Regulation of immune signalling in the malaria mosquito vector, Anopheles : the secreted mosquito leucine-rich repeat protein APL1C is a pathogen binding factor essential for immunity to Plasmodium ookinetes and sporozoites

Natalia Marta Zmarlak

Sorbonne Université

École doctorale *Complexité du Vivant*

Laboratoire de Génétique et Génomique des Insectes Vecteurs, Institut Pasteur, Paris

Regulation of immune signalling in the malaria mosquito vector, *Anopheles*

The secreted mosquito leucine-rich repeat protein APL1C is a pathogen binding factor essential for immunity to Plasmodium ookinetes and sporozoites

Par Natalia Marta Zmarlak

Thèse de doctorat de Science du Vivant

Dirigée par Christian Mitri et Kenneth Vernick

Présentée et soutenue publiquement le 28.06.2021

Devant un jury composé de :

Higuet Dominique. Professeur de la Sorbonne Université, Président.
Christophides George. Chargé de recherche au Royaume-Uni, Rapporteur.
Marois Eric. Chargé de recherche INSERM, Rapporteur.
Smith Ryan. Chargée de recherche aux États-Unis, Examinateur.
Mitri Christian. Thesis Co-Encadrant.
Vernick Kenneth. Directeur d'unité. Directeur de these.

This work is dedicated for my Parents. Thank you for raising me in love, faith and hope.

Pracę te dedykuje moim Rodzicom. Dziękuję Wam za wychowanie mnie w miłości, wierze i nadziei.

.

SUMMARY

ACKNOWLEDGMENTS

I would like to thank my supervisors. Ken, Christian thank you for the opportunity to do this thesis. Thank you for all the time you both always had for me, our discussions and chance to observe your work. Finally, thank you that I could raise under your supervision as a scientist but also as a person.

I would also like to thank all the colleagues of the Genetics and Genomics of Insect Vectors Unit (Kenneth Vernick laboratory) who also attributed to this work, especially Emma who helped me with functional genomics studies, Corinne who always provided me the mosquitoes, Inge who taught me cell culture, Adrien who supervised my RNA sequencing analysis and Manu for advices concerning data analysis. Besides work, I would like to thank all present and previous members of GGIV for the everyday atmosphere that cheered me up during better and worse days of my PhD.

My deep gratitude to the members of Malaria Infection and Immunity (Rogerio Amino laboratory), especially Eduardo Aliprandini and Pauline Formaglio for discussions and advices concerning my immunofluorescence analyses and microscopy. Jean-Michel, thank you for your patience while teaching me salivary glands dissection and infection analysis.

I am grateful to Audrey Salles and Julien Fernandes for providing me skills for Laser Scanning Microscopy and to Jean-Yves Tinevez who helped me with pictures analysis.

My sincere thanks to all the members of CEPIA (Patricia Baldacci platform), for providing me mosquitoes. Special thanks to deceased Marek Szatanik (responsible for CEPIA platform 2015-2019) under whom supervision I made my first internship in Institut Pasteur and who will always stay in my memory as dear friend.

Thanks to all the members of Labo Prepa who took care of my working environment.

Thanks to all my friends in Poland and France. I would like give special thanks to my best friend Ilona who was always available to give me a call as well as to visit me in France. Aurelia and Kuba, thank you for providing scientific advices but also friend shoulder.

Finally, I would like to thank my family, my father Janusz Zmarlak and mother Marta Zmarlak, my brothers Marcin Zmarlak, Szymon Maj and Bartlomiej Zmarlak and their families. Last but not the least I want to thank my fiancé Maxence Feher who is my biggest supporter. Thank you for the faith you have in me and care that you took of our everyday life so I could focus on this thesis.

TABLE OF CONTENTS

TABLE OF CONTENTS

LIST OF FIGURES

LIST OF FIGURES

LIST OF TABLES

LIST OF ANNEX CONTENT

ABBREVIATIONS

A

A. gambiae s.l. – *Anopheles gambiae* sensu lato

AMP – antimicrobial peptides

AP–1 – activator protein 1

APL1 – *Anopheles Plasmodium*-responsive leucine-rich repeat 1

ATB – antibiotic

ATP – adenosine triphosphate

Avr – avirulence

B

BCR – B-cell receptor

bp – base pair

Bti – *Bacillus thuringiensis* var. *israelensis*

C

C3 – complement component 3

CC – coiled coil

cDNA – complementary DNA

CLD – clodronate

CP – connecting peptide

CRISPRs – clustered regulatory interspaced palindromic repeats

D

DAMP – damage associated molecular pattern

DAPI – 4′,6-diamidino-2-phenylindole

DC – dendritic cell

DNA – deoxyribonucleic acid

ds – double stranded

DTT – dichlorodiphenyltrichloroethane

E

ETI – effector triggered immunity

F

FC – fold change

G

GAPDH – glyceraldehyde 3-phosphate dehydrogenase

GFP – green fluorescent protein

GMEC – Global Malaria Eradication Campaign

GNBP – Gram–negative binding–protein

H

HdMv – hemocyte derived microvesicles

HELI – Health and Environment Linkages Initiative

HPX2 – heme peroxidase 2

HR – hypersensitive response

HSP – heat shock protein

I

IBM – *Plasmodium* infected bloodmeal

IFA – immunofluorescence assay

Ig – immunoglobulin

Imd – immunodeficiency

IP – Interpro

IRF3 – interferon regulatory factor 3

IRS – indoor residual spraying

ITN – insecticide-treated nets

IVM – integrated vector management

IκB – inhibitor of nuclear factor kappa B

J

JAK – Janus kinase

L

LAM – lipoarabinomannan

LP – liposomes

LPS – lipopolysaccharide

LRIM – leucine-rich repeat immune

LRR – leucine-rich repeat

LRRCT – leucine-rich repeat C-terminus

LRRNT – leucine-rich repeat N-terminus

LRRV – leucine-rich repeat variable

LSM – laser scanning microscope

LTA – lipoteichoic acid

M

mAb – monoclonal antibody

MAC – membrane attack complex

MAPK – mitogen activated protein kinase

MBL – mannose binding lectin

MHC – major histocompatibility complex

MyD88 – myeloid differentiation primary-response protein 88

N

n.s. – not significant

NA – not applicable

NB – nucleotide binding

NBM – non-infected bloodmeal

NBS – nucleotide binding site

NFkB – nuclear factor kappa-B

NLR – nucleotide-binding leucine-rich repeat receptor

Nod – nucleotide-binding oligomerization domain-like

NOX5 – NADPH oxidase 5

P

pAb – polyclonal antibody

PAMP – Pathogen Associated Molecular Pattern

PBS – phosphate-buffered saline

PCR – polymerase chain reaction

PGN – peptidoglycan

PGRP – peptidoglycan recognition protein

PRI – *Plasmodium* resistant island

PRR – Pathogen Recognition Receptor

qPCR – quantitative PCR

R

RACE – rapid amplification of cDNA ends

RBC – red blood cell

rDNA – ribosomal DNA

RFP – red fluorescent protein

RLK – receptor–like kinase

RLP – receptor–like protein

RNA – ribonucleic acid

RNAi – RNA interference

ROS – reactive oxygen species

S

s.l. – sensu lato

SEM – standard error of mean

SPE – Spätzle–processing enzyme

spp. – species pluralis

Spz – Spatzle

STAT – signal transducer and activator of transcription

sTLR – secreted Toll-like receptor

SUG – sugar meal

T

TCR – T-cell receptor

TEP1 – thioester-containing protein 1

TIR – Toll/interleukine-1 receptor

TLR – toll-like receptor

TM – transmembrane

UP – UniPro

V

VB – VectorBase

VC – vector competence

VLR – variable lymphocyte receptor

W

WHO – World Health Organization

223

I. GENERAL INTRODUCTION

1.1 Malaria – overview

1.1.1 Female *Anopheles* mosquitoes – vector of malaria

Morbidity and mortality caused by mosquito-borne diseases makes a mosquito the most dangerous animal for a human being[1]. The hematophagous female mosquito acquires essential nutrients for egg development by taking blood from vertebrate animals including or humans. Through the bloodmeal, mosquitoes can ingest and eventually transmit pathogenic microbes with injected saliva to the vertebrate host during the next bloodmeal. Many mosquito species are vectors responsible for the transmission of multiple pathogens, including protozoans, viruses, bacteria and nematodes, causing diseases such as malaria, yellow fever, dengue, filariasis or encephalitis. This blood dependency has been used by the pathogens to co-evolve with their respective mosquito hosts to assure their transmission. Mosquito vectors thus bridge the physical barriers that would be impossible for the pathogen to cross through direct contact between humans or animals[2].

Mosquitoes of the genus *Anopheles* are responsible for the transmission of the protozoan parasite *Plasmodium,* the causative agent of malaria, the world's deadliest parasitic disease. In 2019, there were 229 million diagnosed cases of malaria worldwide, with 409 000 human deaths reported. Approximately 94% of global malaria cases occur in sub-Saharan Africa. Children under 5 years old are the most vulnerable group to malaria and constitute two-thirds of all malaria deaths worldwide in 2019[3].

1.1.2 History of malaria, mosquito-vector discovery and vector control

Malaria is one of the oldest human diseases. The first recorded mention that corresponded to malaria symptoms appeared in notes from ~2700 BC. The word "malaria" comes from an Italian appellation of the disease during Middle Age, mal'aria, meaning "spoiled air'", reflecting the doctrine that lasted for over 2500 years, which considered malaria as an aerial infection arising from the marshes. Our understanding of this disease started at the end of the XIX century when a French physician, Alphonse Laveran, discovered *Plasmodium* parasites in a malaria infected patient[4]. For this finding, Laveran won the Nobel Prize in Physiology or Medicine in 1907.

In the 1890s, Patrick Manson proved an association between insects and pathogens causing human and animal diseases. His discovery of mosquito involvement in transmission of filarial worms responsible for lymphatic filariasis suggested that this insect could also be responsible for malaria transmission[5]. Scientists postulated the possibilities of human infection by drinking water contaminated by infected mosquitoes or inhaling dust from dried-up ponds in which infected mosquitoes died. Others suspected that the parasites could be transmitted mechanically from host to host on the proboscis of a mosquito[4,5]. But finally, in 1897 Ronald Ross, after many attempts, successfully infected female mosquitoes with *Plasmodium* from the blood of infected patients, thus resolving all previous speculations. His observations of circular parasites in dissected mosquito midguts (now called oocysts) were followed by research on avian malaria, where he demonstrated the rupture of oocysts leading to sporozoite release in the circulatory system of the mosquitoes (hemocoel) and their migration to the salivary glands, thus completing the parasite life cycle[4,6].

The ground-breaking discovery of R. Ross opened a new avenue in fighting malaria disease, through controlling the essential part of *Plasmodium* parasite transmission by targeting the *Anopheles* mosquito vector. The historic success of malaria eradication

in various parts of the world was mainly achieved by vector control programs. The early malaria vector control programs attempted to eliminate mosquito through environmental management based on knowledge of insect development. The mosquito lifecycle includes four stages: egg, larva, pupae and adult, of which the first three are aquatic. Therefore, early strategies concentrated on limiting the aqueous environment, such as drainage of habitats, oil application to open water bodies, grid-ditching of marshes, modification of river boundaries and other engineering approaches, which decreased mosquito populations by denial of larval habitat[7,8,9]. However, the most efficient tool appeared with the use of insecticides. Since the first half of the 20th century, different classes of insecticides have been successively used: organochlorines, organophosphates, carbamates and synthetic pyrethroids. Use of insecticides greatly limited mosquito-borne diseases and in some areas even eradicated malaria. Indoor residual spraying (IRS) using dichlorodiphenyltrichloroethane (DDT) implemented in the Global Malaria Eradication Campaign (GMEC) in 1955, showed spectacular success in decimating disease vectors. However, despite the efficiency of DDT in reducing mosquito vector populations, safety concerns for humans and their environments led to its ban in many countries in the 1970s. Moreover, at least during the last 20 years, the widespread development of mosquito resistance to the most commonly used insecticides caused serious problems in many areas resulting in recurrent outbreaks of mosquito-borne diseases[10,11,12,13,14,15,16]. Alternative approaches that have already been implemented use natural insecticidal materials obtained from animals, plants, bacteria or minerals instead of chemical insecticides. Classified as biopesticides, entomopathogenic bacteria and fungi, such as *Bacillus thuringiensis* var. *israelensis* (Bti) or *Metarhizium* spp. displayed promising results in mosquito elimination. Nevertheless, their efficacy

varies in different environments, affected by factors such as water pollution or instability to UV radiation[17]. Therefore, according to World Health Organization (WHO) recommendations, insecticide-based strategies, including insecticide-treated mosquito nets (ITNs) and IRS using pyrethroids, remain the mainstay interventions for mosquito vector control. At the same time, the recent WHO Health and Environment Linkages Initiative (HELI) stressed the importance of basic knowledge on mosquito vector behaviour and ecology, in order to develop tailor-made vector management actions in malaria endemic sites. This strategy enables implementation of integrated vector management (IVM), which besides conventional methods in fighting mosquito vector (ITNs and IRS) implements alternative strategies, such as environmental manipulation. IVM is a dynamic and still-evolving field necessary for sustainable and ecologically sound mosquito control strategies[18].

1.1.3 Why is Africa the most malaria endemic continent – what makes a competent mosquito vector?

Plasmodium parasite transmission between humans requires a competent mosquito vector. Vector competence defines the intrinsic ability of a vector to carry, tolerate the development and transmit a microbe and it reflects the susceptibility of a mosquito vector to such microbe[19]. Vector competence is usually measured experimentally as the prevalence of infected and infectious vectors at given times post-microbial exposure[20]. The reasons for high malaria endemicity cases in Africa is a combination of physiologically permissive vector species mainly belonging to the *Anopheles gambiae sensu lato* (*s.l.*) complex and, most importantly, their highly anthropophilic feeding behaviour. The anthropophily of *A. gambiae s.l.* probably originated from the integration of these mosquitoes into human ecosystems about 8000 years ago when

the advent of agriculture led to the new ecological niche of fixed human settlements[19, 21,22].

Among approximately 100 *Plasmodium* species that are infective for different vertebrates, five of them cause malaria in humans: *Plasmodium falciparum*, *Plasmodium vivax, Plasmodium malariae, Plasmodium ovale* and *Plasmodium knowlesi*[23,24]. Today the majority of malaria cases in Africa are caused by *P. falciparum*[23].

A. gambiae was initially considered as a single malaria vector species across the African continent. However, beginning in the 1960s hybridization experiments combined with genetic studies showed that *A. gambiae s.l.* is a complex of at least seven morphologically indistinguishable sibling species, and more taxa continue to be discovered[25,26,27]. Different species display diverse biting behaviour and ecological preferences, including indoor (endophagous) or outdoor (exophagous) biting behaviour. Therefore, indoor targeted vector control strategies are not completely efficient against outdoor-biting taxa or genotypes. This behavioural diversity of *A. gambiae s.l.* increases the challenge in vector control strategies. Mosquito genotyping combined with behavioural and infectious studies are helping to better understand the complexity of the efficient transmission system in order to develop more efficient control strategies.

1.1.4 The complex lifecycle of *Plasmodium* parasite in vertebrate and mosquito

As pointed out, the success of parasite transmission to humans depends on the vector competence of the mosquito. *Plasmodium* has a complex lifecycle that requires two

hosts: the intermediate vertebrate host, and the definitive mosquito host. *Plasmodium* sporozoites are transmitted to the vertebrate host through the saliva of an infected mosquito (**Figure 1**). Sporozoites are carried by blood flow to the liver where they infect hepatocytes. There, the parasites grow and multiply to be released into the blood stream as merozoites, which infect red blood cells (RBCs). Repetitive intraerythrocytic cycles occur to form different stages: rings, trophozoites and schizonts, which release new merozoites that invade non-infected RBCs. The contents of the infected RBCs released upon their lysis stimulate the production of tumour necrosis factor and other cytokines, which are responsible for clinical manifestations of malaria disease. People infected with *Plasmodium* typically experience fever, shivering, cough, respiratory distress, joint pain, headache, diarrhoea, vomiting and convulsions. *P. falciparum* is the most dangerous human malaria species and can be sequestered in microvasculature of different organs, including the brain, which can result in cerebral malaria and potentially death[23,28,29].

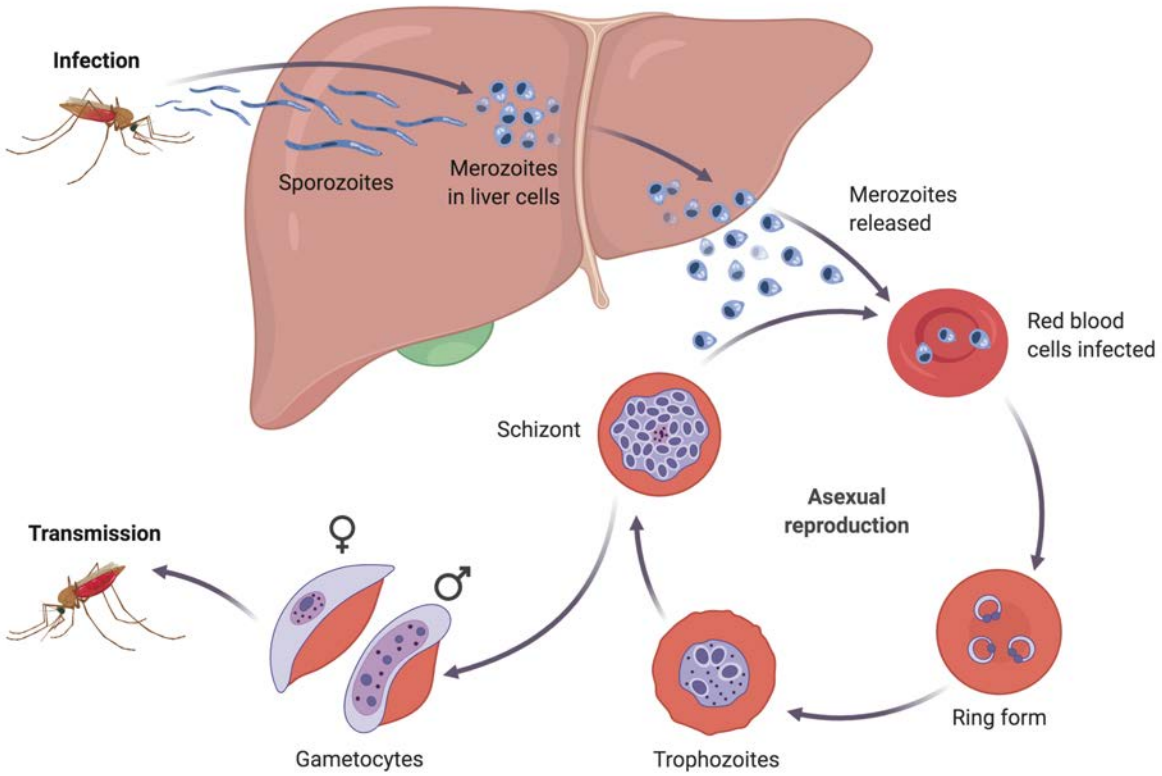

Figure 1. *Plasmodium* parasite asexual development in a human host. Detailed description in the text.

None of the parasite asexual blood stages are infectious to the mosquito. After several erythrocytic cycles, stress and other signals leads to parasite differentiation into female and male gametocytes, maturating through five different stages (I-V). Nevertheless, the mechanism of the parasite commitment to start sexual development still remains ambiguous, as approximately 10% of the merozoites undergo sexual development[30]. Only stage V mature female and male gametocytes are transmissive stages from human to mosquito. Upon a bloodmeal on an infected host, the female mosquito ingests both female and male gametocytes. In the midgut lumen, each male gametocyte produces eight flagellated motile microgametes in a process called exflagellation, induced by environmental and vector factors (**Figure 2**). Released motile male gametes attach and fertilize female gametes within ~30 min after ingestion,

forming zygotes. The zygotes transform into motile ookinetes that traverse mosquito midgut epithelial cells, from the apical to the basal side where they round up to become oocysts. These first steps of the parasite development in the mosquito, from gametocyte fertilization to ookinete traversal, are relatively rapid, taking approximately 24 hours. The subsequent steps are longer in time. Within the sessile oocysts, multiple rounds of mitosis result in thousands of sporozoites. Between 10-12 days after oocyst establishment, mature oocysts undergo membrane rupture, leading to the release of sporozoites in the mosquito hemocoel, which is an open circulatory system, from which sporozoites invade the salivary glands. There, the sporozoites remain metabolically quiescent for the life of the vector, and are transmitted in the saliva to a new host during later bloodmeals[31,32,33,34,35,36].

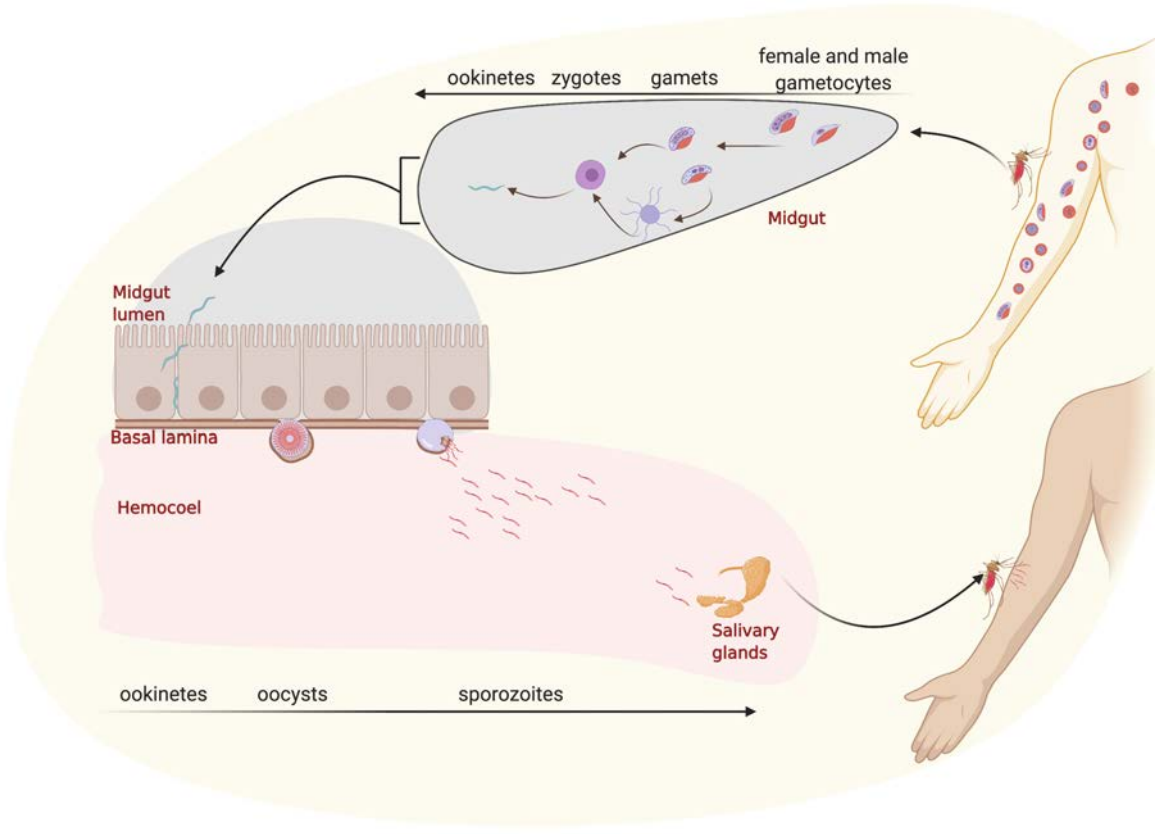

Figure 2. *Plasmodium* development in female *Anopheles*. Detailed description in the text.

1.1.5 Two bottlenecks of *Plasmodium* development in mosquito vector

Even though *Anopheles* female mosquitoes are essential for *Plasmodium* transmission, not all of them are competent vectors for the parasites. In other words, the fact that a mosquito takes a bloodmeal from *Plasmodium*-infected host does not mean that the parasites will successfully develop within the insect vector. Indeed, during the parasite lifecycle, the largest losses in the number of parasites occur inside the mosquito host[37]. This indicates that the mosquito mounts defence mechanisms towards *Plasmodium* that can lead to complete elimination of the parasites from the mosquito host. During the early stages of *Plasmodium* development in the mosquito, from gamete fertilization to ookinete formation, the parasites are still exposed to the vertebrate host immune factors present in the ingested blood sera, which can impede parasite development in the mosquito[38]. The mosquito microbiome, which expands in abundance after the bloodmeal, could have deleterious, neutral, or beneficial effects on early parasite development, and is not yet well understood[39-42]. Finally, digestive enzymes in the mosquito midgut as well as the development of the chitin-based peritrophic matrix around the ingested blood bolus could serve as a mechanical barrier that some ookinetes fail to pass[38]. However, the most dramatic bottlenecks in the *Plasmodium* lifecycle appear during ookinete traversal through midgut epithelium, as out of ~1000 ookinetes invading the midgut epithelium, ~5 may succeed in forming oocysts[43,44].

The next bottleneck is when sporozoites are released from mature oocysts in the hemolymph to invade the salivary glands. It is estimated that approximately 80% of released sporozoites will fail to infect the salivary glands[45,46,47]. During these two main bottlenecks of parasite development in the mosquito, *Plasmodium* is in direct contact

with the insect hemolymph, thus with soluble mosquito immune factors. Therefore, the mosquito hemolymph appears to be a battlefield in which *Plasmodium* parasites are attacked by mosquito defence factors. While the role of mosquito immune factors in the first bottleneck has been clearly demonstrated, this is not the case for the second one, concerning the large sporozoite clearance seen in the hemolymph, and this still needs to be clarified.

1.2 Microbial sensing by the immune system

1.2.1 Basis of microbial immune sensing and evolution

One of the challenges in immunology is to understand how the host organism detects the presence of infectious agents and mounts efficient killing mechanisms against these intruders, without destroying self-tissues. Sensing intruder as “non-self” or as lacking “self-markers” constitutes the starting point of the host response as a defence reaction in all living organisms. For microbial sensing, host-derived factors need to come in contact with the pathogen and generate the signals that will be transduced into a downstream immune response leading to the clearance of the microbes. Even such simple organisms as prokaryotes have defence mechanisms based on restriction enzymes and clustered regularly interspaced palindromic repeats (CRISPRs) that target invading pathogenic phages for degradation[48]. The foundational defence strategies in eukaryotic organisms are generally classified as the innate immune system, a host defence system in which plants and animals share similar inherited molecular modules including for pathogen sensing. The principle of innate immune recognition is based on the detection of constitutive and conserved products from structural microbial surface proteins or from their metabolism. Different pathogens

share unique structures, for example lipopolysaccharide (LPS) or peptidoglycan, which are bacterial surface molecules, characterized as Pathogen Associated Molecular Patterns (PAMPs) and which are not synthetized by eukaryotic cells. The structure of these components is conserved, as they are often essential components for microbial survival and fitness. PAMPs are sensed by host germline-encoded proteins serving as pathogen recognition receptors (PRRs). Activation of PRRs through PAMP recognition transduces an immune signal inside the cells that leads to diverse killing mechanisms of the invaded pathogen (opsonization, activation of complement, phagocytosis, activation of pro-inflammatory signalling pathways, induction of apoptosis etc.).

In the first vertebrates, around 500 million years ago, a more sophisticated mechanism called adaptive immunity, was built upon the innate immune layer. One of the unique features of adaptive immunity is the rearrangement of immune receptor gene segments, which result in development of clonally diverse immune cells called lymphocytes, where each possesses a unique antigen recognition receptor. Somatic recombination leads to the development of a large repertoire of lymphocytes that can recognize distinct microbes and mount highly specific immune responses tailored to the threat. Pathogen recognition occurs through mature effector lymphocytes with cytotoxic and pro-inflammatory functions or plasma cells that secrete antibodies (the soluble forms of the antigen-specific receptors). Moreover, the clonal expansion and long life of primed cytotoxic lymphocytes and plasma cells provide a protective immune memory to prevent reinfection[49,50,51].

The recognition of a microbial intruder leads to the activation of defence mechanisms in the host-organism, leading to the immune responses. The study of *Drosophila melanogaster* was highly relevant to mammalian biology, given the evolutionary conservation of many key signal transduction pathways. In *Drosophila*, the innate

immune system recognizes infectious microbes[52]. *Drosophila* Toll and Immunodeficiency (Imd) immune pathways represent two distinct major arms of the immune response, which are activated by different microbes. Gram-positive bacteria and fungi activate the Toll signalling pathway, whereas Gram-negative bacteria activate the Imd pathway. Both pathways induce humoral and cellular changes in the insect host in order to eliminate or control the invasion of the intruder. Besides Toll and Imd immune-signalling pathway, the Janus kinase (JAK)-signal transducer and activator of transcription (STAT) and RNA interference (RNAi) pathways are immune arms of the antiviral response. Thus, invertebrate innate immunity is able to mount different defence response against distinct pathogens[53].

1.2.2 LRR domain proteins in immunity

LRR motifs have been identified in proteins ranging from viruses to eukaryotes. Despite distinct evolutionary origin, many plant and animal immune receptors or factors including cell-adhesion molecules, hormone receptors, tyrosine kinase receptors or extracellular matrix-binding glycoproteins contain LRR domain. LRR proteins serve as significant mediators in both innate and, replacing immunoglobulin (Ig) domain, in alternative-adaptive immune systems where they play a dual function. Firstly, serving in pathogen sensing, through direct or indirect recognition of the pathogens, and secondly, as signal mediator, through the elicitors of downstream immune signalling they activate. LRR domains vary in their lengths and pattern of conserved residues, mediating ligand binding interactions[54]. In the next parts, I give an overview of distinct conserved immune protein families from different organisms, all carrying the LRR domain required for achieving their protective function.

1.2.2.1 LRR proteins in the innate immune system

1.2.2.1.1 Drosophila Toll receptors

Toll and the members of the Toll-dependent signalling pathway were initially found in *Drosophila* as involved in early embryonic development in the dorso-ventral patterning of the embryo[55,56]. Further studies demonstrated the contribution of Toll signalling pathway in defence against Gram-positive bacteria and fungi[57-59]. Toll protein is a transmembrane receptor with extracellular LRR domain that binds a ligand and an intracellular Toll/interleukine-1 receptor (TIR) domain that takes part in the intracellular signal transduction. Toll is not activated by direct recognition of a PAMP, but it binds instead to the active form of the protein ligand Spätzle (Spz) with a high affinity (*kd=0.4nM*)[60]. Spz is a cytokine that is produced as a pro-form. Spz activation takes place upon proteolytic cleavage in response to infection through serine protease cascades that lead to the activation of Spätzle-processing enzyme (SPE), which is required to activate Spz[57]. Spz binding to Toll induces receptor dimerization through disulphide bridges of conserved cysteine residues[61]. This dimerization induces an intracellular signalling, leading to the phosphorylation of the inhibitor of nuclear factor kappa B (IκB) Cactus (a negative regulator of the Toll pathway). Once phosphorylated, Cactus releases the nuclear factor kappa-B (NF-κB) transcription factor(s) Dorsal or Dif, which migrate to the nucleus and activates the transcription of several genes, such as antimicrobial peptides (AMP)[57]. Apart from humoral response, Toll receptor activation also induces cellular responses in *Drosophila,* such as phagocytosis, melanization or encapsulation[52,57]. The *Drosophila* genome encodes nine Toll receptors that all share a similar molecular structure, with an ectodomain composed mainly of LRR and cysteine-rich flanking motifs. Besides Toll (also known as Toll-1),

533 only Toll-5 and Toll-9 induce the expression of the anti-fungal peptide *drosomycin*[62],
534 whereas Toll-7 was shown to interact with viral pathogens, inducing antiviral autophagy
535 in *Drosophila*[63]*.* Therefore, Toll proteins are responsible for indirect recognition of
536 pathogens and activation of humoral and cellular immune responses in
537 *Drosophila.*[57,61,64,65]

538

539 **1.2.2.1.2 Toll-like receptors (TLR)**
540

541 Identification of Toll receptors in *Drosophila* opened new perspectives to understand
542 the innate immune system, which was understudied in higher organisms in favour to
543 the adaptive immune response. In deuterostomes, Toll-like receptors (TLRs), which
544 are transmembrane proteins, were identified as the major PRRs that underwent
545 purifying and diversifying selection, ranging from 222 TLR genes in sea urchin
546 *Strongylocentrotus purpuratus* to 12 TLR in mouse[66], in order to adapt to a variety of
547 coevolving pathogens. Among mammals, human encodes at least 10 TLRs. In contrast
548 to *Drosophila,* where the Toll-dependent pathway is induced by Gram-positive and
549 fungal pathogens, TLR in mammals are activated upon structurally variant PAMPs
550 from different organisms and that constitute a large repertoire of microbial structures
551 (**Table 1**).

Toll-like receptor	Ligand(s)
	Only signals as a dimer when combined with TLR2 for all its ligands; recognizes *Borrelia burgdorferi* OspA; required for adaptive immune response
	Tri-acyl lipopeptides (bacteria, eg, *M tuberculosis*)
TLR1	Soluble factors (*Neisseria meningitidis*)
	Associates with CD11/CD18, CD14, MD-2, TLR1, TLR6, dectin 1; Lipoprotein/lipopeptides (a variety of microbial pathogens)
	Peptidoglycan
	Lipoteichoic acid
	Lipoarabinomannan (mycobacteria)
	Phenol-soluble modulin (*Staphylococcus epidermidis*)
	Glycoinositolphospholipids (*Trypanosoma Cruzi*)
	Glycolipids (*Treponema maltophilum*)
	Porin (*Neisseria*)
	Zymosan (fungi)
	Atypical LPS (*Leptospira interrogans*)
	Atypical LPS (*Porphyromonas gingivalis*)
	HSP70 (host)
	CMV virions
	Hemagglutinin (H) protein of wild-type measles
TLR2	Bacterial fimbriae
TLR3	Double-stranded RNA in viruses
	Gram-negative enteric LPS (requires coreceptors MD-2 and CD14)
	Additional ligands
	Chlamydial heat shock protein 60
	RSV F protein
	Taxol (plant)
	M tuberculosis HSP65
	Envelope proteins (MMTV)
	HSP60 (host)
	HSP70 (host)
	Type III repeat extra domain A of fibronectin (host)
	Oligosaccharides of hyaluronic acid (host)
	Polysaccharide fragments of heparan sulfate (host)
	Fibrinogen (host)
TLR4	Beta-defensin2
TLR5	Flagellin (monomeric) from bacteria
	See TLR2 (as dimmers with TLR2)
	Phenol-soluble modulin
TLR6	Di-acyl lipopeptides (mycoplasma)
	Responds to imidazoquinoline anti-viral agents (synthetic compounds)
	Loxoribine (synthetic compounds)
	Bropirimine (synthetic compounds)
	Endogenous and exogenous ligands unknown.
TLR7	Single-stranded RNA
	Imidazoquinoline (synthetic compounds)
TLR8	Single-stranded RNA
TLR9	Bacterial DNA as “CpG” motifs
TLR10	Unknown

Table 1. Role of human TLRs in pathogen recognition. Table modified from[67].

Depending on the sensed pathogen, TLRs activate intracellular signalling pathways that induce transcription of various defence factors, including inflammatory cytokines, chemokines, major histocompatibility complex (MHC) and co-stimulatory molecules[68]. TLR activity require dimerization of LRR ectodomain that is proposed to bring together intracellular TIR domains, thus enabling activation of downstream signal transduction process[69]. TLRs dimerization can be homo- and heterologous, and the variety of TLR dimer combinations increases their microbial sensing repertoire[70]. An example of this cooperation was demonstrated for TLR2 heterodimer with either TLR1 or TLR6, where

563 the TLR2 partner determines the specificity of the ligand recognition[71]. In response to
564 microbial invasion, extracellular PAMPs or DAMPs can activate TLRs on the cell
565 surface. However, TLRs can also be found in the intracellular compartment, where
566 they are located in the membranes of endosomes and lysosomes. In particular,
567 intracellular TLRs sense viral and bacterial nucleic acids during viral particles
568 endocytosis and degradation in late endosomes or lysosomes[72]. Moreover, it was
569 suggested that the intracellular localization of these TLRs could enable discrimination
570 between viral DNA and self-DNA. Lastly, secreted TLR (sTLR) were also described,
571 e.g. sTLR2, which has been shown to arise from ectodomain shedding of the
572 extracellular domain[73]. Soluble form of receptor was found in blood and breast milk to
573 inhibit inflammatory reaction. Such reaction is proposed to work in the way that sTLR2
574 could negatively regulate TLR2 activation by behaving as a decoy receptor[74,75].

575 Taken together, the TLR family serves mainly as direct PRRs for microbial sensing
576 that mount innate immune responses as well as playing key role in linking innate with
577 adaptive immunity [67,68,76,77,78,79].

578

579 **1.2.2.1.3 Nucleotide-binding leucine-rich repeat receptors**
580

581 Nucleotide-binding leucine-rich repeat receptors (NLRs) represent the major class of
582 intracellular innate immune receptors found in both animals and plants (described
583 below). In animals, the cytoplasmic detection system induced by NLRs was proposed
584 to play a defence function in host tissues where TLRs are absent or expressed at low
585 levels[80]. This is the case for the intestinal epithelial cells, which are in constant contact
586 with the microbial flora. Therefore, expression of TLRs is down-regulated in these cells
587 in order to avoid high stimulation and aberrant inflammations due to the microbial

PAMPs from microbiome. However, in case of cell infections with invasive pathogens, PAMPs can be transferred to the intracellular compartment and be sensed by NLRs, which initiate the defence response. Proteins classified as NLR belong to diverse families. The best characterized members of the NLR family are the Nucleotide-Binding Oligomerization Domain-like (Nod) receptors Nod1 and Nod2. Both Nod1 and Nod2 recognize peptidoglycan (PGN), but each of them requires distinct PGN molecular motifs. In the centre of the proteins, NLRs are characterized by a nucleotide-binding (NB) domain followed by a variable number of highly polymorphic C-terminal LRRs and diverse N-termini. Activation of the Nod molecules occurs when a bacterial ligand is sensed by the LRR domain[80]. Besides recognition of PAMPs, similarly to TLRs, NLRs can also react to modified-self in the form of DAMPs[81]. NLRs are normally in an “off” state due to the inhibitory function of the LRR domain, thus preventing constitutive protein activation via the NB molecular switch[82,83]. Recognition of the pathogen effector induces the release of the inhibited LRR domain and this conformational change, through ATP binding, leads to NLR oligomerization and activation[82]. Activated NLRs lead to inflammatory responses mediated by NF-κB, Mitogen Activated Protein Kinases (MAPK), or Caspase-1 activation, accompanied by subsequent secretion of proinflammatory cytokines[82].

Thus, NLRs are intracellular sensors of innate immunity that activate defence in cells that do not express TLRs but might also serve as a second layer of immune responses after intruders have bypassed extracellular defence and invaded a cell. [80,84,82,85]

1.2.2.1.4 Plant LRRs

Plants lack adaptive immune response. Nevertheless, during evolution plants acquired multilayer innate immune mechanisms. In this system, LRR proteins play a major role across both transmembrane and cytoplasmic PRRs that sense the pathogens and transduce the signals into activation of immune responses. Transmembrane LRR proteins compose the first layer of defence, sensing the extracellular signals from pathogens. This group of receptors is all composed of extracellular LRR domain and variable, intracellular C-terminus. Therefore, we can distinguish receptor-like kinase (RLK) proteins that have intracellular kinase domain and receptor-like protein (RLP) that lack intracellular kinase domain[86] (**Figure 3A**)

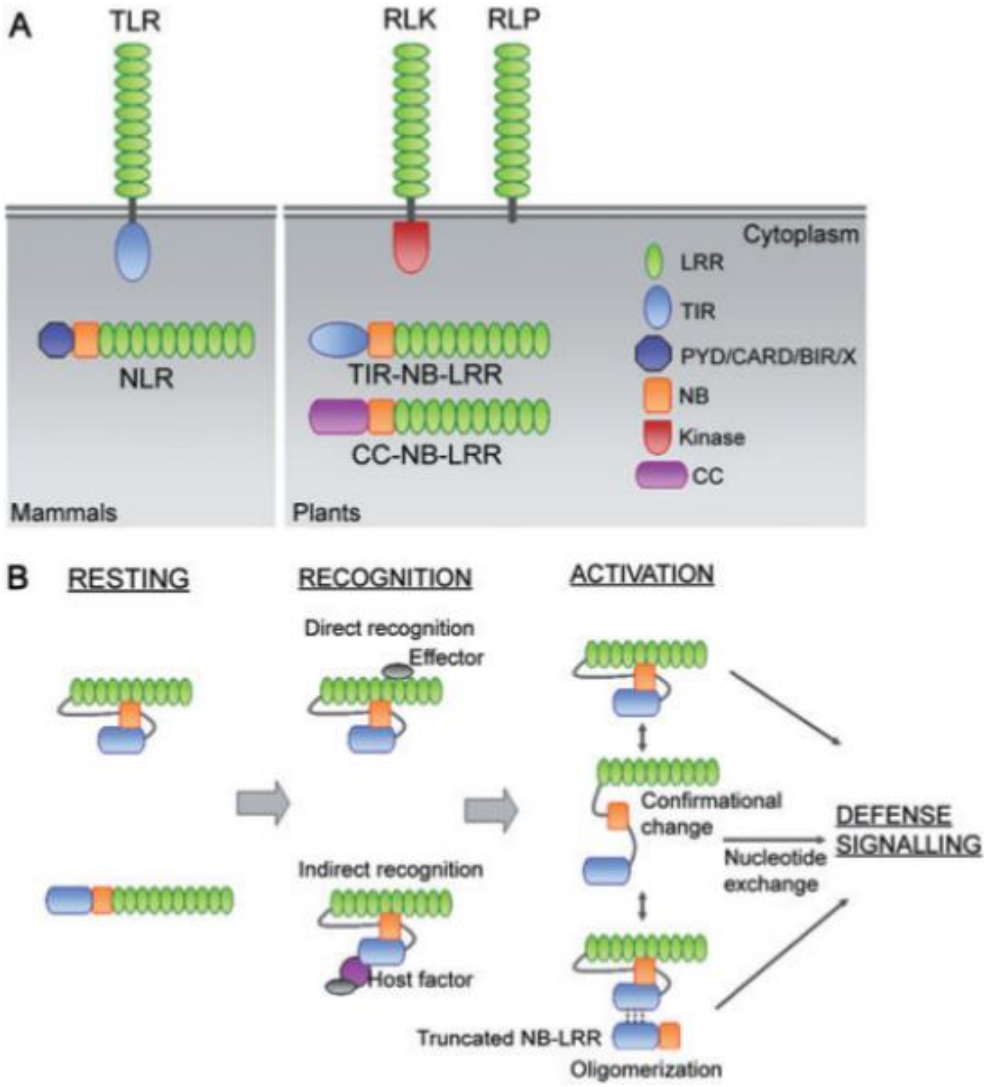

Figure 3. LRR-containing immune receptors, modes of pathogen perception and activation in plants. A. An overview of LRR-containing immune receptors in mammals and plants. **B.** NB-LRR immune signalling activation pathway. Figure reproduced from[86].

Based on N-terminal domain composition, the NB-LRR proteins can be categorized as two types. The common core is composed of C-terminal LRR domain and a central NBS domain, whereas the variable N-terminal domains carry coiled-coil (CC) domain or a domain homologous to *Drosophila* Toll/human interleukin-1 receptor (TIR)[86] (**Figure 3A**). These receptors mediate the activation of the mitogen-activated protein kinase (MAPK) pathway that in turn leads to increased transcription of pathogen-responsive genes, production of reactive oxygen species (ROS), all of which contribute to prevention of pathogen spreading[86,87]. Nevertheless, if a microbe overcomes the

first line of host-defence machinery and enters the cell, a second layer of defence takes over. Plant evolution has generated proteins that detect specific effector molecules, in a mechanism called effector-induced immunity (ETI)[88]. Plant effector-induced immunity is more akin to mammalian adaptive immunity in that pathogen effectors and virulence factors are specifically recognized. The genes encoding the specificity determinants of effector-induced immunity are known as resistance (R) genes. Most known R genes encode proteins belonging to the family of nucleotide binding (NB) LRR proteins (NB-LRR). NB-LRR proteins are involved in the recognition of specialized pathogen effectors (also called avirulence (Avr) proteins) that are thought to provide virulence function in the absence of the proper R gene[88]. Nevertheless, unlike mammalian adaptive immunity, plant defence relies on innate immunity. Therefore, their capability to recognize specifically a large repertoire of pathogen effectors suggests they encode a high number of NB-LRR genes. Indeed, in the genome of *Arabidopsis* there are approximately 150 predicted NB-LRRs[87]. However, this number is probably still below the wide range microbes that plants have to face. This questions of how an effector-induced immune response in plants coordinates resistance to a broad range of pathogens and their corresponding effectors, in sometimes very long-lived individuals, up to centuries, is still not completely clarified. It was proposed that NB-LRR bacterial effector recognition likely evolved as an indirect mechanism. Based on the fact that the majority of characterized bacterial effectors display enzyme activity that modify plant proteins, enzymatic functions of multiple distinct pathogen-effectors target the same host proteins. Therefore, rather than developing receptors for every possible effector, host plants have evolved mechanisms to monitor common plant proteins that are targets of pathogen virulence. Thus, by monitoring perturbations in key host proteins, R proteins such as the NB-LRR, indirectly detect the functional

enzymatic activity of multiple or many pathogen-effectors[87] (**Figure 3B**). NB-LRRs are normally kept in a resting state by intramolecular interactions involving the LRR domain. Pathogen recognition occurs either by direct association between the LRR domain and a pathogen-effector protein or by indirect association mediated by a host protein (**Figure 3B**). Upon ligand binding, conformational changes and/or protein oligomerization leads to the activation of NB-LRR (**Figure 3B**). This is accompanied or followed by exchange of ADP for ATP at the NB domain that leads to defence signalling. The activity of NB-LRR proteins result in activation of defence factors transcription in nucleus or plant hypersensitive response (HR), which is a form of programmed cell death localized to infection sites[86,89,90].

1.2.2.2 LRR-coding receptors in adaptive-like immunity of jawless vertebrates

Jawless vertebrates (agnathans) and jawed vertebrates (gnathostomes) diverged approximately 550 million years ago. While jawed vertebrates are predominant, the jawless clade has only two extant representatives: hagfishes and lampreys. As mentioned above, the arsenal of adaptive immune recognition in gnathostomes is based on Ig domain B and T lymphocyte receptors (BCRs and TCRs) and major histocompatibility complex (MHC) molecules. While none of these proteins are present in agnathans, hagfishes and lampreys were shown to mount adaptive-like immune responses to repetitive antigenic challenges through the expression of unique antigen receptors named variable lymphocyte receptors (VLRs). These VLRs generate antigen-recognition diversity through a gene conversion-like mechanism involving a variable LRR segment domain[91]. Three VLR genes have been identified, VLRA, VLRB and VLRC and they share a similar protein organization with a N-ending LRR-capping motif (LRRNT) followed by 18-residue N-terminal LRR module (LRR1), diverse region

composed of multiple, variable LRR modules (LRRV), 24-residue called end LRRV (LRRVe), a connecting peptide (CP) and a C-terminal LRR-capping motif (LRRCT, **Figure 4**)[92].

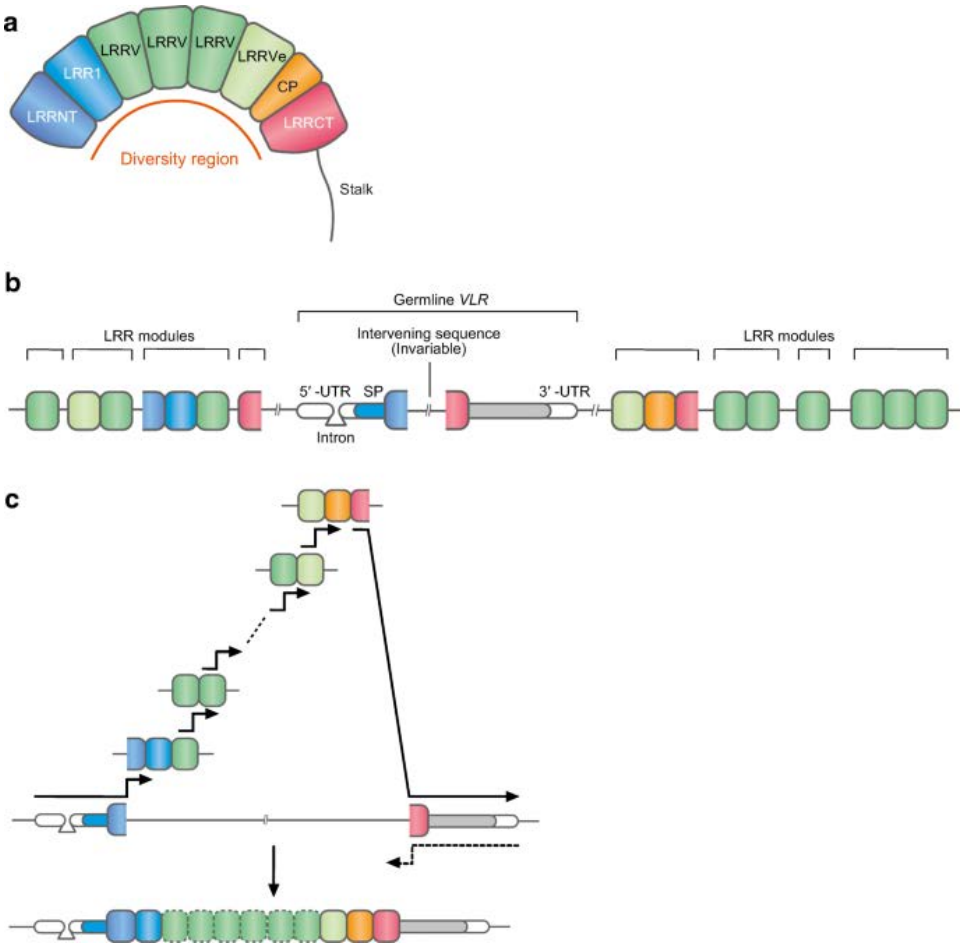

Figure 4. Schematic structure of a VLR protein and VLR gene assembly. A. VLR monomers adopt a horseshoe-like solenoid fold characteristic of the LRR protein family. **B.** The germline VLR gene has a non-functional intervening region instead of the diversity region. Sequences coding for LRR modules (color-coded as in panel **A**) are located in multiple copies adjacent to the germline VLR gene. **C.** In developing lymphocytes, VLR is assembled by a gene conversion-like mechanism. Gene conversion can begin from either end of the gene. Figure reproduced from[92].

This diverse region (LRRV) composed of multiple LRR modules determines receptor specificity. VLRs A, B and C are a membrane-bound protein receptor. However, in addition to be a transmembrane protein, VLRB can also be secreted as a soluble protein. Secreted VLRB molecules occur as pentamers or tetramers of dimers and

have eight to ten antigen binding sites[93], leading to the neutralization of the pathogen and subsequent elimination by phagocytosis or complement pathway activation[92]. In summary, suggesting a convergent evolution, jawed and jawless vertebrates use remarkably different modules (Ig and LRR, respectively) in common strategies, forming transmembrane or soluble antibody receptors as the arm of adaptive immune response [91,92,93,94,95].

706

II. CURRENT KNOWLEDGE, GAPS AND OBJECTIVES

707

708

2.1 Natural resistance to *Plasmodium* highlighted a family of LRR genes termed APL1 (*Anopheles Plasmodium*-responsive leucine-rich repeat)

Like all invertebrates, mosquitoes lack adaptive immune response, thus using their innate immune system to face microbial invasion. The availability of complete genome sequences as well as comparative genome studies between mosquitoes and the arthropod model organism, *Drosophila,* contributed to identification of mosquito immune factors[96,97]. However, *Drosophila* and *Anopheles* diverged from a common ancestor around 250 million years ago and have extremely different lifestyles, especially with the obligate hematophagy of mosquito females. Therefore, while the main immune pathways were found to be conserved, flies and mosquitoes are exposed to different microbial repertoires and thus underwent different evolutionary pressures that have shaped their respective immune systems. While it is difficult to measure fitness trade-offs in nature, identifying the molecular components of natural resistance could help understand how they are genetically structured in wild mosquito vector populations[98]. A field-based genetic mapping survey of wild mosquito populations revealed that about 50% of the *A. gambiae* s.s. tested carried a significant locus controlling susceptibility to natural *P. falciparum*. This genomic locus located on chromosome 2L was mapped in both East and West African wild *A. gambiae* [99,100,101], suggestive of a widespread and shared genetic mechanism of malaria resistance. Candidate gene filtering of the locus by bioinformatics and transcriptional regulation highlighted a family of three genes encoding LRR proteins and named *Anopheles Plasmodium*-responsive leucine-rich repeat 1 (APL1). The genes, APL1A, APL1B and APL1C, share ≥50% peptide identity and have distinct functional activities[102,103].

Functional analysis performed in the laboratory by measuring the presence of midgut oocysts after gene silencing showed that a functional APL1A gene protects against infection with *P. falciparum*, while functional APL1C protects against the rodent malaria parasites, *P. berghei* and *P. yoelii*[102,103]. Furthermore, protection against *P. falciparum* correlates with the transcriptional regulation of APL1A by the isoform Imd/Rel2-S but not Imd/Rel-2F[103], whereas protection against *P. berghei* correlates with the transcriptional regulation of APL1C by the Toll/Rel1 pathway[102]. Gene APL1B protects against both human and rodent malaria parasites in collaboration with APL1A and APL1C, respectively[104]. The APL1 genes display high polymorphism with a rate of non-synonymous variation 10-fold higher than any another *A. gambiae* genes. This pattern is consistent with adaptive maintenance of polymorphism, which can be seen in so-called “trench warfare” models of fluctuating recurrent pathogen epidemics[105]. Such polymorphism results in different encoded protein variants that likely lead to protective phenotypes against distinct pathogens. Indeed, in a study of the *A. gambiae* Ngousso colony, which segregates three different major structural alleles of APL1A, only one allele was associated with protection against *P. falciparum*[106]. This observation highlights that APL1 allelic variation could contribute to natural variation in mosquito susceptibility to *Plasmodium,* and also that studies in different mosquito colonies should take into consideration presence of different genetic forms that could affect the phenotype.

All three APL1 gene genes are comprised of a small 5’ exon followed by a second longer exon separated by a short intron. The encoded proteins are characterized by an N-terminal signal peptide, a series of LRR motifs spanning ~300 amino acids and

a coiled-coil domain at the C-terminus. In addition to common core sequence among the three genes, APL1C (and some allelic variants of APL1A) also carry an N-terminal repeated motif of the amino acids P-A-N-G-G-L (called PANGGL region), with an unknown function[107 106].

Besides the common LRR domain, some of the other LRR genes in *A. gambiae* share a similar protein structure as the APL1 gene members and together constitute a subfamily of LRR immune genes, called leucine-rich repeat immune molecules (LRIM)[107]. Apart from LRR, these proteins include a coiled-coil domain and patterns of cysteine residues that give possibilities for disulphide bridges between two protein partners. The coiled-coil domain was proposed to drive or consolidate interactions such as combinatorial oligomerizations to promote the orientation of the cysteine residues for stabilizing the disulphide bridges. LRIMs also have a signal peptide with, for some members, a transmembrane domain, suggesting they are secreted into the mosquito hemolymph or exposed on cell membranes. The PANGGL domain present in APL1C and some APL1A allelic forms is exceptional for these proteins and was not found in any other mosquito protein[107]. The LRIM family can be classified in four groups: “Long” subgroup that includes APL1 genes, the “Short” subgroup, the Transmembrane (TM) LRIM and Coil-less subgroups. The “Long” and “Short” subgroups differ each other from the length of their LRR domain[107]. The variable LRRs domains among LRIMs form a stable arc or horseshoe-like fold that could facilitate protein interactions (**Figure 5**).

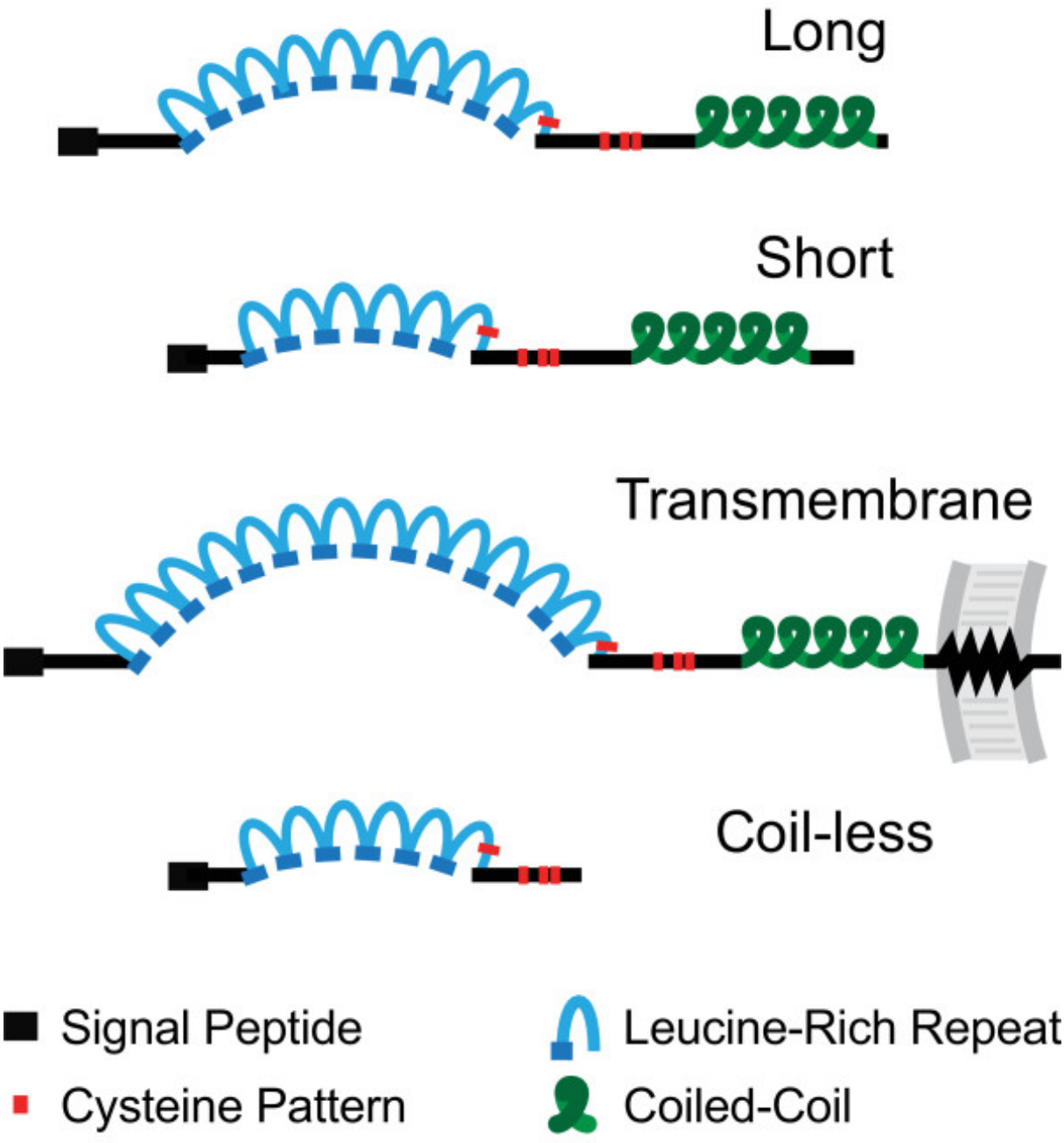

Figure 5. Classification of mosquito LRIM proteins. Figure reproduced from[107].

The structure of LRIMs promotes genes interaction and was best studied in the case of APL1C, which forms a heterodimer with LRIM1 via interaction of their C-terminal coiled-coil domains and a single disulphide bond[108]. This dimerization is absolutely necessary for the antimalarial activity of the *Anopheles* complement-like protein, TEP1 (thioester-containing protein)[109,110].

Nevertheless, not only LRIMs, but other LRR proteins can biochemically interact in binding assays with APL1C or LRIM1, and possess the same protective phenotypes as LRIM family genes, which could generate combinatorial complexity for immune recognition and response[104,107,111,112].

2.2 APL1 functional activity and the mosquito complement system

APL1C and LRIM1 form a heterodimer necessary for the antimalarial activity of the *Anopheles* complement-like protein, Thioester-containing Protein 1 (TEP1)[108,111]. The two other APL1 genes (APL1A and APL1B) also have the capacity to heterodimerize with the LRIM1 protein, suggesting that LRIM1 may act as a common core protein for different heterocomplex formation with APL1 as well as other LRR proteins, including the LRIM members[104]. This is consistent with the role of LRIM1 as an antagonist of both *P. berghei* and *P. falciparum* midgut infection, and also against Gram-negative bacteria[104,113,114].

TEP1 is a structural and functional homolog of vertebrate complement factor C3 and of members of the α2-macroglobulin family (A2Ms)[115,116].

In vertebrates, the complement system is composed of soluble and cell-membrane proteins, acting together in the cascade leading to pathogen clearance through their phagocytosis or membrane attack complex (MAC) formation. There are three complement pathways (**Figure 6**): i) the classical pathway, which is initiated by an antibody-antigen complex ii) the lectin pathway where the mannose or different sugar

811 moieties present on the microbial surface are bound by mannan-binding lectin (MBL)
812 iii) the alternative pathway which is initiated by the spontaneous hydrolysis of the C3
813 factor. This pathway is either self-amplified on the surfaces of microbes or inhibited in
814 the case of host self-surfaces. Despite distinct arms of pathogen recognition, all three
815 pathways induce subsequent proteolysis events and converge to the central C3 factor.
816 Upon proteolytic cleavage, C3 produces anaphylatoxin C3a that recruits neutrophils
817 and monocytes at the site of infection. This promotes inflammation and C3b opsonin
818 inducing phagocytosis and/or downstream reactions with other complement factors, all
819 ending with MAC formation (**Figure 6**)[117,118].

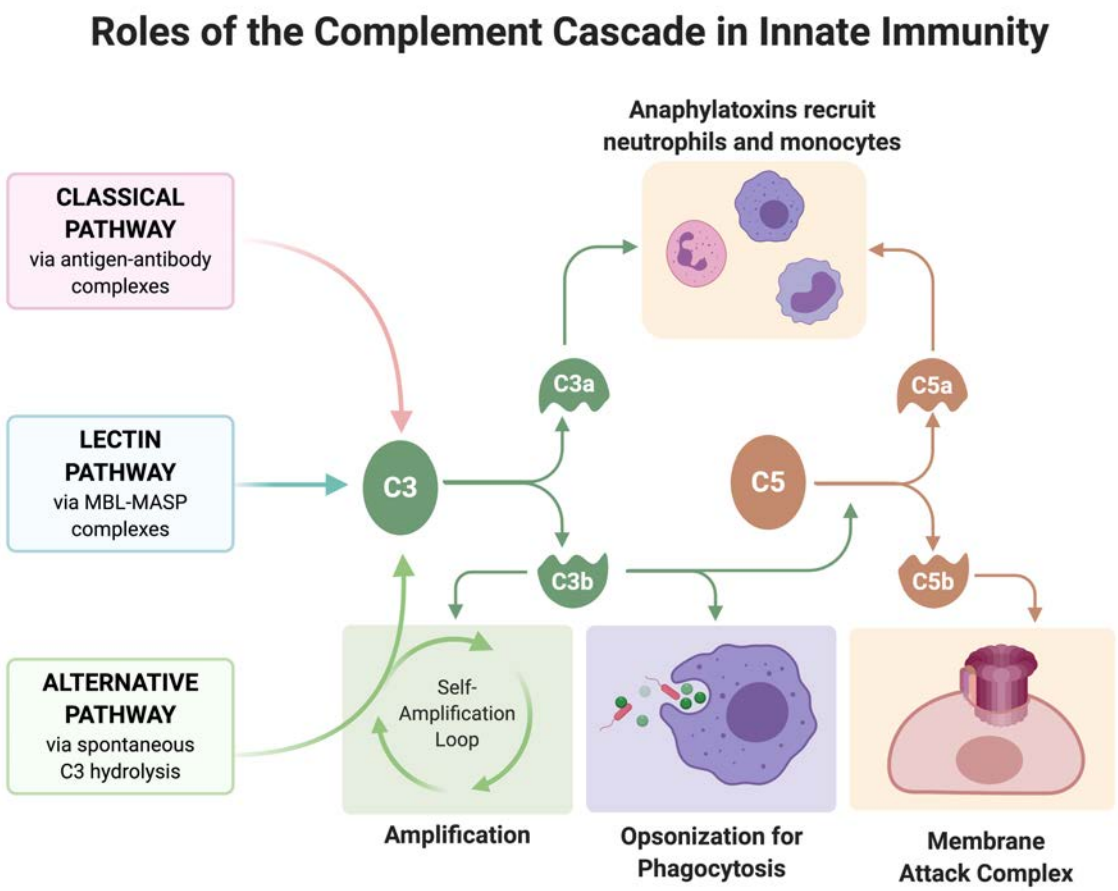

820

821 **Figure 6**. **Complement pathway activation and outcome in vertebrates.**
822

823 In *A. gambiae*, the TEP1-mediated complement-like pathway is the best described

immune effector mechanism. TEP1 is secreted into the hemolymph as a full-length protein before being cleaved to the active form. The cleaved TEP1 form called $TEP1_{cut}$ is stabilized in the hemolymph by the heterodimer LRIM1/APL1C to form a complex. This interaction with the LRR heterodimer is necessary to maintain a functional thioester bond that can covalently attach to the parasite surface[119]. In the absence of APL1C or LRIM1, TEP1 is unable to specifically bind to the parasite surface, and deposits apparently non-specifically on self-tissues, the thioester bond being hydrolysed over time, resulting in non-functional precipitation of TEP1[109,110]. TEP1 was demonstrated to bind to different pathogens, including Gram-positive and Gram-negative bacteria and *P. berghei* ookinetes in mosquito midguts[115], mediating their killing[120]. Like the APL1 gene family, TEP1 genes are highly polymorphic in *A. gambiae* genome with distinct alleles correlating with susceptibility or resistance to *Plasmodium*[115,121]. Variation of resistance and susceptible alleles are associated with variable loops within the thioester domain[119].

Besides the interaction with TEP1, the APL1C-LRIM1 heterocomplex can also interact with other TEP family members, such as TEP3 and TEP4, indicating that LRIM members can form multiple distinct immune complexes[111]. Functional analysis *A. coluzzii* detected a protective phenotype of TEP4 for *P. falciparum* but not rodent malaria species, whereas TEP3 displayed the inverse protective phenotype[104]. This protective specificity mirrors the distinct antagonistic activity observed for APL1A and APL1C proteins against *P. falciparum* and *P. berghei*, respectively.

2.3 Scope of the thesis

The phenotype of APL1 function in the anti-*Plasmodium* response has been described, but the molecular mechanism of activity is not known. The only structural mechanistic information is related to their ability to form, in the case of APL1C, a heterodimer with another LRR, LRIM1, which stabilizes the active $TEP1_{cut}$ protein. In addition, unlike LRIM1, which dimerizes with all three APL1 genes, APL1A and APL1C display a discriminating protective phenotype against human and rodent malaria parasites species, respectively. Consistently, a recent study revealed specificity in complement-like pathway activation towards Gram-negative bacteria through protease cleavage of the APL1C C-terminus in the LRIM1/APL1C complex[122]. Thus, LRIM1 which has the capacity to bind to the three APL1 genes, might constitute a common structural scaffold where activities directed towards distinct pathogens may be determined by the APL1 partner. Therefore, I postulate the following hypotheses:

1. APL1C might act as a pathogen specificity component in its heterocomplex with the common scaffold component LRIM1, which would explain how the complement-like effector activity of the otherwise nonspecifically-binding TEP1 protein is brought into proximity with the target pathogen surface.
2. Because APL1C is secreted into the hemolymph, APL1C could also display functional activity against free sporozoites in the hemocoel to limit *Plasmodium* invasion of the salivary glands and thus transmission.
3. APL1 proteins, similar to other LRR proteins, may act in signal transduction to initiate immune signalling cascades, and if so, the architecture of the pathways may be reflected at least in part by transcriptional regulation of target genes.

To examine these assumptions, I used as a study model the rodent malaria *P. berghei* and *A. coluzzii* mosquitoes, and thus focused on APL1C as a model system for the APL1 immune gene family.

872

873 # III. RESULTS

3.1 APL1C protein is a pathogen binding factor for the midgut ookinete stage of *Plasmodium*

3.1.1 Blood feeding induces an extracellular layer of APL1C surrounding the midgut

The active, cleaved TEP1 form is bound in the hemolymph by the heterodimer LRIM1/APL1C to form a complex to allow specific deposition on the surface of the ookinetes exiting the mosquito midgut[115,109]. However, while TEP1 was detected on midgut ookinetes, the localisation of the LRR partners during this process is not known. Therefore, I detected APL1C on mosquito midguts after a *P. berghei*-infected bloodmeal (IBM) 24 h post-feeding by immunofluorescence assay (IFA) on permeabilized midguts, using a polyclonal anti-APL1C antibody (pAb)[102]. Non-infected bloodmeal (NBM) and unfed (UF) midguts served as the controls (for the experimental design see Annex **Figure S1**). IFA followed by confocal microscopy analysis showed that while no APL1C signal was detected on UF midguts, a layer of APL1C protein surrounding the midgut epithelial cells was detected on both NBM and IBM midguts (**Figure 7A**). Quantitative and comparative analysis of the APL1C protein signal intensity between IBM, NBM and UF mosquito midguts confirmed significant statistical difference either between UF and NBM ($p<0.0001$), or between UF and IBM ($p<0.0001$) (**Figure 7B**). The comparison between IBM and NBM midguts was not statistically different (Annex, **Table S1**). I queried the exact APL1C positioning through reconstructed optical sections of confocal stack midgut images (**Figure 7C**, projected

as orthogonal views on the right side and below the stack picture). This analysis revealed that APL1C protein was localised on the basal side of the midguts tissue.

The simplest interpretation is that the observed IFA midgut presence of APL1C is a proxy for the concentration of systemic APL1C in the mosquito hemolymph, which diffuses through the porous basal lamina[123]. This conclusion is strengthened by the similar localisation pattern detected using a diffusible dextran the size of APL1C (**Figure S2**). I cannot eliminate the possibility that the midgut extracellular APL1C detected after a bloodmeal could be specifically targeted to the midgut, although there is no known mechanism that would explain this. Thus, I conclude that mosquito blood feeding causes elevated levels of APL1C protein within the hemolymph, which can be conveniently measured using dissected midguts as a proxy assay that is simpler than perfusion of hemolymph from individual mosquitoes. The APL1C in the extracellular space surrounding the midgut epithelium could serve as part of an initial immune sentinel barrier.

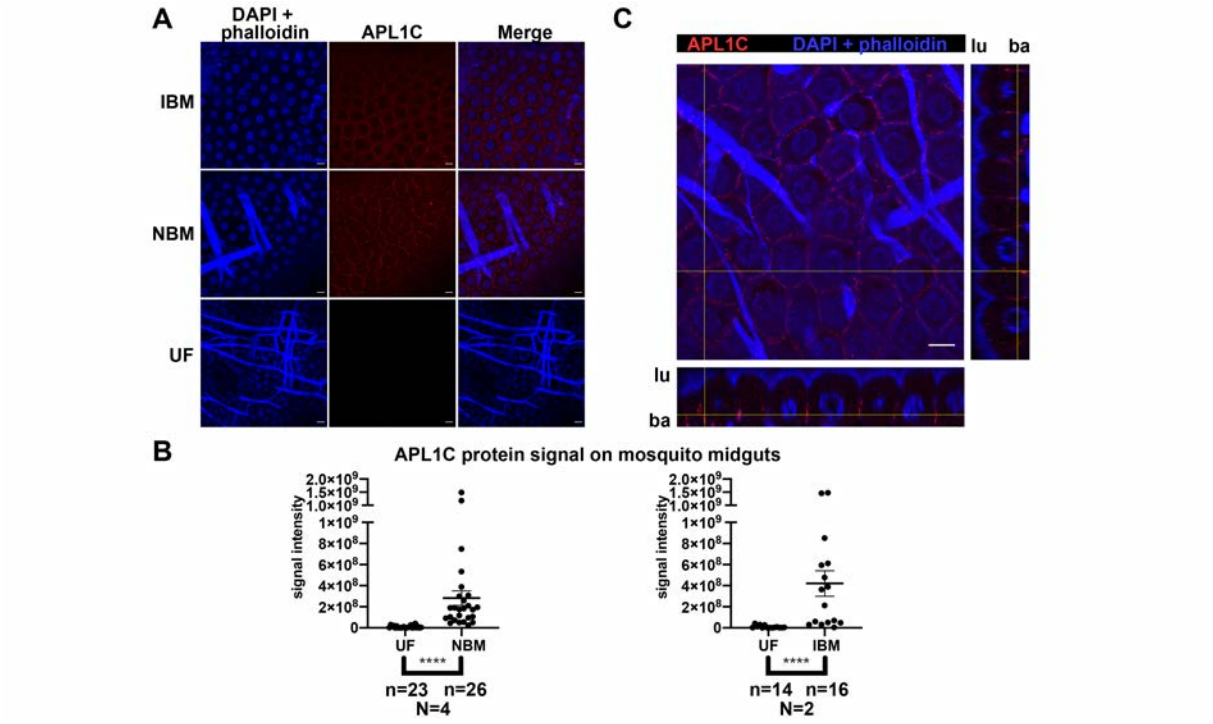

913

914 **Figure 7. Blood feeding induces the presence of APL1C protein on the basal side of the**
915 **mosquito midgut. A.** Immunostaining analysis of the midguts from mosquitoes subjected to
916 *P. berghei*-infected bloodmeal (IBM), normal bloodmeal (NBM) and unfed control (UF).
917 Depicted pictures are representative for at least two replicates in each group. For the in vivo
918 system, all immunostaining analysis were performed with an anti-APL1C pAb followed by
919 fluorophore-conjugated IgG secondary antibody (red). Nuclei and actin were stained with DAPI
920 and Phalloidin (blue). The scale bar is 10 µm. **B.** Quantitative analysis of the APL1C signal
921 between IBM, NBM and UF midguts reveals increase of APL1C protein on the midguts after
922 IBM and NBM. Graph labels and statistical tests for this figure: tests of APL1C protein signal
923 intensity on the midgut indicate each midgut subjected for the analysis as a dot, bars represent
924 mean with ±SEM. Sample sizes (N) show the number of independent replicate experiments,
925 (n) the total number of midguts dissected across replicates. Data were analysed by measuring
926 APL1C signal intensity (RawIntDen) using ImageJ v1.52p and the intensity from each midgut
927 was compared between the two conditions by Mann-Whitney test. All statistical differences
928 were first tested independently within replicates (individual p-values in Annex, **Table S1**), and
929 if individual replicates showed a common trend of change, individual p-values were combined
930 using the meta-analytical approach of Fisher (significance level of Fisher-combined p-value:
931 **** p-value <0.0001). **C.** The XZ and YZ orthogonal views of the NBM stack picture show
932 APL1C protein localising extracellularly, on the basal side (ba) of the midguts. No APL1C
933 signal was found on midgut lumen (lu). The scale bar is 10 µm.

934

935 The specificity of the anti-APL1C pAb was confirmed on midguts collected from
936 mosquitoes depleted for APL1C gene expression by RNAi-mediated gene silencing.
937 *A. coluzzii* mosquitoes were injected with double-stranded RNA of APL1C gene

(dsAPL1C) or dsGFP (for control group) and blood fed 72 h post-treatment. APL1C gene expression was efficiently silenced at 72 h post dsAPL1C treatment as compared to dsGFP-injected controls, measured by quantitative polymerase chain reaction (qPCR, **Figure 8A**). IFA analysis of the midguts 24 h after NBM revealed APL1C protein signal in dsGFP controls and no signal in APL1C-silenced midguts (**Figure 8B**). Hence, the IFA signal observed on the mosquito midgut samples is specific for presence of the APL1C protein.

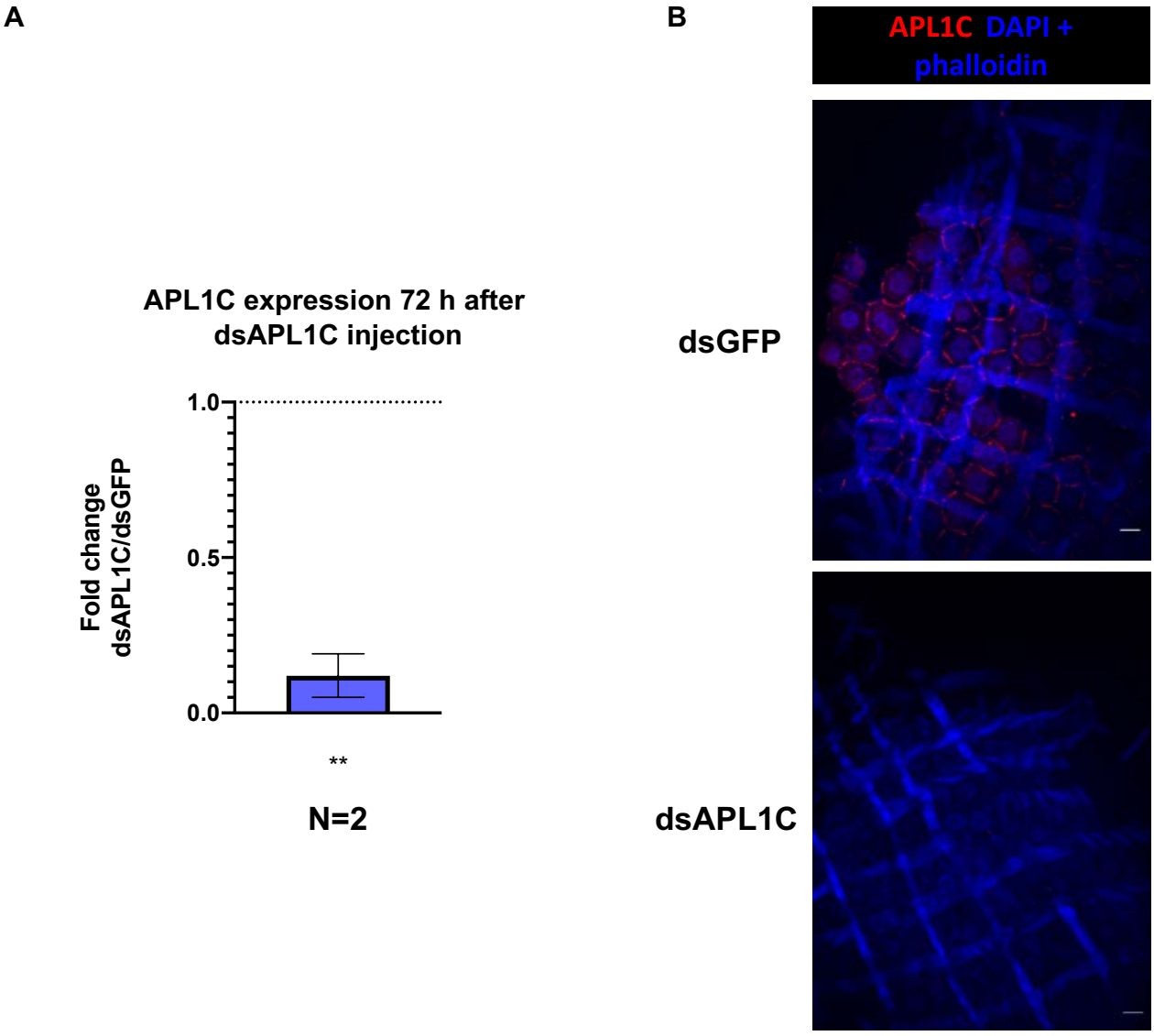

Figure 8. Anti-APL1C pAb labelling is specific to the APL1C protein. A. APL1C silencing was verified by qPCR measurement between dsAPL1C and dsGFP (dotted line) 72 h post-treatment (corresponding to expression status at the time of the NBM). The ratio of the

normalized APL1C cDNA detection in “dsAPL1C” versus “dsGFP” treatments was computed using triplicates from the same cDNA dilution. Graph represents mean with ±SEM of the expression fold change between “dsAPL1C” and “dsGFP” control from two biological replicates (N=2). Data for qPCR analysis was analysed by unpaired t-test (significance level of t-test p-value: ** p-value <0.01). **B.** Immunostaining analysis of NBM mosquito midgut after APL1C gene silencing reveals no APL1C signal on APL1C-silenced midguts. APL1C protein images are from midguts of dsGFP-injected control mosquitoes. The scale bar is 10 µm.

3.1.2 APL1C presence on the basal side of the midgut epithelium is microbiome independent

I showed that NBM is sufficient to cause presence of the APL1C protein on *A. coluzzii* midguts. Since mosquito blood feeding induces expansion of the bacterial flora[39], I queried the role of the microbiome as a potential signal promoting elevated APL1C abundance on the midgut epithelium. Prior to a bloodmeal, two groups of mosquitoes were treated or not with a wide-spectrum antibiotic (ATB) cocktail. The ATB efficiency on the microbiome was confirmed by qPCR measuring bacterial ribosomal DNA (rDNA 16S) (**Figure 9A**). After the bloodmeal, IFA analysis showed that APL1C presence was still elevated on the midguts in the +ATB midguts group, and with an intensity similar to that of -ATB control group (**Figure 9B**), indicating the bacteria microbiome expansion post-NBM does not influence APL1C abundance detected on the midgut.

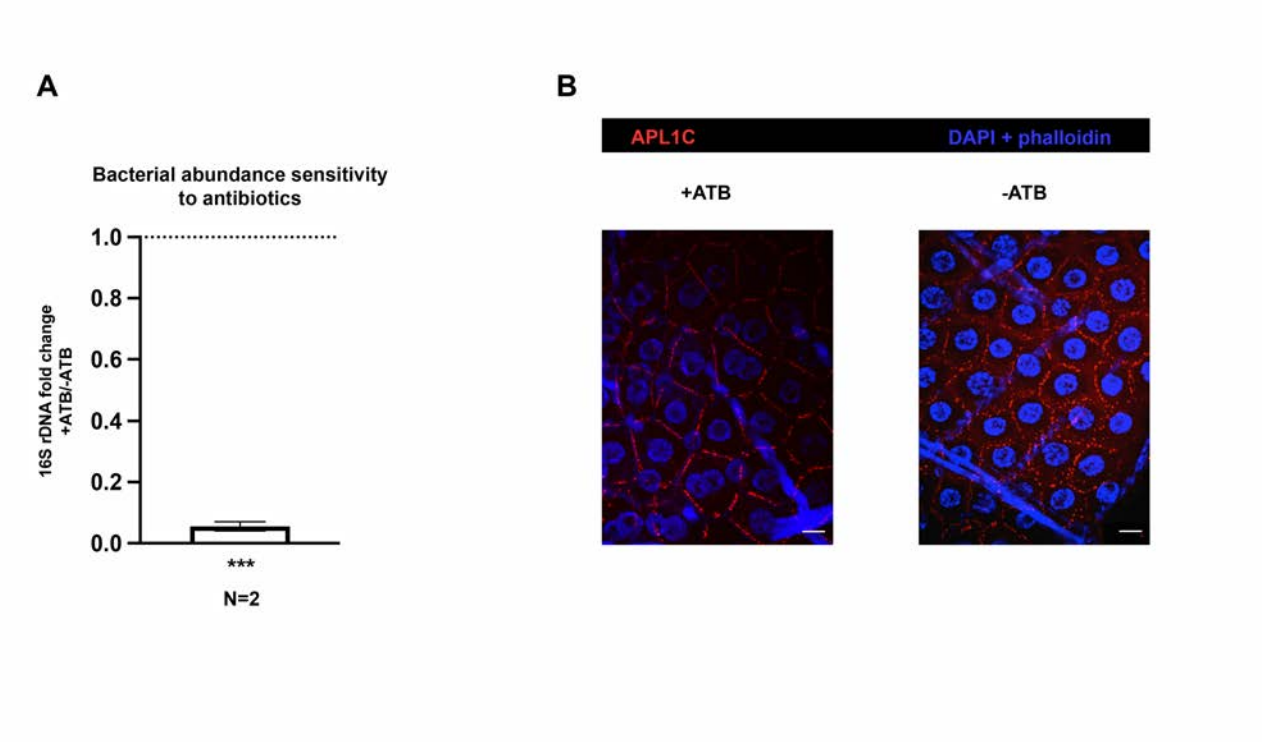

Figure 9. The mosquito microbiome does not influence APL1C protein abundance on the midgut 24 h after NBM. A. Bacterial abundance was significantly reduced after antibiotic treatment. Antibiotic efficiency on bacterial abundance was confirmed by qPCR detection of 16S rDNA in controls (-ATB, dotted line indicates y=1.0) and ATB-treated (+ATB), 24h post NBM. The ratio of the normalized 16S rDNA detection in "+ATB" versus "-ATB" treatments was computed using triplicates from the same cDNA dilution. Graph represents mean with ±SEM of the expression fold change between "+ATB" and "-ATB" control from two biological replicates (N=2). Bacterial qPCR data were analysed by unpaired t-test using (*** p-value <0.001). **B.** Immunostaining analysis of the +ATB midguts group shows that bacterial depletion did not diminish APL1C abundance on NBM midguts. Images are representative of two independent biological replicates of 3–7 midguts each. The scale bar is 10 µm.

3.1.3 APL1C binds to *Plasmodium* ookinetes exiting the basal side of the midgut epithelium

Elevated hemolymph APL1C levels are induced by NBM, and are also present in the hemolymph within the midgut extracellular space delimited by the basal lamina. Therefore, I assessed whether APL1C binds to *Plasmodium* ookinetes. IFA analysis on midguts collected 24 h post-IBM displayed APL1C signal on some parasites, but the majority of parasites were negative for APL1C (**Figure 10 A** and **B** "Merge"

column). Overall, 18% of live (GFP) ookinetes present in the infected midguts were positive for APL1C (**Figure 10C).** In addition, APL1C occasionally labelled structures previously reported as stalk-form ookinetes[124], but these structures were negative for GFP (**Figure 10C**). It suggests that these GFP-negative forms were probably undergoing lysis, and GFP protein leaked from dead parasites. This is consistent with the description of mosquito complement leading to parasite lysis and previous observations, in which parasite ookinetes labelled by TEP1 at 24 h post-infection were found both, live (GFP-positive) and dead (GFP-negative)[115 125].

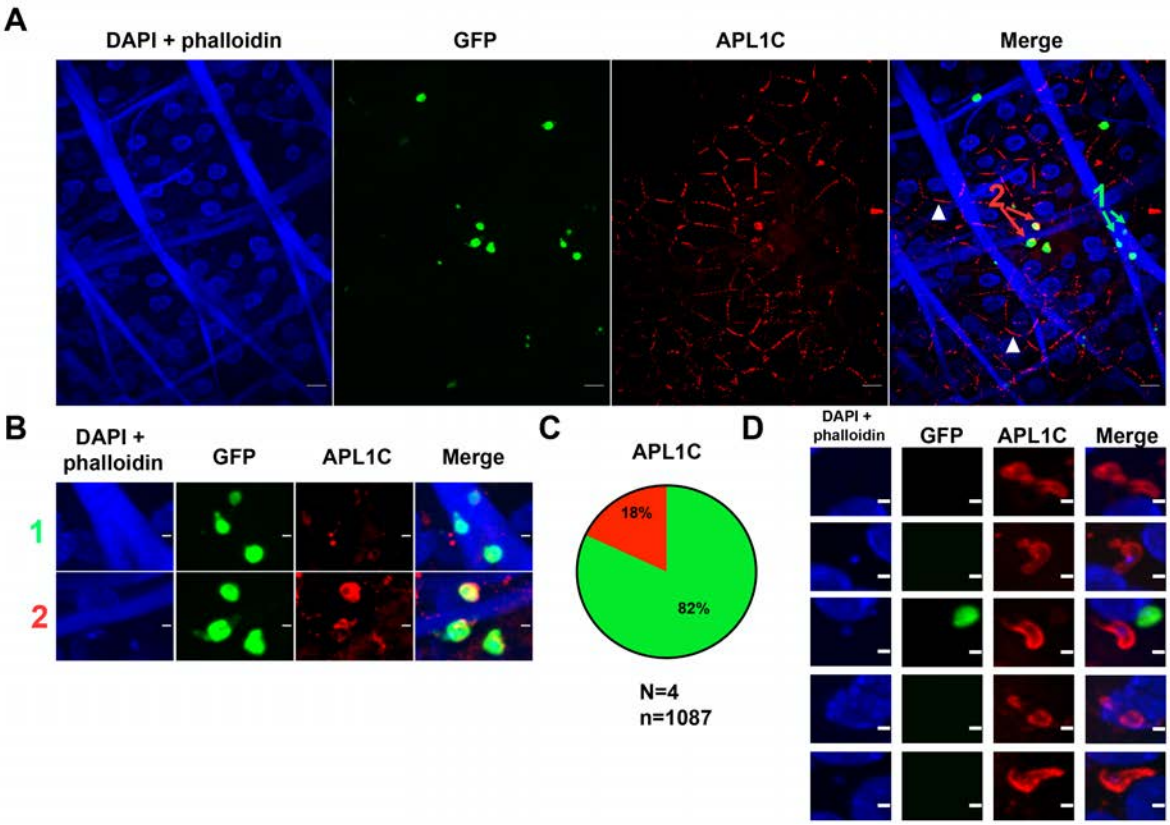

Figure 10. APL1C binds to ookinetes in *A. coluzzii* midguts. A. Immunostaining analysis of IBM mosquito midguts 24h post-infection shows GFP-expressing ookinetes (green) associated with APL1C protein (red arrows on the "Merge" picture) and APL1C-negative parasites (green arrow on the "Merge" picture). Scale bar is 10 µm. **B.** Enlarged projections of APL1C-negative parasites (1) and APL1C-positive parasites (2) from (A). The scale bar is 2 µm. **C.** Depending on APL1C binding, GFP-positive parasite numbers (n=1087 number of the parasites scored across the replicates) were scored and are shown in the pie chart (red: APL1C-positive parasites, green: APL1C-negative parasites) as the mean percentage obtained from four independent experiments (N=4, 4 to 7 midguts per each replicate). **D.** APL1C labelling localises with dead ookinetes in mosquito midgut. Immunostaining analysis

of mosquito midgut infected with GFP-expressing parasites (green) at 24 h post-infection. The APL1C staining reveals APL1C protein signal (red) with a shape related to ookinete structure but where GFP signal from the parasite is lacking, probably due to parasite lysis. Note nucleus staining in the DAPI + phalloidin channel. The scale bar is 2 µm.

Ookinete traversal through the midgut epithelium is a dynamic process, and 24 h after IBM the majority of parasites are still found in the blood bolus, while some are intracellular and only a minority have exited from epithelial cells[126]. Despite permeabilization of the midgut tissues during the IFA analysis, only 18% of GFP-positive parasites were APL1C-labeled. An additional control was performed using anti-GFP antibody which labelled 93% of parasites in the midguts, confirming efficient permeabilization and antibody access within the tissue (Annex, **Figure S3**). Therefore, I determined the localization (apical and/or basal) of APL1C-labelled parasites on the midgut epithelium. Reconstructed optical sections of the confocal stack images revealed that APL1C-labeled parasites were strictly located at the basal side of the midgut epithelium (**Figure 11A**). In contrast, the ookinetes that were crossing or that remained on the apical side of the midgut epithelium lumen were not labelled with APL1C (**Figure 11B**). This result is consistent with the 18% APL1C-labeled parasites, as it was reported that between 24 and 25 h post-infection, around 15% of them reach the basal lamina[126].

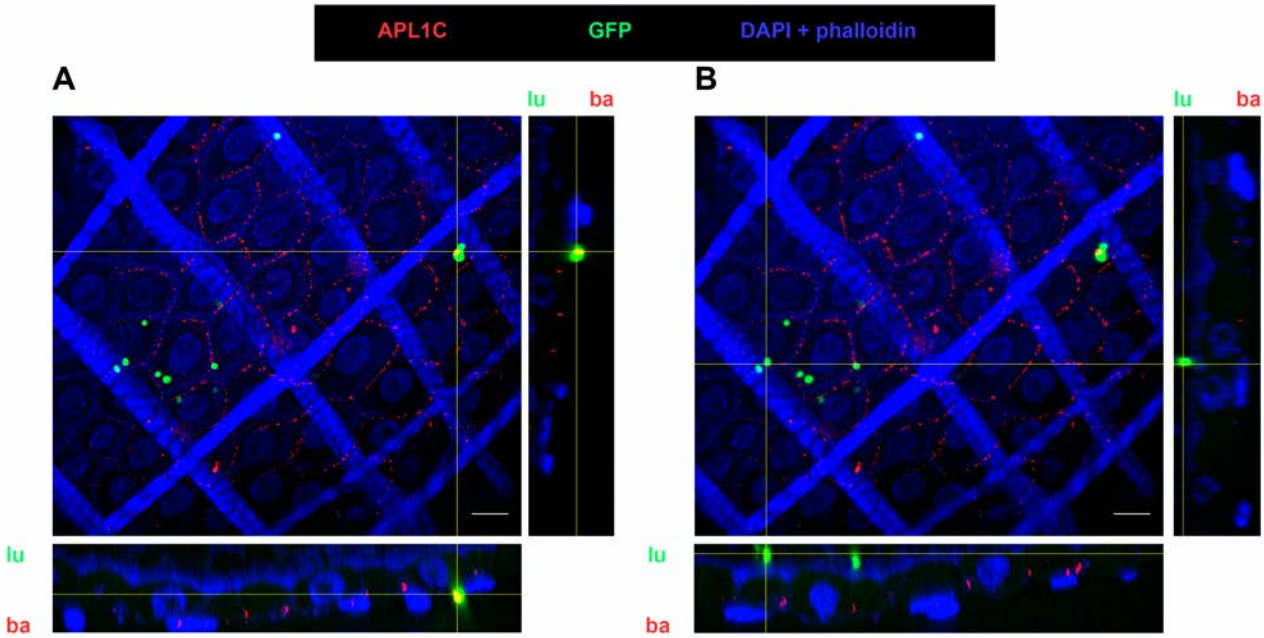

Figure 11. APL1C binds to the ookinetes located on the basal side of the midgut. XZ and YZ orthogonal views of the stack pictures links APL1C protein binding with parasite spatial localisation in mosquito midguts. Yellow lines depict the parasite, which spatial localisation is presented on the sides of the stack picture. **A**. Illustration of a parasite traversing the midgut epithelium that is labelled with APL1C on the basal side of the mosquito midgut. **B.** The parasites that did not traverse the midgut epithelium and remained on the apical side of the mosquito midgut are not labelled with APL1C. The midgut lumen (*lu*) and basal site *(ba)* of the midgut are depicted on the orthogonal view pictures. The scale bar is 10 µm.

3.1.4 LRR proteins bind autonomously to the ookinete surface (coll.: C. Lavazec, Institut Cochin, Paris)

As APL1C has been shown to act in a heterodimeric complex with LRIM1[109], we wished to determine whether LRIM1 could also be detected on the ookinete surface. We developed a powerful *ex vivo* model of mosquito hemocoel immunity using the 4a3A hemocyte-like cell line. Cells were transfected to express, either separately or

simultaneously, V5-tagged LRIM1 (V5-LRIM1) or V5-APL1C (used as positive control for the binding). After verifying that both V5-APL1C and V5-LRIM1 protein constructs were secreted at day 3 post transfection from hemocyte-transfected cells in the medium (Annex, **Figure S4**) we investigated their labelling on fluorescent-GFP parasites. To validate the *ex vivo* system, we phenocopied APL1C binding to the parasites on the midgut epithelium observed *in vivo*. Transfected cells were exposed to *A. coluzzii* midguts infected with *P. berghei* (24 h post-IBM) and we found that V5-APL1C as well as V5-LRIM1 were co-localized with parasites (**Figure 12A**). The V5-RFP-transfected proteins, used as negative control, displayed no labelling on the GFP parasites (**Figure 12A**), although as expected it was secreted into the medium (Annex, **Figure S4**). In addition to validation of the *in vivo* system, these results indicated that as for APL1C, the subunit partner LRIM1 also binds to the parasite, and in similar proportions for V5-APL1C or V5-LRIM1-labelled parasites (12% and 10% respectively) (**Figure 12B**). Interestingly, the proportion of labelled parasites did not increase in cells co-transfected with both tagged-LRRs (11%) as compared to the single transfected treatments (**Figure 12B**). This observation is consistent with but does not prove that labelled parasites are bound with LRIM1/APL1C heterodimers.

To distinguish extracellular ookinetes from those that were still within the lumen or epithelial cells, we immunostained non-permeabilized infected midguts using *P. berghei*-specific Pbs28 antibody. Only 18% of the GFP ookinetes were labelled with the Pbs28 antibody (**Figure 12B**), indicating those that reached the basal side of the midgut at 24 h post-IBM.

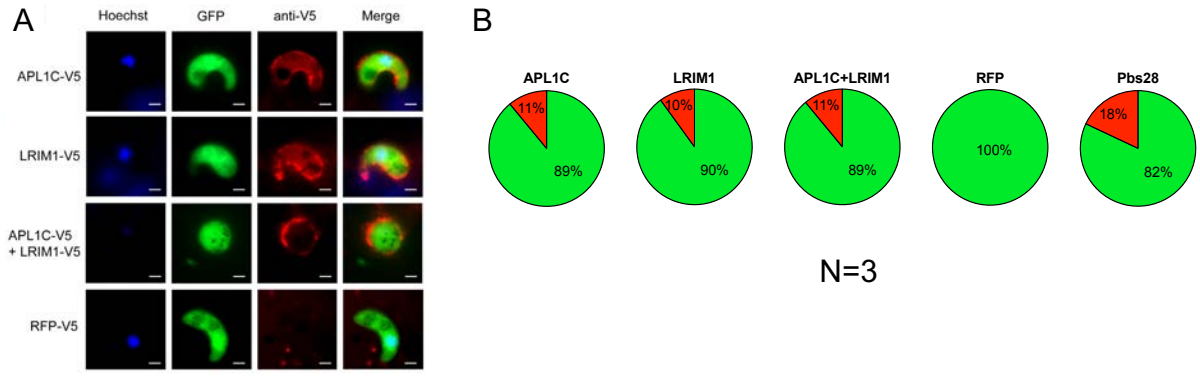

Figure 12. APL1C and LRIM1 both bind to *P. berghei*. **A.** Immunostaining analysis of mosquito midguts infected with GFP parasites (green) after 2 h incubation in culture medium from transfected 4a3A cells. Staining with an anti-V5 monoclonal antibody (mAb) followed by fluorophore-conjugated IgG shows parasites associated with V5-APL1C and V5-LRIM1 tagged proteins (red). Nuclei were stained with Hoechst 33342 (blue). The scale bar is 2 µm. **B.** V5-positive parasites and V5-negative parasites after staining with anti-V5 antibodies in each condition were scored and illustrated in pie charts (red: V5-positive parasites, green: V5-negative parasites) as the mean percentage obtained from three independent experiments (N=3, 3–10 midguts per experimental point). The proportion of parasites reaching the basal side of the midgut epithelium at 24 h post-infection was scored using the anti-Pbs28 antibody (red: Pbs28-positive parasites, green: Pbs28-negative parasites). *Data from collaboration: C. Lavazec, Institut Cochin, Paris.*

We then tested whether APL1C and LRIM1 parasite binding is dependent on the presence of TEP1 protein. Cells were transfected to express V5-tagged APL1C and/or V5-tagged LRIM1 as above, but with TEP1 gene expression silenced (dsTEP1 or dsGFP as control). Depletion of TEP1 protein was confirmed by Western blot using an anti-TEP1 antibody (**Figure 13A**). *A. coluzzii* midguts collected 24 h post-infection were incubated in medium from transfected cells. Depletion of TEP1 did not alter the proportion of V5-LRR-labelled parasites as compared to the dsGFP controls, whether APL1C and LRIM1 were expressed individually or simultaneously (**Figure 13B**). These results indicate that while TEP1 requires at least APL1C or LRIM1 for specific parasite binding, the reciprocal is not true, suggesting that TEP1 binding on the parasite must occur indirectly and secondarily, mediated by LRR binding to the parasite surface.

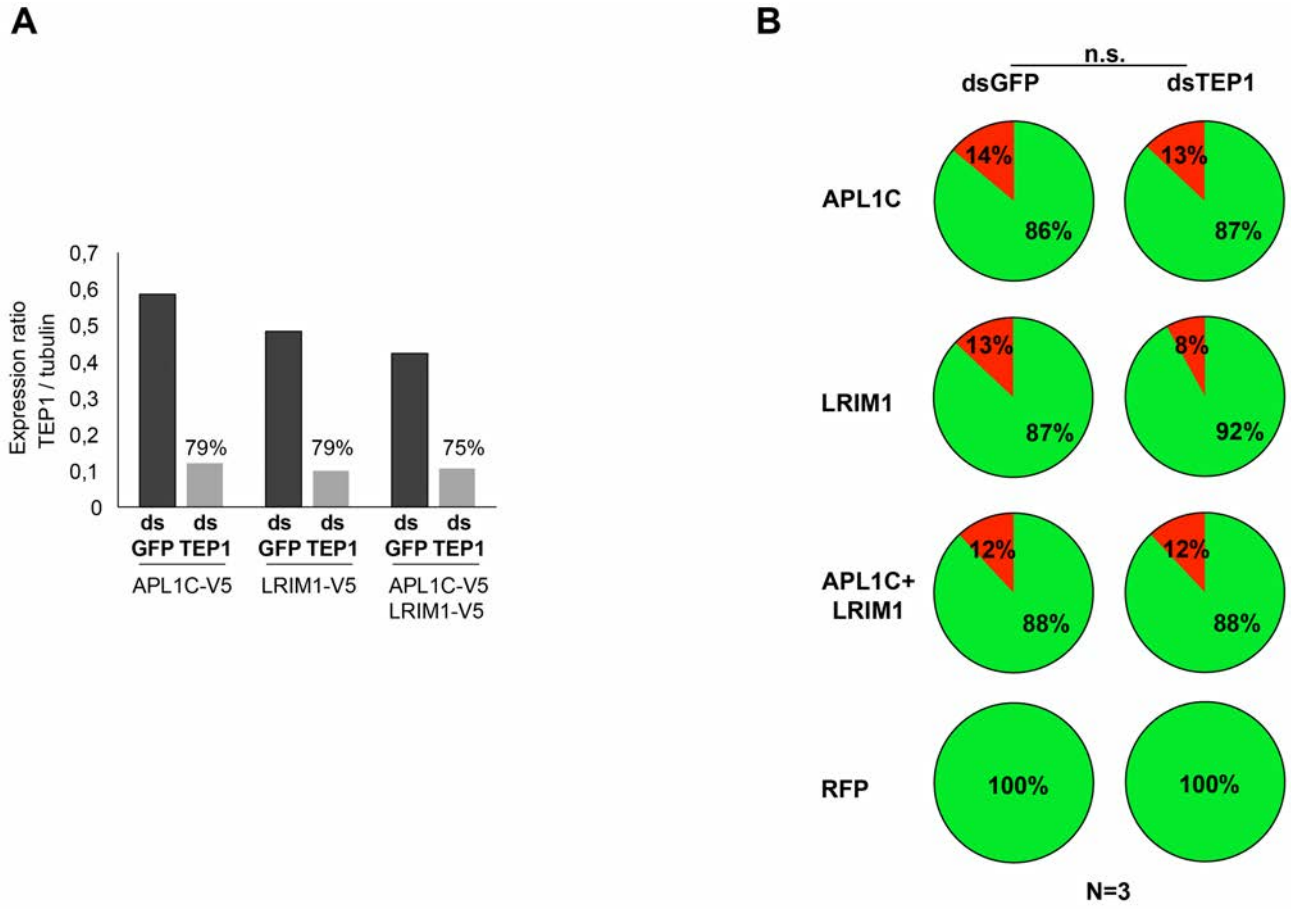

Figure 13. APL1C and LRIM1 both bind to *P. berghei* ookinetes independently of TEP1 presence.

A. TEP1 protein is successfully depleted by dsTEP1 in 4a3A cells. Expression ratios of protein levels TEP1/tubulin were quantified by densitometry. The efficiency of the gene silencing effect was monitored at day 6 by immunoblotting analysis of cells and culture medium of the 4a3A cell line using an anti-TEP1 antibody and an anti-tubulin antibody. For each condition, the ratio of protein levels TEP1/tubulin was calculated and the percentage of TEP1 signal reduction relative to tubulin was quantified in dsTEP1-transfected cells as compared to dsGFP transfected cells. **B.** APL1C and LRIM1 binding to the parasites are TEP1 independent. Proportions of parasites associated with V5-tagged proteins in cells depleted for TEP1, after staining with anti-V5 antibodies. Parasite numbers in each condition were scored and are shown in the pie chart (red: V5-positive parasites, green: V5-negative parasites) as the mean percentage obtained from three independent experiments (3–10 midguts per experimental point). DsGFP transfected cells were used as a control. Numbers of V5-positive and V5-negative parasites from each replicate were compared between the two conditions by chi-square test (significance level of chi-square: n.s.=not significant). *Data from collaboration: C. Lavazec, Institut Cochin, Paris.*

3.1.5 Phagocytic hemocytes are required for wildtype APL1C levels in the hemolymph

Recent results demonstrated the specific contribution of the phagocytic hemocyte cells for the binding of invading ookinetes by the mosquito complement system[127]. Therefore, I investigated the contribution of the phagocytic cells for APL1C protein abundance in the hemolymph, measured as above using IFA to detect APL1C levels present on dissected midguts. Phagocytic cells were chemically depleted by injecting liposome-encapsulated clodronate (CLD) as described[127] prior to an IBM, with empty liposomes (LP) as a control. The liposome capsule prevents systemic toxicity of CLD to the mosquito, while phagocytosis of the encapsulated CLD and subsequent release of CLD specifically leads to the death of the phagocytic hemocytes. The efficiency of phagocyte depletion was measured by quantifying the expression of two phagocyte markers 24 h post treatment, eater and nimrodB2, in pools of eight whole mosquitoes. Expression of these two markers was significantly reduced by CLD treatment as compared to LP controls (**Figure 14A**).

Depletion of phagocytic hemocytes by CLD treatment decreased APL1C gene expression (**Figure 14B**). Depletion of phagocytic hemocytes by CLD treatment also reduced the abundance of APL1C protein in the hemolymph, as measured by IFA signal intensity on dissected midguts from CLD and LP treated mosquitoes at 24 h post-IBM ($p<0.01$ **Figure 14B** and Annex **Table S1**). These results indicate that phagocytic hemocytes are required both for APL1C gene expression as well as normal APL1C protein levels in the mosquito hemolymph.

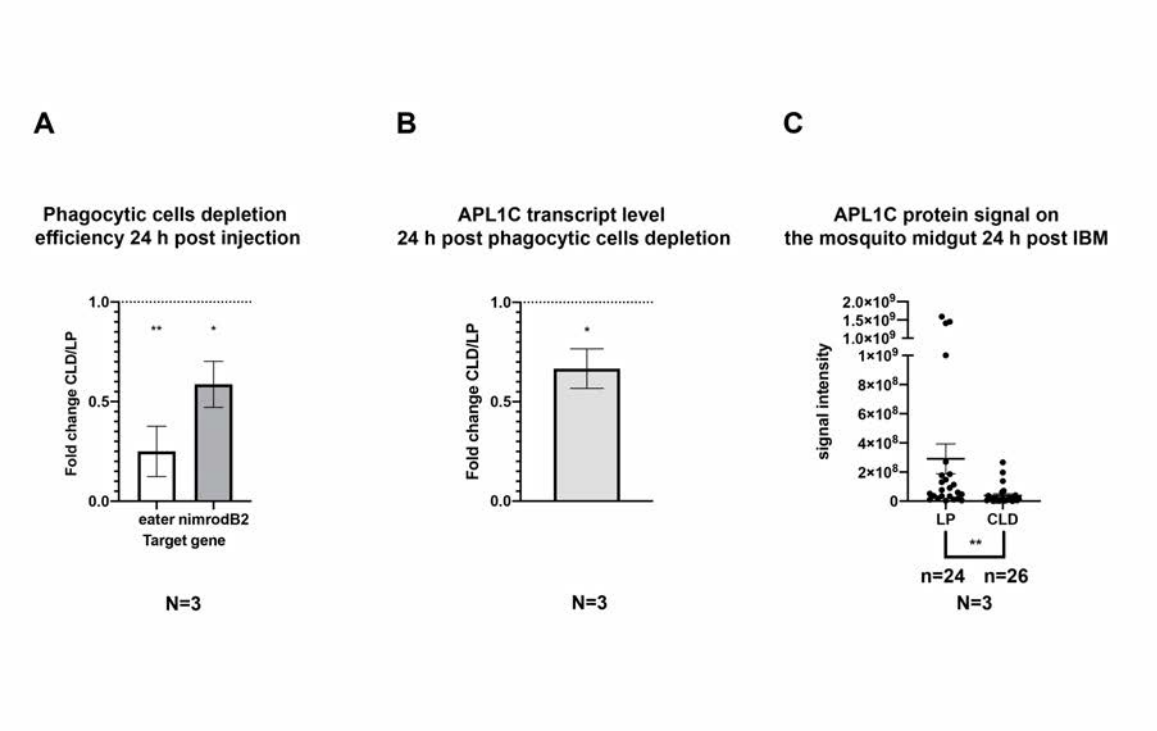

Figure 14. Full APL1C gene expression and protein abundance in the hemolymph requires phagocytic hemocytes. **A.** Phagocytic hemocytes were depleted by clodronate treatment (CLD). CLD-mediated phagocyte depletion was verified by qPCR measurement of phagocyte markers, eater and nimrodB2 between CLD-treated mosquitoes and liposome controls (LP, indicated as dotted line), 24 h post-treatment prior to IBM. The ratios of normalized eater, nimrodB2 transcript detection were computed using triplicates from the same cDNA dilution, and graph represents mean with ±SEM of the expression fold change from three biological replicates (N=3). qPCR was analysed by unpaired t-test (* p-value<0.05; ** p-value<0.01). **B.** APL1C expression was reduced in CLD-treated mosquitoes. Analysis of APL1C expression was performed as described in **A. C.** Hemolymph APL1C protein abundance measured as IFA signal intensity on midguts dissected from mosquitoes treated with CLD prior to IBM. Data points on graph indicate single midguts, bars indicate mean with ±SEM. The number of independent replicate experiments (N) the total number of midguts dissected across replicates (n) are indicated. Data were analysed by measuring APL1C signal intensity (RawIntDen) using ImageJ v1.52p and the intensity from each midgut was compared between the two conditions by Mann-Whitney test. All statistical differences were first tested independently within replicates (individual p-values in Annex **Table S1**), and if individual replicates showed a common trend of change, individual p-values were combined using the meta-analytical approach of Fisher (significance level of Fisher-combined p-value: ** p-value <0.01).

3.1.6 Nitration pathway activity is required for full APL1C abundance in hemolymph

The release of microvesicles by mosquito hemocytes appears to be correlated with the deposition of TEP1 upon the ookinete surface, because depletion of the nitration pathway simultaneously abolished release of hemocyte-derived microvesicles (HdMv) and impaired TEP1 binding to the parasites [128]. This observation led to the hypothesis that factors delivered by HdMv may promote TEP1 binding to ookinetes, although the contents of the HdMv are unknown. APL1C is expressed in hemocytes and its presence is required for TEP1 binding to parasites. Therefore, I evaluated whether APL1C could be a component of the HdMv payload to deliver APL1C into the hemolymph and ultimately to the midgut surface.

First, APL1C subcellular localization was determined by IFA with APL1C antibody on perfused hemocytes and on 4a3A hemocyte-like cells, revealing that APL1C protein is found in vesicle-like structures in perfused hemocytes (**Figure 15A**). This observation is consistent with our previous report of localization of APL1 family gene APL1A within hemocyte vesicles[106] and with the hypothesis that APL1C may be secreted from hemocytes in microvesicles. Next, the nitration pathway was inactivated by co-silencing the genes for heme peroxidase (HPX2) and NADPH oxidase 5 (NOX5), with the aim to inhibit the release of HdMv. Mosquitoes were treated with dsNOX5/HPX2 or control dsGFP prior to an IBM, and the efficiency of HPX2 and NOX5 depletion was confirmed by RT-qPCR. (**Figure 15B**).

Midguts from each group were collected 24 h after *Plasmodium* infection and APL1C abundance on the midgut was quantified using IFA with APL1C antibody. Midguts from mosquitoes depleted for NOX5/HPX2 displayed decreased APL1C abundance as compared to dsGFP treated controls ($p<0.0001$) (**Figure 15C** and Annex **Table S1**). Western blot analysis of extract from whole mosquitoes confirmed that the observed phenotype did not result from APL1C protein decrease after inhibition of the nitration

pathway, and in fact APL1C protein was slightly increased in silenced mosquitoes as compared to dsGFP controls (**Figure 15D**), which could be explained if APL1C protein is retained in non-released HdMv. Overall, these results indicate that an active nitration pathway is necessary for wild-type levels and localization of free APL1C in the hemolymph, as measured by APL1C abundance captured on the midgut.

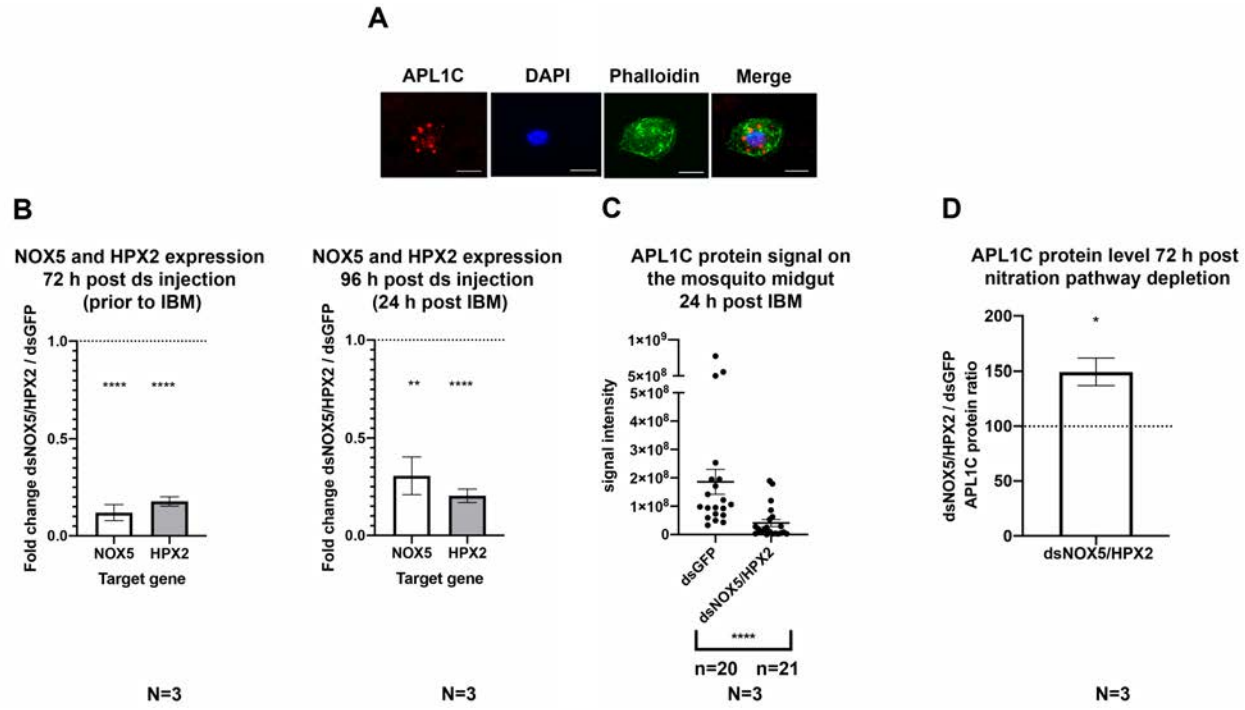

Figure 15. Nitration pathway activity mediates APL1C protein presence in mosquito hemolymph. A. Immunostaining analysis of perfused hemocytes from mosquitoes indicates that APL1C is localized in subcellular vesicles (red). Cells were stained with Hoechst 33342 to label nuclei (blue) and phalloidin for actin (green). Scale bar, 5 µm. *Data from collaboration: C. Lavazec, Institut Cochin, Paris.* **B.** Expression of NOX5 and HPX2 genes is decreased after treatment with dsNOX5/HPX2. NOX5 and HPX2 silencing was verified by qPCR measurement between dsNOX5/HPX2 and dsGFP (dotted line) 72 h post-treatment (before IBM). The ratio of normalized NOX5 or HPX2 cDNA detection in "dsNOX5/HPX2" versus "dsGFP" was computed using triplicates from the same cDNA dilution. Graph represents mean with ±SEM of the expression fold change between "dsNOX5/HPX2" and "dsGFP" control from three biological replicates (N=3). Data for qPCR analysis was analysed by unpaired t-test (significance levels of t-test p-values: ** p-value <0.01; **** p-value <0.0001). **B.** NOX5 and HPX2 silencing was verified accordingly to **(A)** 96 h post treatment (24 h after IBM). **C.** Nitration pathway elicits APL1C presence in the hemolymph, measured by detection of protein captured in the extracellular space of dissected midguts. Quantitative analysis of the APL1C signal on the midguts from the mosquitoes in which the nitration pathway was depleted as compared to controls reveals decreased APL1C protein in mosquitoes depleted for nitration activity. Graph labels and statistical tests for this figure: tests of APL1C protein signal intensity on the midgut

indicate each midgut subjected for the analysis as a dot, bars represent mean with ±SEM. Sample sizes (N) show the number of independent replicate experiments, (n) the total number of midguts dissected across replicates. Data were analysed by measuring APL1C signal intensity (RawIntDen) using ImageJ v1.52p and the intensity from each midgut was compared between the two conditions by Mann-Whitney test. All statistical differences were first tested independently within replicates (individual p-values in Annex **Table S1**), and if individual replicates showed a common trend of change, individual p-values were combined using the meta-analytical approach of Fisher (significance level of Fisher-combined p-value: **** p-value <0.0001). **D.** The APL1C protein level in whole mosquitoes increases upon nitration pathway depletion. Immunoblot analysis of APL1C protein level 72 h after dsNOX5/HPX2 treatment. Protein extracts from mosquitoes injected with dsNOX5/HPX2 and dsGFP (control) were subjected to a Western blot with an anti-APL1C pAb and anti-GAPDH antibody as a loading control. The normalized APL1C signal density was compared between “dsNOX5/HPX2” and “dsGFP” mosquitoes (dotted line). Graph represents mean with ±SEM of the protein ratio between “dsNOX5/HPX2” and “dsGFP” from three biological replicates (N=3). Data were analysed by Image Lab 6.0.1 and statistically analysed by unpaired t-test (significance level of t-test * p-value<0.05).

3.2 APL1C protein is a pathogen binding factor for the hemocoel sporozoite stage of *Plasmodium*

3.2.1 Sporozoites affect APL1C protein abundance

Only a small proportion of the thousands of sporozoites released by each oocyst invade the salivary glands, while the majority of sporozoites are destroyed in the mosquito hemocoel by an unknown mechanism[46]. Phagocytosis of sporozoites by hemocytes was observed, but was numerically insufficient in itself to explain sporozoite clearance from the hemocoel. Thus, the mechanism of sporozoite destruction in the hemocoel remains unknown.

To examine the activity of APL1C against released sporozoites in the hemocoel, the abundance of APL1C protein was first measured by Western blot at four time points during *Plasmodium* development in the vector: young oocysts at 4 d post-bloodmeal, late oocysts before sporozoite release at 10 d post-bloodmeal, early sporozoite release

at 12 d post-bloodmeal, and late sporozoite release at 18 d post-bloodmeal. Unfed mosquitoes (UF) were used as controls. At 4 d post-bloodmeal, APL1C protein was increased in both IBM and NBM mosquitoes as compared to UF, but there was no difference between IBM and NBM, indicating that the early stage induction of APL1C protein was dependent only on the bloodmeal and not infection (**Figure 16**). At 10 d and 12 d post-bloodmeal, APL1C abundance in both IBM and NBM mosquitoes was equivalent to the UF controls, indicating that APL1C levels return to baseline after the effect of the bloodmeal decays. Notably, at 18 d post-bloodmeal during sporozoite release, APL1C protein abundance was significantly higher in IBM as compared to either NBM or UF mosquitoes, which were not different from each other (**Figure 16**). The APL1C increase at 18 d post-IBM indicates that APL1C induction at this time point was dependent only on the presence of circulating sporozoites. This result suggests that APL1C is a component of immune signalling responding to free sporozoites, and could help to limit salivary gland invasion and thus transmission of *Plasmodium*.

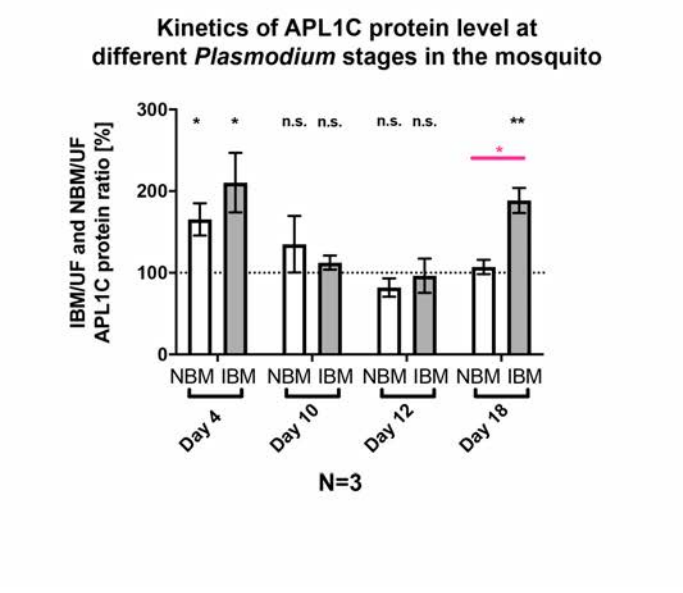

Figure 16. APL1C protein level is increased by blood feeding and sporozoite release in *A. coluzzii*. Immunoblot analysis of APL1C protein levels after IBM. Protein extract from whole mosquitoes collected at day 4 (early oocyst), day 10 (mature oocyst, before sporozoite release), day 12 (early sporozoite release) and day 18 (late sporozoite release) were probed with an anti-APL1C pAb and anti-GAPDH antibody as a loading control. NBM and UF samples

were used as controls for each time point. The normalized APL1C signal was compared between NBM or IBM mosquitoes versus UF mosquitoes (dotted line). APL1C protein level increases at day 4 after NBM or IBM and at day 18 after IBM as compared to controls. Graph represents mean with ±SEM of the protein ratio between “IBM” or “NBM” and “UF” control from three biological replicates (N=3). Data were analysed by Image Lab 6.0.1 and statistically analysed by unpaired t-test (significance levels of t-test p-values: n.s., not significant; * p-value<0.05; ** p-value <0.01).

3.2.2 APL1C activity in the hemocoel limits sporozoite invasion of salivary glands

Based on the APL1C protein increase in mosquitoes at the time of high sporozoite release at 18 d post-IBM, APL1C was tested for a protective role against sporozoites. Mosquitoes were treated with dsAPL1C or control dsGFP at 9 d post-IBM, approximately 3 d before the beginning of sporozoite release (experimental design, **Figure S5**). Silencing efficiency was confirmed for APL1C transcript and protein, and was persistent until at least 10 d post-treatment (**Figure 17A** and **B**). Salivary glands were dissected at 19 d post-IBM and sporozoites were counted using fluorescence microscopy for each individual mosquito. APL1C-depleted mosquitoes displayed increased sporozoite infection prevalence, that is, the proportion of positive versus negative glands, as compared to dsGFP controls ($p<0.0001$) (**Figure 17C**, Annex, **Table S2**). There was no effect on infection intensity, that is, the numbers of sporozoites in positive glands (Annex, **Table S2**). Thus, APL1C activity controls the efficiency of sporozoite invasion of salivary glands, and therefore should influence vector competence for parasite transmission.

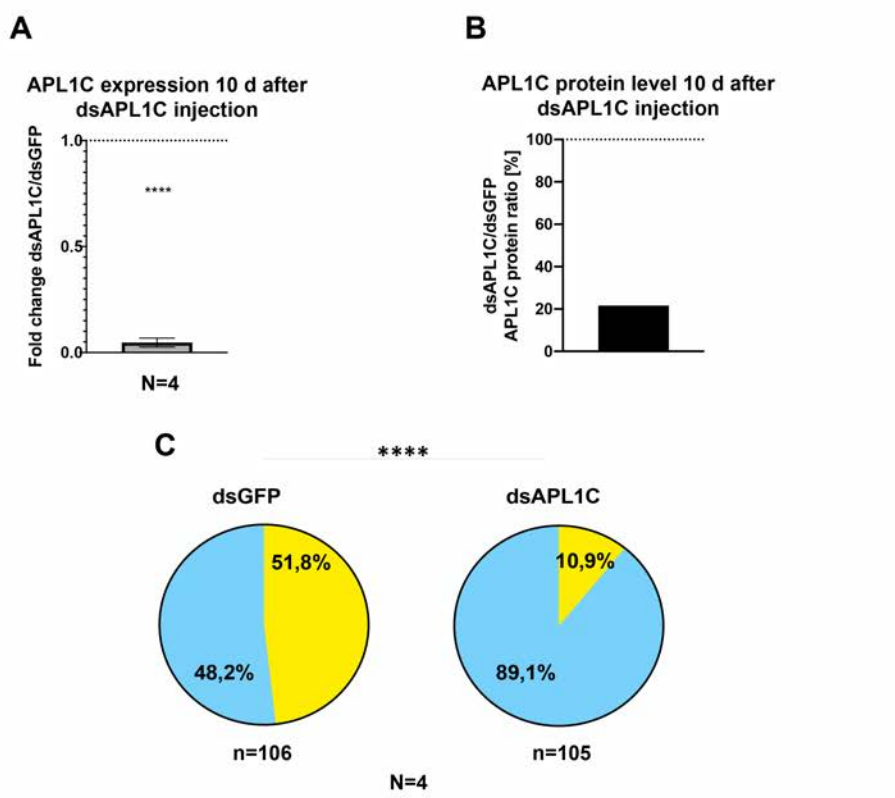

Figure 17. APL1C activity limits sporozoite invasion of salivary glands. A. Silencing of APL1C gene expression is efficient until at least 10 d after dsAPL1C treatment, the time point when salivary glands were dissected. APL1C silencing was verified by qPCR measurement between dsAPL1C and dsGFP (dotted line) treatments. The ratio of the normalized APL1C cDNA detection in "dsAPL1C" versus "dsGFP" treatments was computed using triplicates from the same cDNA dilution. Graph represents mean with ±SEM of the expression fold change between "dsAPL1C" and "dsGFP" control from four biological replicates (N=4). Data for qPCR analysis was analysed by unpaired t-test (significance level of t-test **** p-value <0.0001). **B.** APL1C protein level is efficiently decreased 10 d after dsAPL1C treatment. Graph represents the protein ratio between "dsAPL1C" and "dsGFP" control (depicted as a dotted line), measured by densitometry. GAPDH density signal was used to normalize APL1C signal in both dsGFP and dsAPL1C treatments, and the normalized APL1C signals were then compared between these two treatments. **C.** APL1C depletion led to increased sporozoite infection prevalence of the salivary glands. The proportions of the sporozoite-infected salivary glands (blue) or non-infected (yellow) in dsAPL1C and dsGFP treated mosquitoes were scored (n=total number of salivary glands dissected across the replicates) and are illustrated in the pie chart as the mean percentage obtained from four independent experiments (N=4). Prevalence from each replicate was compared between the two conditions by chi-square test. All statistical differences were first tested independently within replicates (individual p-values in Annex **Table S2**), and if individual replicates showed a common trend of change, individual p-values were combined using the meta-analytical approach of Fisher (significance level of chi-square **** p-value <0.0001).

3.2.3 APL1C binds to free *Plasmodium* sporozoites in the mosquito hemolymph

The simplest model to explain APL1C inhibition of sporozoite invasion into the salivary glands is similar to the above proposed model for ookinete immunity, where LRR proteins recognize and bind to the pathogen, then recruiting the TEP1 effector for lysis of the cell. Therefore, we tested whether APL1C binds directly to sporozoites. Sporozoites were perfused from IBM mosquitoes at 17 d post-IBM and IFA was performed using APL1C antibody. The majority (97%) of sporozoites were labelled with APL1C antibody (**Figure 18A** and **B**), indicating that APL1C protein binds to sporozoites in the mosquito hemocoel. As a control, 2 of 210 sporozoites perfused from APL1C-silenced mosquitoes were detectably labelled with APL1C antibody (**Figure 18C** and **D**). These results demonstrate that APL1C protein binds to free sporozoites in the hemolymph, which is consistent with its protective activity against salivary gland infection shown above.

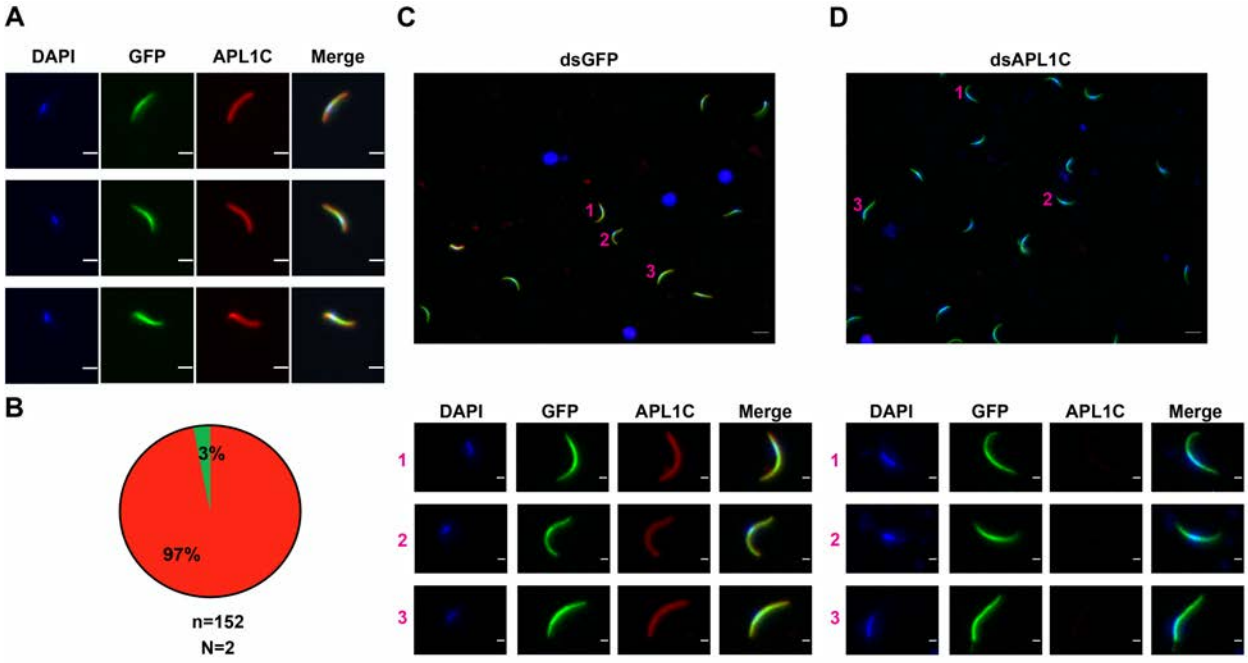

Figure 18. APL1C protein binds to free sporozoites in mosquito hemolymph. **A.** Immunostained GFP sporozoites (green) from mosquitoes perfused 17 days post-IBM are labelled with APL1C protein (red). Nuclei were stained with DAPI (blue). Images are representative of two independent biological replicates. The scale bar is 5 µm. **B.** The proportion of circulating sporozoites (n=152) labelled with APL1C protein was scored and illustrated in a pie chart as a mean percentage from two independent experiments (red: APL1C-positive sporozoites, green: APL1C-negative sporozoites). **C.** Sporozoites perfused from dsGFP-injected mosquitoes are labelled by APL1C protein. The main picture depicts merge (scale bar 10 µm), whereas pictures below show 3 channels of enlarged projections of sporozoites (scale bar 2 µm), indicated by the numbers on the merge picture. **D.** Sporozoites perfused from dsAPL1C-treated controls are not labelled by APL1C protein. The main picture depicts merge (scale bar 10 µm), whereas pictures below 3 channels of enlarged projections of sporozoites (scale bar 2 µm), indicated by the numbers on the merge picture.

3.2.4 APL1C protective activity against sporozoites does not require the complement proteins TEP1 or TEP3

For killing of rodent *Plasmodium* midgut ookinetes, it was previously shown that a physical complex of the APL1C-LRIM1 heterodimer with either one of the thioester proteins TEP1 or TEP3 is required[104,111]. Therefore, the role of TEP1 and TEP3 in APL1C-mediated sporozoite protection was queried. Expression of TEP1 and TEP3

was silenced individually or simultaneously by treatment with dsRNA at 9 d post-IBM, and sporozoite infection prevalence and intensity in the salivary glands was measured at 19 d post-IBM (experimental design, **Figure S5**). Silencing efficiency was confirmed at 10 d after dsRNA treatment (**Figure 19A)**. Neither TEP gene, alone or together, displayed an influence on sporozoite infection of salivary glands (**Figure 19B**). These results indicate that while TEP1 and TEP3 both display anti-ookinete function in the mosquito midguts[104,111,129] [115], they do not contribute to APL1C-mediated anti-sporozoite function. APL1C may recruit different TEP family members for sporozoite protection, or sporozoite destruction could be mediated by a distinct mechanism that does not include a TEP effector. Further work will be required to distinguish between these models.

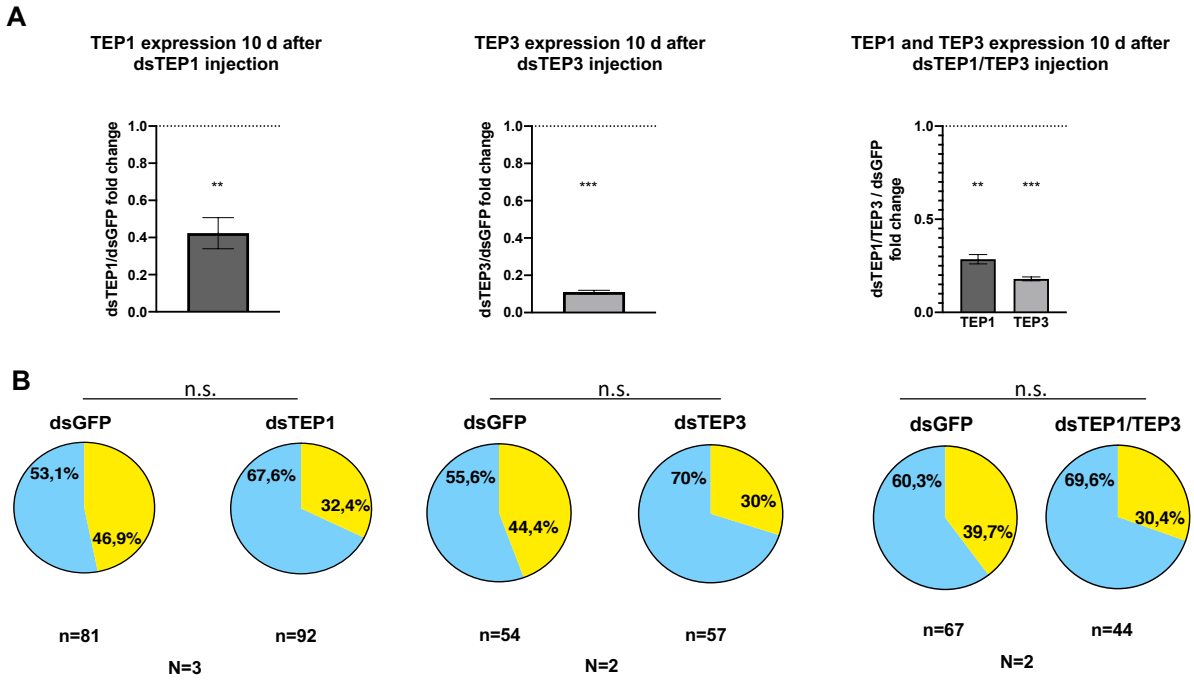

Figure 19. APL1C protective activity against sporozoites does not require the complement proteins TEP1 or TEP3. A. TEP1 and TEP3 expression are efficiently silenced at the time of the salivary gland dissection (10 days post-dsTEP1, dsTEP3 or dsTEP1/TEP3 treatments). TEP1 and TEP3 silencing was verified by qPCR. The ratio of normalized TEP1 or TEP3 cDNA detection in “dsTEP1”, “dsTEP3” or “dsTEP1/TEP3” versus “dsGFP” treatments was computed using triplicates from the same cDNA dilution. Graph represents mean with ±SEM of the expression fold change between “dsTEP1”, “dsTEP3” or “dsTEP1/TEP3” as

compared to the "dsGFP" control from all biological replicates (N) depicted in **B**. Data for qPCR analysis was analysed by unpaired t-test (significance levels of t-test p-values: ** p-value <0.01; *** p-value <0.001). **B.** TEP1, TEP3 or simultaneous TEP1/TEP3 depletion does not affect sporozoite salivary gland infection. The salivary glands dissected among all the replicates were scored (n=total number of salivary glands dissected in all replicates) and represented in pie charts as the mean percentage of sporozoite-infected salivary glands (blue) or non-infected (yellow) obtained from indicated number of biological replicates (N). The percentages of dsTEP1, dsTEP3 or dsTEP1/TEP3 salivary gland infection prevalence were compared with dsGFP injected control. Infection prevalence from each replicate was compared between the two conditions by chi-square test. All statistical differences were first tested independently within replicates (individual p-values in Annex **Table S2**), and if individual replicates showed a common trend of change, individual p-values were combined using the meta-analytical approach of Fisher (significance level of chi-square: n.s.=not significant).

3.3 Implication of the APL1 LRR family in immune signal transduction

APL1C binds to both ookinete and sporozoite parasite stages, and appears to be a component of pathogen sensing for free sporozoite presence in the hemocoel. APL1C may generate signals leading to the expression of additional downstream immune factors. To test the hypothesis that APL1 family proteins lead to downstream immune signalling, a transcriptomic analysis using RNA sequencing (RNAseq) was carried out to detect the transcriptional effects of APL1A and APL1C activity (**Figure 20**). Because the phenotypes of each gene are largely mediated by different immune pathways[103,102], it was expected that the transcriptional effects of each gene would be different.

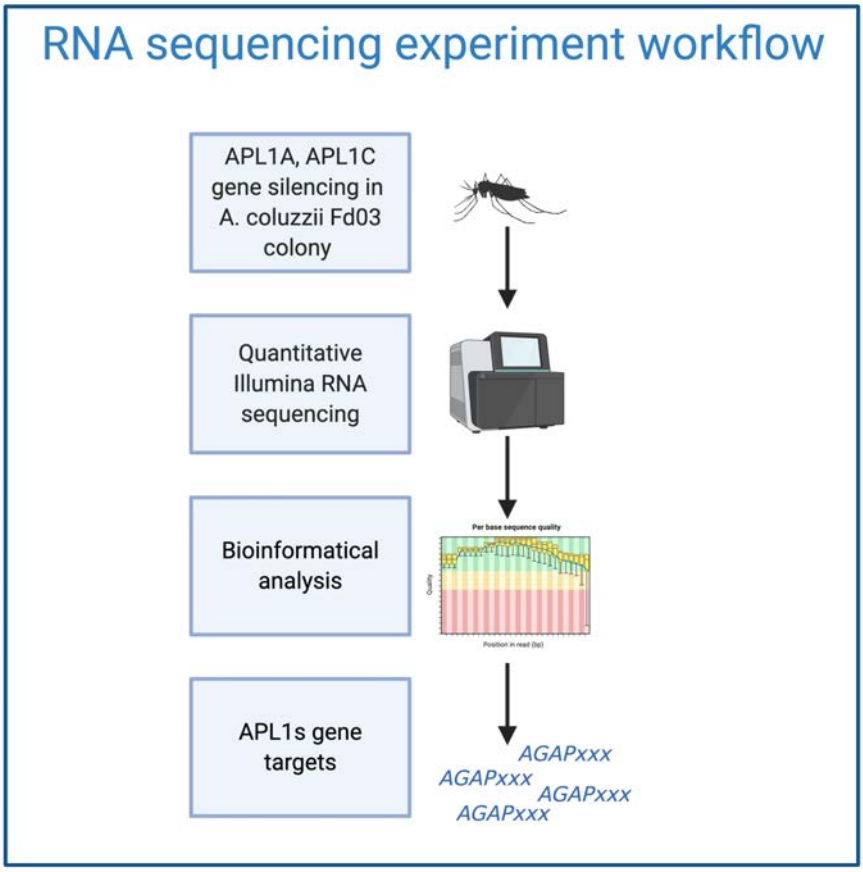

Figure 20. Overview of the RNAseq experiment. The APL1A or APL1C genes were silenced in *A. coluzzii*, with dsGFP treatment as the control, and RNAs were subjected to RNAseq. Bioinformatic analysis identified differentially expressed genes for each silenced gene as compared to the control.

3.3.1 APL1A and APL1C gene silencing in *A. coluzzii*

The APL1 genes are characterized by their exceptional genetic diversity observed in wild mosquitoes as well as in the lab-reared colonies[105,106]. This genetic variability within each gene include gene insertion-deletions[106], and variants in the region targeted for gene silencing using dsRNA could affect silencing efficiency. Therefore, I identified the potential APL1A and APL1C variants segregating in the studied mosquito colony (Fd03) to verify that they are sensitive to the designed dsAPL1A and dsAPL1C fragments targeting the gene 3'UTRs[102,103]. 3' Rapid Amplification of cDNA Ends (3'

RACE) was used to sequence APL1A and APL1C 3'UTR variation. Five different APL1A 3' variants were identified, and all of them overlapped and would be sensitive to the designed dsAPL1A fragment (**Figure 21A**). Among 22 sequenced clones, 18 represented one major structural variant with 8 bp and 9 bp insertions compared to the reference sequence, resulting in a shifted stop codon (stop codon depicted as 'TAG' on **Figure 21A**). Another variant (1 clone) lacked a stop codon. A third variant included two deletions of 308 bp and 15 bp, as compared to the reference sequence, which also shifted the stop codon. This variant also displayed a 9 bp insertion after the stop codon. The two remaining other variants are the closest to the reference sequence, with a stop codon located at the same position.

For APL1C, over 31 sequences analysed, 4 different structural variants were identified. All of them overlapped with the dsAPL1C fragment (**Figure 21B**). All variant cases encoded the stop codon in the same place as the reference sequence (**Figure 21B**). The differences between the variants were observed in the 3'UTR region. These differences included insertion-deletion events as compared to the reference sequence (**Figure 21B**).

Thus, sequence analysis indicated that all APL1A and APL1C gene variants identified in the Fd03 colony used in this study should be efficiently targeted by the synthesized dsAPL1A and dsAPL1C fragments.

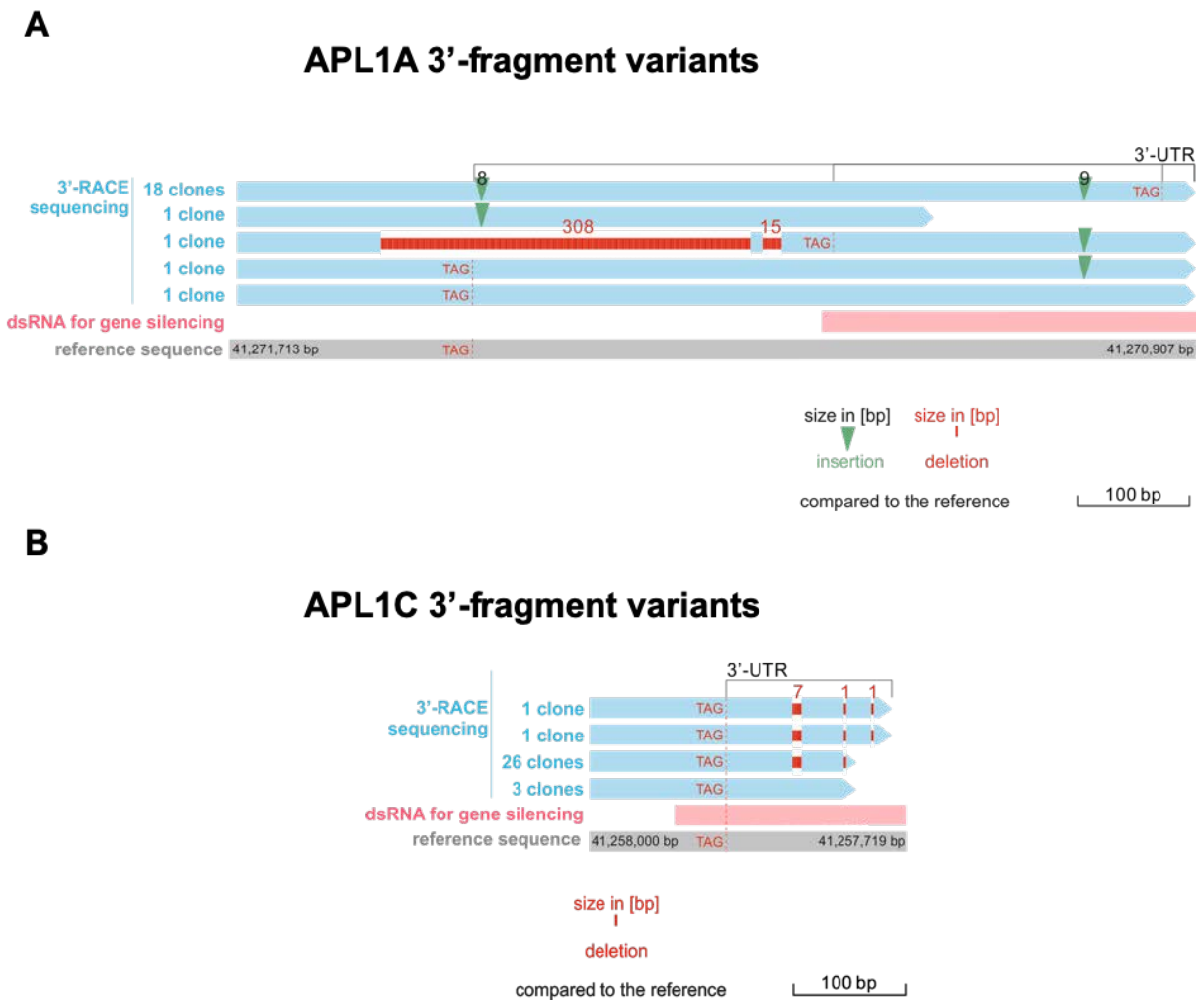

Figure 21. 3' APL1A and APL1C fragments identified by 3' RACE overlap with dsAPL1A and dsAPL1C fragments. A. 3'RACE of APL1A gene identified 5 different 3'APL1A fragment variants. **B.** 3'RACE of APL1C gene identified 4 different 3'APL1C fragment variants.

3.3.2 Kinetics of APL1A and APL1C silencing

The next step was to establish the correct time point(s) after gene silencing to collect samples for RNAseq. Ideally, as depicted in **Figure 22**, it would be the best to capture the first layer of the genes affected by APL1A and APL1C silencing and avoid the subsequent layer(s) of indirectly affected genes and secondary effects. Collecting the samples at latter time points (red arrow, **Figure 22**) would increase the number of

differentially expressed genes to test and decrease their informativeness for identifying the proximal target genes of putative APL1 signalling.

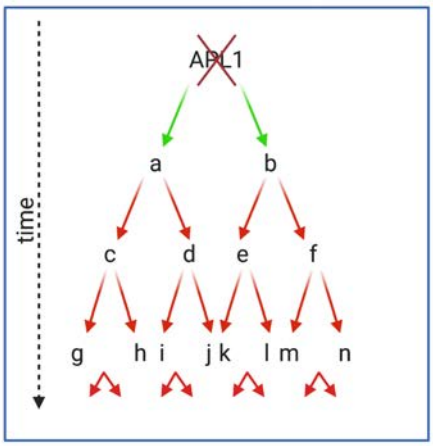

Figure 22. The potential time effect after APL1 depletion on the number of the affected genes. 'a' and 'b' correspond to the hypothetical first layer of genes directly affected by depletion of APL1 (green arrows). The influence of APL1 on downstream expression could be caused by any combination of transcriptional, translational and post-translational effects. The red arrows indicate the genes that are secondary, tertiary and subsequently affected by the time post-APL1s depletion.

In order to determine the optimal time to harvest RNA for collecting mosquitoes after gene silencing, pools of eight mosquitoes were collected at 6, 12, 24, 30, 48 and 72 h for each treatment (dsAPL1A, dsAPL1C and dsGFP). Efficiency of APL1A and APL1C transcript silencing was measured by qPCR and determined as expression fold change of the dsGFP control group. Silencing of APL1A was efficient already at 6 h with 70% of transcript decrease. For the next time points (12, 24, 30, 48 and 72 h post-treatment), APL1A transcript was further decreased to at least 90% below controls (**Figure 23A**). For APL1C transcript levels were decreased by 90% at 6 h post-dsRNA treatment, which persisted until 72 h post-treatment. Therefore, I screened earlier time points post-dsAPL1C treatment (0, 1, 2 and 4 h), in order to test how the silencing efficiency evolved. The results illustrated in **Figure 23B** showed that the major effect of gene silencing occurred 1-2 h after dsRNA treatment.

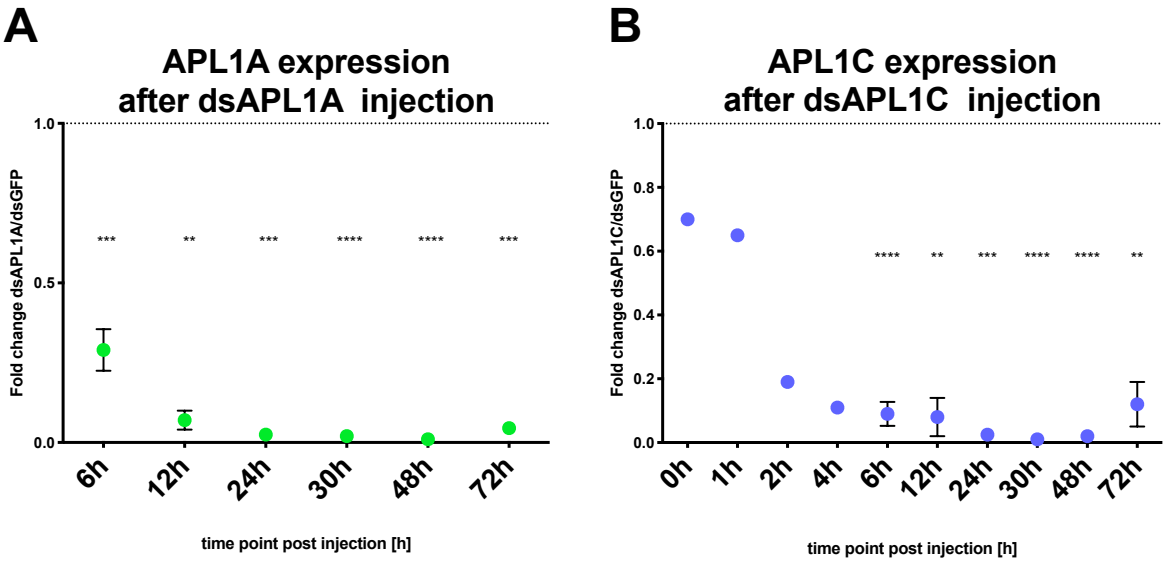

Figure 23. APL1 gene silencing efficiency after dsRNA treatment. A. The kinetics of APL1A transcript depletion after dsAPL1A treatment in *A. coluzzii*. APL1A silencing was verified by qPCR measurement relative to dsGFP controls (dotted line). The ratio of the normalized APL1A cDNA detection in "dsAPL1A" versus "dsGFP" treatments was computed using triplicates from the same cDNA dilution. Graph represents mean with ±SEM of the expression fold change between "dsAPL1A" and "dsGFP" control from at least two biological replicates. **B.** The kinetics of APL1C transcript depletion after dsAPL1C treatment. APL1C silencing was verified by qPCR and computed as above. For **A** and **B** data for qPCR analysis was analysed by unpaired t-test (significance levels of t-test p-values: ** p-value<0.01; *** p-value <0.001; **** p-value <0.0001).

APL1C protein levels were also measured at the same time points. Pools of eight mosquitoes were collected at 6, 12, 24, 48 and 72 h post dsRNA and proteins extracted from mosquitoes were quantified by Western blot.

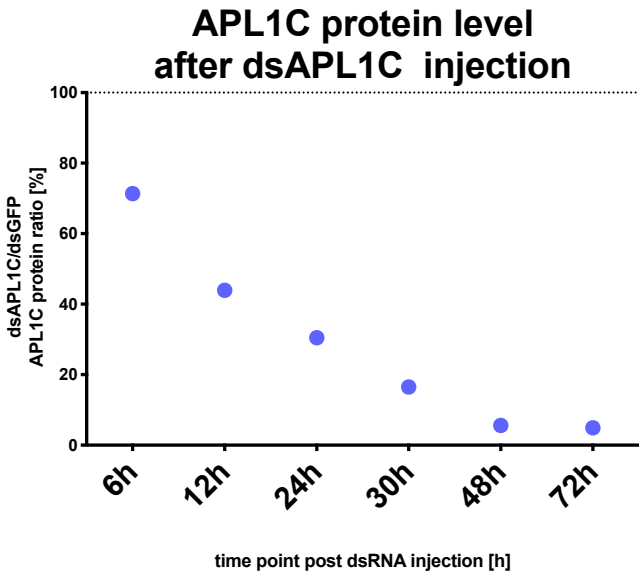

Figure 24. The kinetics of APL1C protein levels after dsAPL1C. The graph represents the level of APL1C protein in dsAPL1C-treated mosquitoes normalized with the dsGFP control (depicted as a dotted line), measured by densitometry. GAPDH density signal was used to normalize APL1C signal in both "dsGFP" and "dsAPL1C" treatments, and the normalized APL1C signals were then compared between "dsAPL1C" and "dsGFP" conditions.

The amount of APL1C protein decreased by 50% at 12 h post-dsRNA and more than 90% reduction at 48 and 72 h as compared to dsGFP controls (**Figure 24**). It was estimated that 50% protein reduction at 12 h post-dsRNA treatment should be appropriate to identify the more proximal gene expression affected by APL1C silencing. The protein analysis could not be conducted for APL1A protein because of the absence of specific antigen targets for APL1A antibody production. However, analysis of the transcript level showed that APL1A silencing was as efficient as APL1C at 12 h post-dsRNA treatment (**Figure 23A**). Taken together, for both APL1A and APL1C silencing, I decided to collect mosquito RNA samples at 12 h post-dsRNA treatment, as the earliest time-point that would preferentially capture the most proximal response genes to APL1 depletion. Four independent biological replicates were performed, where mosquitoes were injected with dsAPL1A, dsAPL1C or dsGFP as control. For each replicate, total RNAs were extracted from a pool of eight collected

females, at 12 h post-dsRNA treatment. APL1A or APL1C silencing efficiency was confirmed in each replicate by qPCR analysis (**Figure 25A** and **B**). In addition, APL1C protein decrease in dsAPL1C-injected mosquitoes was confirmed by Western blot analysis (**Figure 25C**).

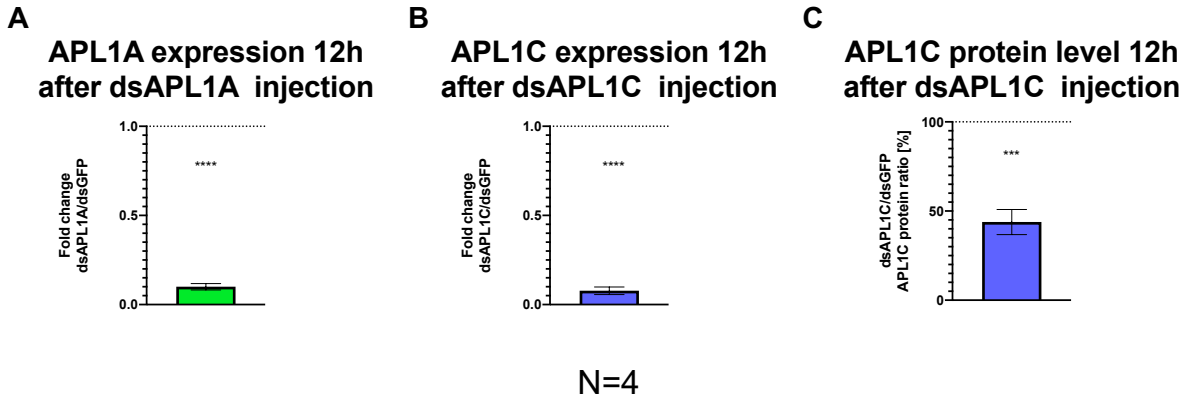

Figure 25. APL1 genes silencing controls prior to the RNAseq analysis. A. APL1A expression is silenced 12 h post dsAPL1A treatment. APL1A silencing was verified by qPCR measurement between dsAPL1A and dsGFP (dotted line) treatments. The ratio of the normalized APL1A cDNA detection in "dsAPL1A" versus "dsGFP" treatments was computed using triplicates from the same cDNA dilution. Graph represents mean with ±SEM of the expression fold change between "dsAPL1A" and "dsGFP" control from four (N=4) biological replicates. **B.** APL1C expression is silenced 12 h post dsAPL1C treatment. APL1C silencing was verified by qPCR measurement between dsAPL1C and dsGFP (dotted line) treatments. The ratio of the normalized APL1C cDNA detection in "dsAPL1C" versus "dsGFP" treatments was computed using triplicates from the same cDNA dilution. Graph represents mean with ±SEM of the expression fold change between "dsAPL1C" and "dsGFP" control from four (N=4) biological replicates. **A** and **B** data for qPCR analysis was analysed by unpaired t-test (significance level of t-test p-value: **** p-value <0.0001). **C.** APL1C protein level is decreased by more than 50% at 12 h post dsAPL1C treatment. The graph represents the level of APL1C protein in dsAPL1C-injected mosquitoes normalized with the dsGFP control (depicted as a dotted line), measured by densitometry. GAPDH density signal was used to normalize APL1C signal in both dsGFP and dsAPL1C treatments. Graph represents mean with ±SEM from four biological replicates (N=4). Data were analysed by Image Lab 6.0.1 and statistically analysed by unpaired t-test (significance level of t-test p-value: *** p-value <0.001).

3.3.3 RNAseq and bioinformatic analysis

Differentially expressed genes were identified bioinformatically (see Materials and Methods). Results of the differential analysis are presented graphically as volcano and

MA plots (**Figure 26**, **Figure 27**) as well as summarized in **Table 2**. As depicted on the volcano plot, the comparison between dsAPL1A and dsGFP highlighted surprisingly only one candidate gene displaying a statistically significant modulated expression upon APL1A gene depletion (**Figure 26A**). Overall, the mosquito transcriptome was nearly non-affected by the lack of APL1A. In contrast, depletion of APL1C at the same time point highly influenced mosquito transcriptome profile, with gene candidates that were statistically significantly down- or upregulated (**Figure 26B**).

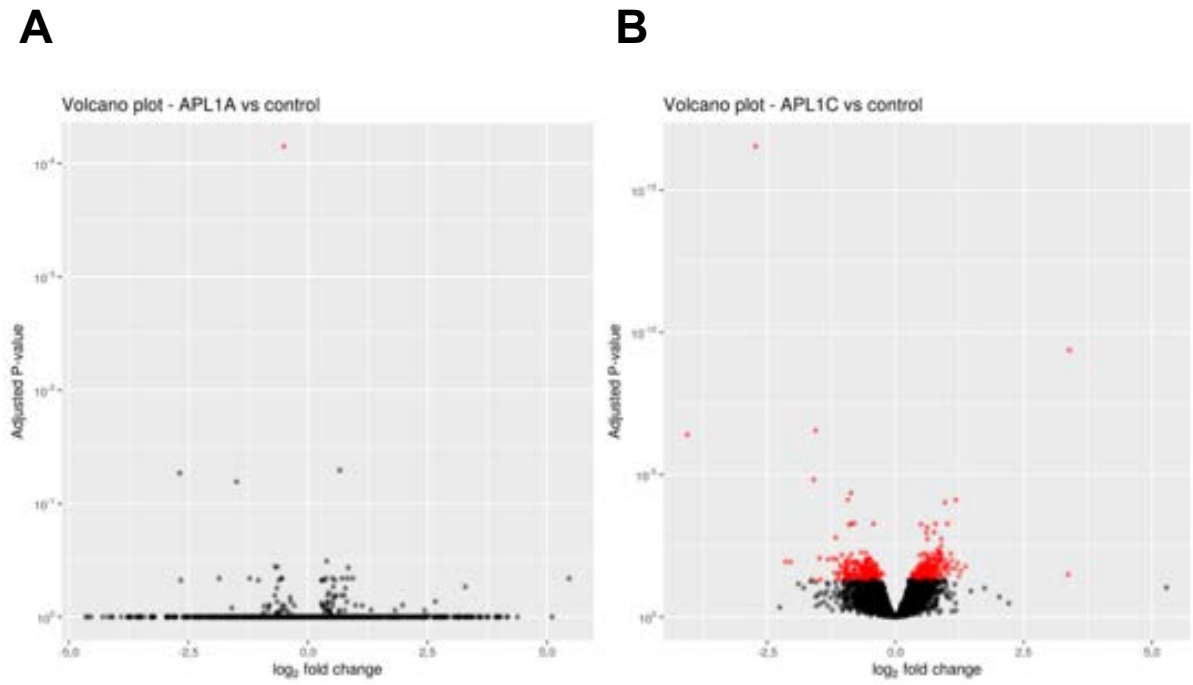

Figure 26. Volcano plots visualize the differential expression analysis of RNAseq taken in dsAPL1A vs dsGFP (A) and dsAPL1C vs dsGFP conditions (B). Each dot represents a gene, which expression was compared between the tested conditions (APL1A-depleted mosquitoes vs dsGFP control or APL1C-depleted mosquitoes vs dsGFP control). Red dots correspond to significantly different genes based on adjusted p-value. For each pairwise comparison, raw p-values were adjusted for multiple testing using the Benjamini and Hochberg procedure[130]. Genes with adjusted p-values below 0.05 were considered differentially expressed

MA-plots for both tested conditions display similar profile among tested conditions (**Figure 27**). Nevertheless, APL1C depletion influenced the expression of a greater number of genes than APL1A depletion **(Figure 27B**).

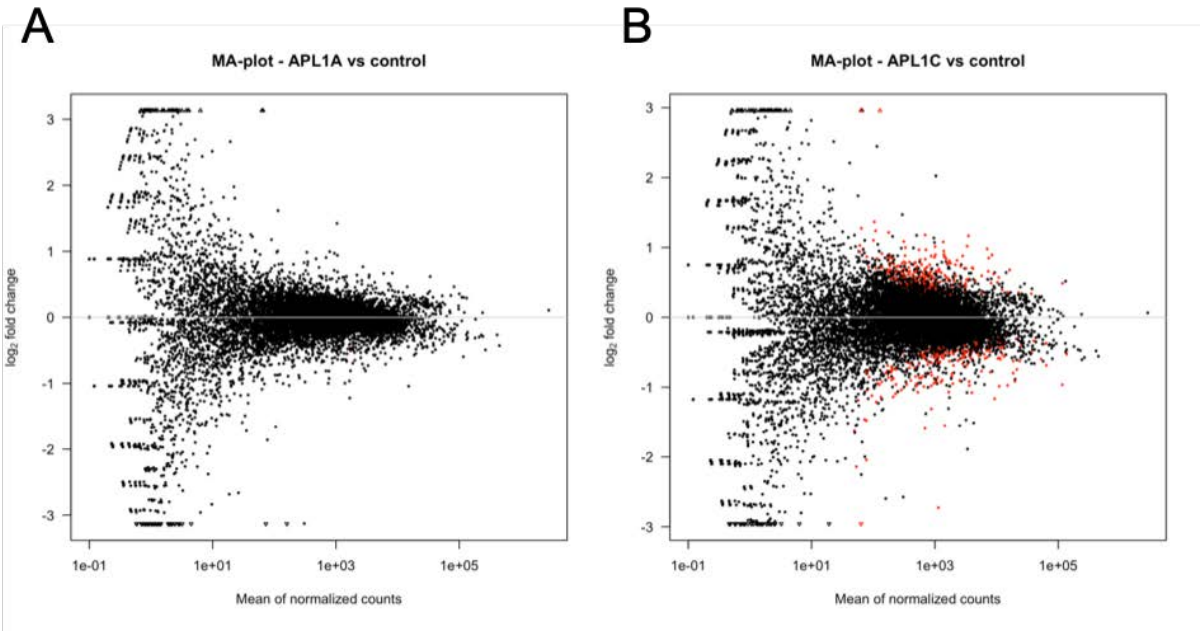

Figure 27. MA-plots visualizing the log ratio of differential expression as a function of the mean intensity taken in dsAPL1A vs dsGFP (A) and dsAPL1C vs dsGFP conditions (B). Each dot represents a gene which expression was compared between the tested conditions**.** Differentially expressed features are highlighted in red and the triangles correspond to features having a too low/high log2(FC) to be displayed on the plot.

Table 2 summarizes significantly down- or upregulated genes in mosquitoes depleted for APL1A or APL1C. As reported graphically, APL1A depletion caused downregulation of only one gene, and none were upregulated. In contrast, APL1C silencing significantly regulated 423 genes, 200 downregulated and 223 upregulated.

Tested condition	Downregulated	Upregulated	Total number of differentially expressed genes
dsAPL1A vs dsGFP	1	0	1
dsAPL1C vs dsGFP	200	223	423

Table 2. Number of up-, down- and total number of differentially expressed genes in each compared condition. The gene was defined as differentially expressed if adjusted p-value <0,05.

The only candidate gene from APL1A depleted mosquitoes encodes “defective in cullin neddylation protein” (AGAP002513). Among APL1C-downregulated and upregulated gene candidates, 112 and 154 genes have an annotated function, respectively (Annex, **Table S4** and **Table S5**).

3.3.4 qPCR validation of the RNAseq gene candidates.

The APL1C gene candidate gene targets revealed by the RNAseq experiment were tested by qPCR analysis. Candidates with adjusted p-values<0,05 and log2 foldchange (log2FC) cut-off of -1 (16 genes) and log2FC cut-off of 0,87 (27 genes), for down- and upregulated genes, respectively, were tested. Results showed that the expression of tested genes correlated between RNAseq and qPCR experiments ($p<0.0001$ **Figure 28**), thus validating performed RNAseq analysis.

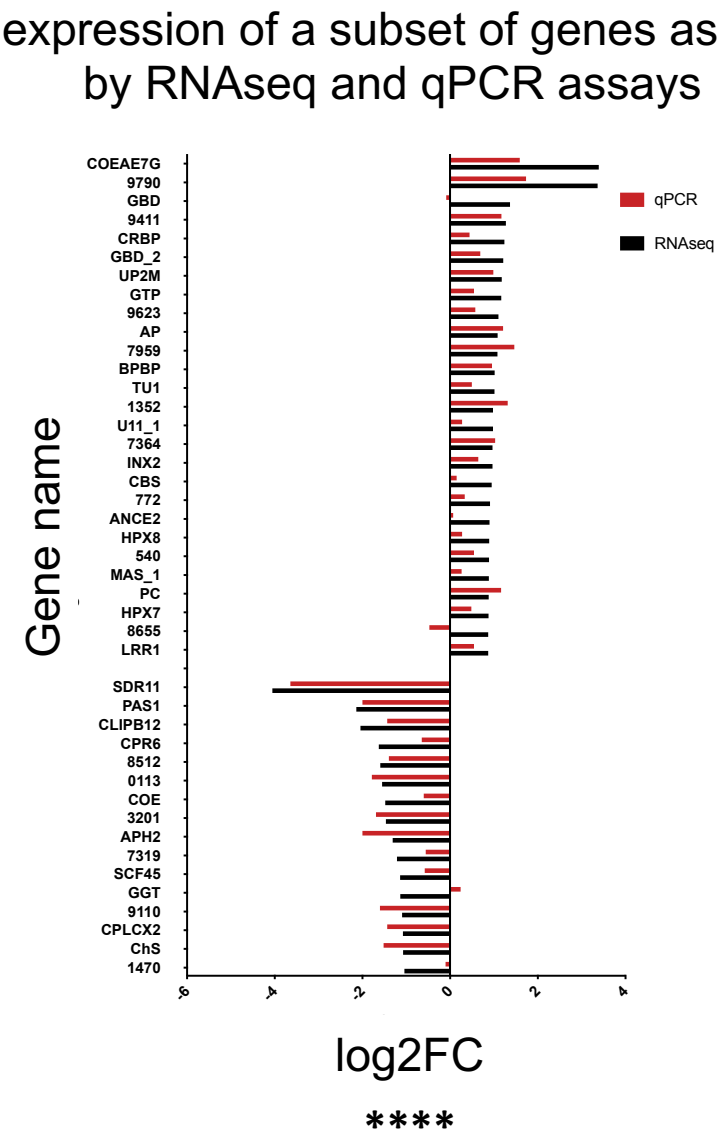

1580

1581 **Figure 28. qPCR gene expression analysis validates RNAseq APL1C gene targets.** Gene
1582 expression is reported as expression log2 foldchange [log2FC, x-axis] measured between
1583 “dsAPL1C” and “dsGFP” conditions. Expression of each tested gene is depicted as a red bar
1584 for qPCR analysis and black bar for RNAseq analysis. For gene calling (y-axis), annotated
1585 genes are called with their gene name or aberrations of gene function, whereas the genes
1586 without annotated function are called by the last four digits of their AGAP number. The
1587 correlation between qPCR and RNAseq was tested by computing Pearson correlation
1588 coefficients. Significance levels of Pearson correlation **** p-value <0.0001).

3.3.5 APL1C controls expression of immune-like genes in the mosquito

The 423 genes significantly affected by APL1C depletion were each screened for encoded protein domains displaying immune-like function, such as LRRs[99,104,110], TEPs[104,111,120,131], CLIP-serine proteases[132-135], serine proteases inhibitors (serpins)[136,137], ankyrin repeats[138], immunoglobulins[139], heme peroxidase[140,141] and angiotensin-converting[142-145]. Among the downregulated genes, 22 genes encodes for such immune-like domains (**Table 3**), whereas 6 genes were identified with such domains among the up-regulated genes (**Table 4**). Interestingly, within 22 downregulated-immune-like genes, I identified nimrod B2 and Scavenger receptors coding genes, both being implicated in phagocytosis in mosquitoes[146,147].

Gene ID	Gene name	FoldChange	log2FoldChange	p-adj	Gene description	Gene description source
AGAP009217	CLIPB12	0,243	-2,043	0,012	CLIP-domain serine protease	VB
AGAP029110	N/A	0,469	-1,093	0,029	C-type lectin-like/link domain superfamily	IP
AGAP001470	N/A	0,486	-1,041	0,007	Leucine-rich repeat, typical subtype	IP
AGAP005496	LRIM12	0,487	-1,039	0,018	leucine-rich immune protein (Short)	VB
AGAP007045	LRIM15	0,514	-0,961	0,015	leucine-rich immune protein (TM)	VB
AGAP028028	LRIM16A	0,514	-0,959	0,012	Leucine-rich immune protein (TM)	UP
AGAP010814	TEP6	0,517	-0,952	0,024	thioester-containing protein 6	VB
AGAP008368	TEP14	0,527	-0,924	0,039	thioester-containing protein 14	VB
AGAP029054	NimB2	0,527	-0,923	0,018	nimrod B2	VB
AGAP028064	LRIM16B	0,535	-0,901	0,042	Leucine-rich immune protein (TM)	UP
AGAP028680	N/A	0,558	-0,842	0,025	Leucine-rich repeat, cysteine-containing subtype, F-box domain	IP
AGAP008091	CLIPE1	0,573	-0,804	0,001	CLIP-domain serine protease	VB
AGAP028167	N/A	0,581	-0,783	0,034	Proteinase, regulatory CLIP domain, Serine proteases	IP
AGAP001375	SRPN12	0,587	-0,768	0,012	serine protease inhibitor (serpin) 12	VB
AGAP004846	SCRB9	0,667	-0,583	0,017	Class B Scavenger Receptor (CD36 domain)	VB
AGAP004643	SCRB6	0,674	-0,569	0,011	Class B Scavenger Receptor (CD36 domain)	VB
AGAP007061	N/A	0,69	-0,535	0,035	Leucine-rich repeat, typical subtype	IP
AGAP029564	N/A	0,694	-0,527	0,037	Immunoglobulin-like domain, CD80-like, immunoglobulin C2-set	IP
AGAP008366	TEP2	0,72	-0,475	0,018	thioester-containing protein 2	VB
AGAP007556	N/A	0,724	-0,465	0,035	Immunoglobulin subtype 2, Fibronectin type III	IP
AGAP008914	N/A	0,757	-0,401	0,026	Basic-leucine zipper domain	IP
AGAP006645	N/A	0,809	-0,307	0,034	Leucine-rich repeat, typical subtype	IP

Table 3. List of the immune-like genes, which expression is downregulated upon APL1C depletion. Genes are enlisted according to the descending expression fold change between "dsAPL1C" and "dsGFP" (control) treatments. The columns include gene ID referred as the AGAP number; gene name, N/A stands for not annotated gene; expression foldchange and log2foldchange, adjusted p-value (p-adj), gene description including encoded protein function or predicted protein domain based on the databases: VB-VectorBase Community Annotation, IP-Interpro, UP-UniPro.

Gene ID	Gene name	FoldChange	log2FoldChange	p-adj	Gene description	Gene description source
AGAP009751	ANCE2	1,868	0,901	0,00605	angiotensin-converting enzyme 2	VB
AGAP004038	HPX8	1,858	0,893	0,0032	heme peroxidase 8	VB
AGAP004036	HPX7	1,838	0,878	0,02739	heme peroxidase 7	VB
AGAP003591	N/A	1,826	0,869	0,00944	LRR-repeat protein 1	VB
AGAP011534	N/A	1,51	0,594	0,02302	Ankyrin repeat Ankyrin repeat and LEM domain-containing pro	IP
AGAP004563	ANCE9	1,313	0,393	0,04951	angiotensin-converting enzyme 9	VB

Table 4. List of the immune-like genes, which expression is upregulated upon APL1C depletion. Genes are enlisted according to the ascending expression fold change between "dsAPL1C" and "dsGFP" (control) treatments. The columns include gene ID referred as the AGAP number; gene name, where N/A stands for not annotated gene; expression foldchange and log2foldchange, adjusted p-value (p-adj), gene description including encoded protein function or predicted protein domain based on the databases: VB- VectorBase Community Annotation, IP-Interpro, UP-UniPro.

IV. DISCUSSION

4.1 Dual functionality for APL1C as guard and PRR-like factor

The LRR APL1 proteins are the key components of the mosquito defence against *Plasmodium* infection[99,102,103]. However, little was known about the mechanism of APL1 function in mosquito anti-*Plasmodium* defence. This thesis work showed that APL1C can bind to both *Plasmodium* ookinetes and sporozoites and thus acts as a pathogen binding factor. Therefore, I propose that APL1C could behave as a PRR in heterocomplex with LRIM1 for initiating complement-like cascade via $TEP1_{cut}$ stabilization and binding to the parasites at least in mosquito midgut, which probably elicit a signalling pathway, as shown that APL1C controls the expression of several genes in *A. coluzzii.* In addition, it was observed that APL1C presence on the mosquito midguts was not restricted to the parasite surface, as it could form hemolymph-originated, extracellular layer on the basal side of the midgut epithelial cells. The APL1C protein level is induced by the bloodmeal independently from the presence of the parasite, which suggests that APL1C acts as a guard protein in mosquito hemolymph, where beneath basal lamina of the midgut, it could form a state of immune readiness to face *Plasmodium* and probably other potential microbes that may emerge from the blood-engorged midguts. The bloodmeal thus constitutes a generalized signal that induces APL1C and other immune factors that may recognize a large range of blood borne potentially pathogenic microbes. In the case of the malaria parasites, when the ookinetes traverse the midgut epithelium and reach the basal side of the cells into the extracellular space, APL1C appears ready to “catch” the parasites through a binding process for blocking their further development. It has been recently reported

that mosquito infection with Gram-negative, but not Gram-positive bacteria specifically induces APL1C cleavage by a still unidentified protease[122] . My thesis work showed that APL1C binds to the *Plasmodium* ookinetes but we still do not know if this binding requires or not the cleavage process, or if the cleavage of APL1C occurs posteriori of the parasite binding. Another possibility would be that previously reported cleavage of APL1C is bacteria-specific, and thus does not occur in the case of *Plasmodium* parasites. PRR have been described mainly as transmembrane but can be also present as soluble receptors. The peptidoglycan recognition proteins (PGRPs) are conserved in both vertebrates and insects. In *Drosophila,* transmembrane, cytosolic and soluble forms of PGRPs display recognition and catalytic properties linked to their capacity to bind PGN[148-150]. C-type lectins (CTLs) are another example of PRRs that occur extracellularly and are either secreted or membrane-bound. C-type lectins are pattern recognition receptors that function in both mammalian and insect innate immunity through the carbohydrate recognition domain. In A. gambiae two CTLs cooperate to defend the mosquito against Gram-negative bacterial infections. CTL function was also assessed towards mosquito *Plasmodium* infection, where two CTL, CTL4 and CTLMA2 protect the ookinetes against a potent mosquito innate immune response, melanization [151,152]. However, the most intriguing resemblance with the APL1C-LRIM1 LRR protein complex is the jawless vertebrate VLRB proteins. They are secreted LRR-antibody-like receptors inducing the classical-complement cascade[92] and circulate as disulphide-bridged multimers[153]. Therefore, the combinatorial immune LRR protein complexes could constitute a repertoire of antibody-like structures in *Anopheles* mosquitoes for facing distinct microbial infections.

4.2 The HdMvs, a source of secreted APL1C, mediated by the nitration pathway?

Phagocytic hemocytes represent more than 80% of total hemocytes in mosquitoes[154,155] and were reported to affect TEP1 binding to the ookinete on infected midguts[127]. Presented results demonstrated the important role of the phagocytic cells as a source of APL1C expression. APL1C proteins, which are expressed in hemocytes, and especially in phagocytic hemocytes, are localized in cytoplasmic vesicles. This suggests that, consistent with the presence of a signal peptide on its protein sequence, APL1C is secreted through this vesicle structure. Nitration has been shown to control release of hemocyte-derived microvesicles (HdMv) that were proposed to transport key factors mediating subsequent TEP1 binding and lysis of ookinetes [128]. It was found that silencing the nitration pathway, and thus inhibiting the release of HdMv, also reduced APL1C abundance in the midgut extracellular space, strongly suggesting that AP1C may be part of the payload of HdMv. To demonstrate this assumption, one possibility would be to physically isolate and collect these HdMvs and perform either a proteomic study or, more directly, a Western blot analysis using anti-APL1C antibody.

4.3 APL1C presence in hemolymph at the basal side of the midgut epithelium is not PAMP dependent

Nitric oxide (NO) production was correlated with *Plasmodium* ookinete invasion of the midgut epithelium[156] and was described as mediating protein nitration of ookinete-invading epithelial cells ('Time Bomb' model)[157]. Activation of the nitration pathway

leads to ookinete tagging as a danger (or non-self) signal, which promotes the activation of the mosquito complement cascade[140]. This suggests that activation of the immune response in mosquito is not initiated by *Plasmodium* PAMP but by parasite-induced tissue damage signals (DAMP) such as nitration. In line with this assumption, a study showed that TEP1 binds damaged sperm cells in a male mosquito in nitration pathway-dependent manner[158]. In the case of APL1C, presented results showed that a non-infected bloodmeal (NBM) also induced APL1C protein levels in mosquito. Because bloodmeals increase the abundance of the bacterial flora[39], I tested whether the enteric microbiome can induce elevated APL1C levels in the hemolymph, the source of the APL1C protein measured by IFA on dissected midguts. However, a similar abundance of APL1C protein between ATB-treated and control midguts groups, ruled out the microbiome as potential signal elicitor leading to increased APL1C protein level. Therefore, an alternative hypothesis for this signal would be related to the mechanical stretching of the midgut induced by the bloodmeal, which could damage the cellular integrity of the epithelium. To test this hypothesis, we could perform a blood-free feeding that would mimic the mechanical distension of the midgut epithelium and assess APL1C presence on the midgut epithelium.

Another possibility for the induction signal would be related to the physiological stress induced by bloodmeal chemical components or metabolites. Digestion of vertebrate haemoglobin results in the production of large amounts of free heme, a cytotoxic molecule that generates reactive oxygen species, which can disrupt phospholipid bilayers of cell [159]. Thus, the oxidative stress induced by the bloodmeal could serve as a danger signal, inducing the presence of LRR protein in the hemolymph, which diffuses through the porous basal lamina into the extracellular space around the midgut.

Taken together, knowing that APL1C presence on the midgut in the absence of *Plasmodium* is even not microbiome-related strengthens the hypothesis of a PAMP-independent source of signal to induce APL1C secretion in the hemolymph.

4.4 The sophisticated sporogony control by APL1C

Little attention has been paid on the mosquito immune response against the last stage of *Plasmodium* development, which are the sporozoites. My results showed that APL1C protein binds to the released sporozoites in the hemolymph, and more importantly, it also controls sporozoite infection prevalence in the salivary glands. The temporal behaviour of APL1C protein during sporogonic development appeared consistent with its immune functionality against the ookinete and the late sporozoite stages. APL1C protein levels were unchanged at the time corresponding to the oocyst stage, suggesting that it is not active against this parasite stage. This is consistent with other reports that the oocyst stage does not seem to stimulate immune responses. Indeed, oocyst surface proteins such as laminin are in fact mosquito host-derived factors[35], and these could hide the oocyst from the immune system recognition. The oocyst acquires metabolic resources from the mosquito for its enormous growth and internal cell divisions to generate thousands of sporozoites, however this appears to occur quietly from an immune perspective, until oocyst rupture. Therefore, potential inflammatory responses or cell apoptosis leading to DAMPs production are probably not prominent during the oocyst stage.

In addition, thesis results showed that APL1C protective function against the sporozoites does not involve the same factors as operate against the ookinete stage. TEP1 and TEP3 that were both reported to control *P. berghei* ookinetes and to interact

with the APL1C/LRIM1 complex[104,111] are not involved in protection against sporozoite salivary gland invasion. However, I cannot rule out that the control of sporozoites in collaboration with APL1C would require other TEP factors. In addition, it has been reported that unlike to the ookinete that harms the midgut epithelial cells, this is not likely the case for the sporozoites on the salivary gland epithelium as neither NOS increase, nor apoptosis has been reported[137]. Finally, a low proportion of phagocytized sporozoites was observed[46], suggesting that the phagocytic cells are activated during sporozoite release, and this activation might contribute to APL1C release in the hemolymph. Taken together, additional work is still needed to fully elucidate the killing mechanism of the sporozoites induced by APL1C.

4.5 Whole transcriptome analysis reveals differential signalling function of APL1 genes

Genomic and evolutionary studies revealed that immune-related genes and especially microbial-sensor coding genes such as PRR evolve faster than other insect genes[160-162]. The APL1 gene family underwent an expansion from a single ancestral gene to three genes in the lineage of African *Anopheles*[163]. The expanded APL1 genes acquired distinct immune activities, as exemplified by functional differences in anti-*Plasmodium* responses[103]. My RNAseq data analysis of APL1A and APL1C silencing treatments revealed distinct profiles of downstream-modulated genes. While depletion of APL1A expression did not induce differences in overall transcriptome, APL1C depleted treatment led to high number of modulated genes. Interestingly, APL1C appears to be orthologous to the ancestral single APL1 gene of *Anopheles*[163].

Therefore, it should likely still display the more ancestral APL1 functions, while the APL1A and APL1B paralogs are derived forms and evolved new functions. APL1C might protect against a broader spectrum of microbes as compared to, for example, APL1A, which could respond to a more specialized microbial profile. Consistently, functional studies revealed that, in addition to the rodent malaria parasites, APL1C protects against *E. coli* bacteria[122].

Even though my thesis did not concentrate on the allelic variation of each gene, my 3' RACE sequencing study of APL1A and APL1C identified allelic variants. It was previously reported that among distinct APL1A alleles segregating in the Ngousso *A. coluzzii* colony, only the APL1A^2 allele was associated with the protective phenotype of APL1A in P. falciparum challenge experiments[106]. My RNAseq experiment used the Fd03 colony, which has not been tested in a similar association study. Therefore, it cannot be excluded that current Fd03 colony may not carry the APL1A^2 allele, or another protective APL1A allele. The underlying hypothesis would be that protective variants would lead to a stronger transcriptional response, detectable by RNAseq, as compared to non-protective alleles. Further genomic and functional experiments would be necessary to test this hypothesis.

V. CONCLUDING REMARKS AND FUTURE PERSPECTIVES

CONCLUDING REMARKS AND FUTURE PERSPECTIVES

My thesis work gave insight in the function of LRR proteins in *A. coluzzii* mosquito. Focusing on the antimalarial APL1C gene as a representative of immune LRR family member, my results showed that it acts as pathogen binding factor in the mosquito hemolymph. I present evidence that APL1C and LRIM1 are directly associated to the *Plasmodium* ookinete surface, that APL1C binding to the parasite requires activity of the nitration pathway and the participation of phagocytic hemocytes. In addition to limiting the midgut stage of infection, presented results revealed that APL1C binds to the surface of free sporozoites in the hemocoel, and is required to limit salivary gland infection by sporozoites. These results are consistent with a model in which APL1C protein acts as a pathogen recognition factor released from hemocytes at elevated levels following a bloodmeal (**Figure 29**), diffuses in the hemolymph to form a protective layer in the midgut basal extracellular space and also protects the open systemic compartment from microbes (such as sporozoites) escaping the epithelial barrier of the midgut. APL1C release after a bloodmeal is triggered by nitration that could function as a DAMP. The bloodmeal induction of APL1C creates a state of immune readiness on the midgut epithelium against microbes ingested with the blood that could infect the mosquito. Furthermore, APL1C appears to be an active recognition factor in the hemolymph, where it binds to sporozoites and apparently tags them for killing by unknown effectors.

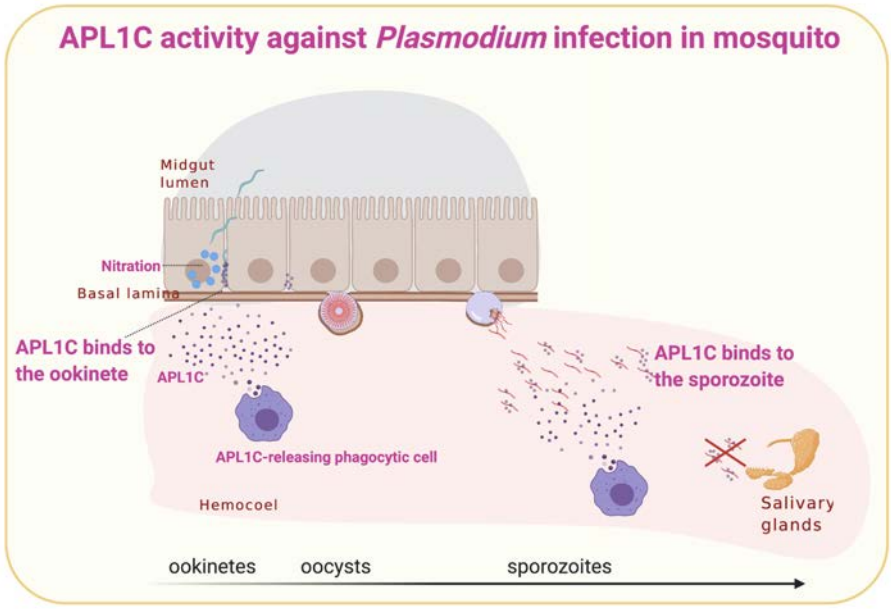

1805 **Figure 29. Proposed model of APL1C function in anti-*Plasmodium* response.** Detailed
1806 description in text.

1807

1808 Assuming that as PRR-like factors APL1 genes might elicit a signal transduction
1809 pathway, I performed a RNAseq analysis to identify the downstream factors of APL1A
1810 and APL1C. Consistently with their distinct activity, the results revealed distinct
1811 transcriptomic profiles between both genes. These results are consistent with the
1812 hypothesis that mosquito immune LRR proteins are functional counterparts of the
1813 immunoglobulin-based receptors that vertebrates use for antigen recognition, although
1814 the parasite surface ligands remain unknown.

1815 Lastly, it would be interesting to enlarge these findings to other members of the LRR
1816 family and assess the pathogen-specificity of their combinatorial binding property, as
1817 this family could represent the first secreted LRR pathogen recognition factors in the
1818 invertebrates.

VI. MATERIALS AND METHODS

Ethic statement

This study was conducted in strict accordance with the recommendations from the Guide for the Care and Use of Laboratory Animals of the European Union (European Directive 2010/63/UE) and the French Government. The protocol was approved by the "Comité d'éthique en expérimentation animale de l'Institut Pasteur" CETEA 89 (Permit number: 2013–0129), by the French Ministry of Scientific Research (Permit number: 202195.02) and undertaken in compliance with Institut Pasteur Biosafety Committee (protocol CHSCT 14.114).

Mosquitoes

Mosquitoes *Anopheles coluzzii* colony Fd03 initiated in Mali [164] was reared at 26˚C and 80% humidity, on a 12 h light/dark cycle with access to cotton soaked in 10% sucrose solution, in Genetics and Genomics of Insect Vectors Unit insectary, Institut Pasteur, Paris, France.

Mouse infections with *Plasmodium berghei*

All experiments were performed with three-week-old female Swiss *Mus musculus* mice (Janvier, France). Mice were inoculated with 10^5 red blood cells (RBCs) infected with GFP-expressing under the *hsp70* regulatory regions *P. berghei* parasite[165]. Four days post-treatment, blood samples were taken from the tail, and parasitemia was determined by flow cytometry. Furthermore, male gametocyte maturity was verified by performing an exflagellation test as previously described[166].

Mosquito feeding on non-infected mice or *P. berghei*-infected mice

For all the experiments, *P. berghei*-infected mice were used at 4-8% parasitemia, with mature gametocytes. Exflagellation tests were performed to evaluate the maturity of male gametocytes. First, both non-infected and infected mice were anesthetized by intraperitoneal (IP) treatment of ketamine (Imalgene 1000 at 125 mg/kg) and xylazine (Rompun 2% at 12.5 mg/kg), then mosquitoes were allowed to feed on the anesthetized mice for 20 min. Unfed mosquitoes were discarded and fed mosquitoes were maintained at 21°C and 70% relative humidity on 10% sucrose solution as previously described [103].

Midguts immunofluorescence assay (IFA)

Immunostainings were performed as previously described [128]. Briefly, mosquitoes were subjected to *P. berghei*-infected bloodmeal (IBM), non-infected bloodmeal (NBM) or 10% sucrose solution (unfed, UF) and incubated at 21°C. 24 h after, midguts from each condition were dissected in sterile 1× PBS, fixed for 40s in 4% paraformaldehyde for easier removal of the blood and opened longitudinally in sterile PBS to remove the blood bolus. Cleaned midguts were then fixed in 4% paraformaldehyde in 1× PBS for 1 hour at room temperature and rinsed five times in sterile PBS for 5 minutes each. In a next step, midguts were permeabilized, and blocked in PBT (PBS supplemented with 1% bovine serum albumin (BSA) and 0.1% Triton X-100) for 2 h at room temperature. Midguts were then incubated overnight with a rabbit polyclonal anti-APL1C antibody (pAb) [102] (1:600 in PBT) at 4°C. The next day, midguts were rinsed five times (10 min each) with PBT, followed by a 2-hour incubation at room temperature with Alexa Fluor 647-conjugated anti-rabbit IgG secondary antibody (Thermofisher) (1:500 in PBT) at room temperature. Then, midguts were rinsed five times in PBT (10 min each).

Immunostained tissues were counterstained for 10 min with 405 phalloidin-iFluor (actin, 1:1,000 abcam) and subsequently for 10 minutes with DAPI (nuclei, 10 µg/ml, Thermofisher). All incubations were performed with 12 rpm rocking. Lastly, tissues were rinsed in sterile PBS and mounted in Vectashield (Vector Laboratories). Antibody accessibility to whole midgut tissue (permeabilization control) was performed as described above, using anti-GFP Alexa Fluor 647-conjugated primary antibody (Thermofisher).

Confocal Microscopy

Midguts where APL1C signal was subjected for quantitative analysis were imaged on a laser-scanning confocal microscope (LSM700, Carl Zeiss Jena). All acquisitions were configured as follow: pinhole size 1 Airy unit; DAPI/Phalloidin channel: 405nm laser, SP490 filter; APL1C channel: LP640 filter, laser 633nm; images are 1024 x 1024, digitised over 16-bit; Z step interval: 0.33 µm; objective 40x, oil, NA=1.3, Plan-Neofluar. Ookinetes were subjected for microscope analysis using High-speed spinning-disk confocal system [(UltraVIEW ERS; Perkin Elmer, mounted on an inverted Axiovert 200 microscope (Carl Zeiss)].

Image analysis

Images were analysed with Fiji [167]. 3D Images were filtered first with a 3x3 median filter then with a Gaussian filter with sigma=0.7 pixels. The 3D stacks were then projected using Maximum Intensity Projection. A selection was created using an intensity threshold using ImageJ ‘default' method. Finally, **Figure 7B**, **Figure 14C** and **Figure 15C** report the mean intensity for the channel APL1C in the selection.

Dextran injection

Using a Nanoject II injector (Drummond Scientific), cold-anesthetized *A. coluzzii* females were injected intrathoracically with 138 nl of 70 kD dextan 488-conjugate of concentration 10 mg/ml. 1,5 h post-injection, midguts were dissected, fixed and counterstained with DAPI and phalloidin as described above. Injections were performed with a glass capillary needle as previously described[102,168].

Plasmids construction

APL1C and LRIM1 alleles were amplified by PCR from *A. coluzzii* Ngousso mosquitoes using the primers flanking the coding regions of each gene (**Table S6**) and cloned into a dual His- and V5-tag insect expression vector (pAc5.1 V5-His, Invitrogen). To generate a plasmid control, RFP (Red Fluorescent protein) coding sequence from the mammalian expression vector pTagRFP (Evrogen) was cloned in the pAc5.1 V5-His expression vector using EcoRI and NotI restriction enzymes. To ensure RFP protein secretion in the culture medium, the signal sequence from APL1C was amplified from *A. coluzzii* Ngousso mosquitoes with the primers (**Table S6**) and cloned in the pAc5.1 V5-His-RFP expression vector.

Insect cell culture and transfection

A. coluzii derived 4a-3A hemocyte-like cells were cultured in monolayer at 27°C in Insect X press medium (Lonza) supplemented with 5% fetal bovine serum (GIBCO BRL) and 50µg/ml gentamycin (Sigma). Before transfection, 1.10^5 cells were allowed to grow in an 8-wells Lab-Tek chamber slide system (Thermo Scientific) for one hour. Cells were transfected with the expression vector using cellfectin II reagent (Invitrogen) according to the manufacturer's protocol.

Ex vivo midgut assay

24 h post *P.berghei*-infected blood feeding (IBM), *A. coluzzii* Ngousso midguts were dissected in PBS and placed for 2 h at 21°C in culture medium of 4a-3A hemocyte-like cells that were transfected 3 days before with pAc5.1 V5-His-RFP, pAc5.1 V5-His-APL1C or pAc5.1 V5-His-LRIM1 expression vectors. After incubation, transfected cells and dissected midguts treated for immunostaining analysis with a mouse V5 monoclonal antibody (mAb, Invitrogen) at 1:500 or a mouse Pbs28 mAb (without permeabilization)[169], followed by 1 h with Alexa Fluor 594-conjugated anti-mouse IgG secondary antibody at 1:2,000. Nuclei were stained with Hoechst 33342. After mounting in SlowFade Gold antifade reagent (Molecular Probes), samples were observed using a Leica DM 5000 B fluorescent microscope.

Double-stranded RNA synthesis and gene silencing

Double-stranded RNAs were synthesized from PCR amplicons using the T7 Megascript Kit (Ambion) as described previously[102]. The sequences of the primers used for synthesis of dsRNA for each gene are enlisted in Annex **Table S7**. 500 ng of dsRNA were injected into the thorax of cold-anesthetized *A. coluzzii* females using a nano-injector (Nanoject II, Drummond Scientific). dsGFP was used as a control. Treatments were performed with a glass capillary needle as previously described[102,168]. The efficiency of the gene silencing was monitored by quantitative Polymerase Chain Reaction (qPCR) and western blot analysis where specific antibody was available.

RNA extraction and RT

Total RNA was extracted with TRIzol reagent (Invitrogen). cDNAs were generated using M-MLV reverse transcriptase (Invitrogen) from 1 μg of total RNAs in 40 μL.

Quantitative polymerase chain reaction (qPCR)

Using cDNA or genomic DNA, all qPCRs were performed as described in [104], using SYBR green supermix (KAPA SYBR FAST ABI, Sigma-Aldrich) and the CFX96 Touch Real-Time PCR Detection System (Biorad). Ribosomal protein *rpS7* gene was used as an internal control. The quantification of each gene was obtained as a ratio of the *rpS7*. All the primers sequences are enlisted in Annex **Table S7**. Analysis of the expression of transcript relative to *rpS7* was performed according to the 2−ΔΔCt method [170]. PCR conditions of the run were: 95°C for 10min, then 40 cycle of [95°C for 15 sec, 60°C for 1min (plateread), melting curve analysis].

Protein extraction and western blotting from whole mosquitoes

Pools of 8 mosquitoes were placed in tubes containing glass beads with 150µl of freshly prepared 1X RIPA buffer (Cell Signalling) and 1X protease inhibitor cocktail (Roche). Samples were grinded in FastPrep using 3 cycles of 30s with 1400 rpm shaking each (with 30s breaks between each cycle to avoid sample heating). Grinded samples were centrifuged for 5 min, 18,000g, 4°C. Collected supernatant was sonicated in ice and centrifuged for 15 min, 18,000g, 4°C. Reduced protein samples were prepared by adding XT sample buffer (Bio-Rad), 1X DTT and heating at 95°C for 5 min. Samples were loaded and separated on 4-12% Criterion SDS-PAGE gels (Bio-Rad). Protein from equivalent of 0.2 mosquito were transferred to the membrane using Trans-Blot Turbo Transfer System (Bio-Rad), after which immunoblots were blocked for 1 hour in 5% BSA in TBST (Tris-buffered saline, 0.1% Tween 20). Immunoblots were probed overnight with a rabbit pAb anti-APLC antibody at 1:5,000 with 5% BSA in TBST. Next day, membranes were rinsed three times in TBST for 10 minutes each, stained by a mouse anti-GAPDH antibody (Thermofisher) at 1:4,000 and followed by horseradish peroxidase-conjugated anti-mouse IgG secondary antibody (Thermofisher) at 1:8,000, which was used as a loading control. Detection step was

performed using the Enhanced chemiluminescence (ECL) system (Biorad) following the manufacturer's instructions. The levels of APL1C were quantified by densitometry using the Image Lab analysis software (BioRad). To normalize expression, the ratio of the GAPDH density from the control sample to the GAPDH density from sample of interest was determinate as a normalization factor. APL1C band intensity was normalized using GAPDH normalization factor.

Mosquito antibiotic treatment (ATB)

Mosquitoes were treated with an antibiotic (ATB) cocktail: penicillin 62.5 µg/mL, streptomycin 100 µg/mL and gentamicin 50 µg/mL in 10% sucrose solution directly after emergence and were kept under ATB pressure for three days, and ATB solution were changed every day. Mosquitoes treated (+ATB) or non-treated (-ATB) (for control) were fed on naive mouse for 20 min. Unfed mosquitoes were discarded and fed mosquitoes were maintained at 21°C and 70% relative humidity. For the (+ATB) group the antibiotic pressure was maintained after the feeding until their collection for midgut dissection.

Microbiota analysis

Dissection was performed as described previously [171]. Briefly, before dissection, mosquitoes were washed in 75% ethanol for 5 min, and then three times in sterile PBS to eliminate non-attached bacteria, thus preventing bacteria contamination during dissection. For each biological replicate, midguts were collected from each mosquito group (-ATB) and (+ATB), frozen immediately on dry ice and stored at −80°C until processing. To assess antibiotic effectiveness, mosquito midguts from each group (-ATB) and (+ATB) were collected 24h post-feeding. Bacterial DNA was extracted with DNeasy PowerSoil Kit (QIAGEN). The V4 region of the 16S rDNA (Annex, **Table S7**)

was used for measuring the total bacterial abundance by quantitative PCR. DNA samples from each independent biological replicate were used to perform distinct qPCR in triplicate and fold changes obtained between (+ATB) and (-ATB) were combined as a mean and illustrated graphically.

Clodronate-chemical depletion of phagocytic cells

Phagocyte Depletion Using Clodronate Liposomes was performed as previously described [172]. Briefly, female mosquitoes were injected intrathoracically with either 101.2nL of control liposomes (LPs) or CLDs in concentration 1.25mg/ml (standard macrophage depletion kit; Encapsula NanoSciences) using a Nanoject II injector (Drummond Scientific). Liposome treatments were performed 24 h before mosquito exposure to *P. berghei* IBM. The efficiency of phagocytic cell depletions using CLD was tested by measuring the expression level of two phagocytic markers: eater and nirmrodB2 by qPCR comparing CLD and LP injected mosquitoes, using pool of 8 mosquitoes from each batch.

Nitration pathway depletion

Nitration pathway depletion was performed as previously described [128]. Briefly, female mosquitoes were injected intrathoracically with either 1μg of dsNOX5/HPX2 (500ng for each) or dsGFP as a control using a Nanoject II injector (Drummond Scientific). Ds treatments were performed 72 h before mosquito exposure to *P. berghei* IBM. The efficiency of nitration pathway depletion was tested by measuring the expression level of NOX5 and HPX2 by RT-qPCR between dsNOX5/HPX2 and dsGFP injected mosquitoes prior to IBM (72h post treatment) and 24h post IBM (96h post treatment) from pool of 8 mosquitoes from each batch.

Sporozoite salivary glands collection

The salivary glands (SG) from infected mosquitoes were collected at day 19 post infection (10 days post ds GFP and dsAPL1C treatment), as previously reported with minor modifications[173]. Briefly, mosquitoes were rinsed one time in ethanol and two times in PBS. Then, each mosquito was placed on the glass side with PBS. Mosquito dissection and SG collections were gently performed under the stereomicroscope using the needles of the insulin syringes. SG were collected separately for each mosquito. Briefly, each pair of isolated SG was placed separately and individually in a 1.5-ml microcentrifuge tube containing 20µl of 1× PBS on ice. Then each tube was gently crushed with a pestle for microtubes in order to release the sporozoites from the salivary glands. The solution was homogenized by vigorous pipetting. Sporozoites were shortly centrifuged on the 35µm filter to remove remaining salivary glands debrides. 10 µl of the solution was placed in a Kova slide. Once the parasites were settled, presence and number of sporozoites were measured with an epifluorescence microscope using a GFP filter.

Hemolymph sporozoites IFA

Mosquitoes were perfused with 4% PFA in 1xPBS straight to poly-L-lysine microscopy chamber (Ibidi GmbH). Slides were centrifuged for 2 min at 500g and fixed for 30min with subsequent centrifugation for 2min at 500g centrifugation in order to settle down the sporozoites. Fixed samples were rinsed three times in PBS and blocked for one hour in 1% BSA and 1X PBS prior to overnight incubation with anti-APL1C pAb (1:300 in 1% BSA in 1X PBS) at 4°C with 12 rpm rocking. The next day, samples were rinsed three times in 1% BSA in 1X PBS for 10 minutes each and incubated for two h with the secondary anti-rabbit Alexa Fluor 647 antibody (Thermofisher) diluted 1:500 in 1% BSA and 1X PBS at room temperature with 12 rpm rocking. Then, samples were rinsed three times in 1% BSA and 1X PBS for 10 minutes each and stained with DAPI.

Immunostained samples were rinsed in PBS and observed under the inverted Axio Observer fluorescence microscope (ZEISS).

Statistical analyses

Differences in APL1C protein signal intensity in midguts were tested using Wilcoxon–Mann–Whitney test. All statistical differences were first tested independently within replicates (individual p-values in Annex, **Table S1**), and if individual replicates showed a common trend of change, then individual p-values were combined using the meta-analytical approach of Fisher[174]. For qPCR analysis using the 2−ΔΔCt method, difference in deltaCt distribution across the independent biological replicates was statistically tested using Student t-test. For western blot analysis, normalized band intensity was compared by Student t-test. Differences in salivary glands infection prevalence were tested using the Chi-Square test. All statistical differences were first tested independently within replicates (individual p-values in Annex, **Table S2**), and if individual replicates showed a common trend of change, individual p-values were combined using the meta-analytical approach of Fisher[174].

3’ Rapid Amplification of cDNA Ends (3’RACE)

Total RNA from pool of 8 females were subjected to a first strand cDNA synthesis at the poly(A) tail of mRNA using the adapter primer (AP) according to the manufacturer (Invitrogen). Amplification of 3’ fragments of APL1A and APL1C were performed by PCR. Two rounds of PCR were performed: first, using the with Gene-Specific Primers (GSPs) designed for each APL1A and APL1C and producer provided Abridged Universal Amplification Primer (AUAP) that targets the cDNA complementary to the 3’ end of mRNA. Second PCR round was performed with a second, nested-GSP for APL1A and APL1C (Annex **Table S7**) and AUAP primers. For each gene, GST and

nested-GST were located before stop codon of the reference gene sequences. The PCR amplicons were subsequently cloned using TOPO cloning system (Invitrogen) and plasmids were collected, purified (QIAGEN) and subjected for sequencing.

RNA sequencing experiment and bioinformatic analysis

RNA sequencing

Anopheles mosquitoes were injected with dsGFP, dsAPL1A or dsAPL1C. For each condition, a pool of 8 mosquitoes was collected at 12 h post-treatment. Total RNA extractions from intact mosquitoes were performed on each pool using TRIzol reagent (Invitrogen). This experiment was repeated four times, yielding to a total number of 12 samples. All RNA-seq was performed at the University of Minnesota Genomics Center (genomics.umn.edu).

Details for RNA sequencing experiment and analysis

Prior to the library composition, RNA from each sample was quantified using fluorimetry (RiboGreen assay) and RNA integrity was assessed using capillary electrophoresis (Agilent BioAnalyzer), generating an RNA Integrity Number (RIN). After passing quality check, libraries were prepared according to TruSeq Stranded mRNA library creation. Samples were sequenced using NextSeq 150SR High-Output (400M reads/lane) ±33M reads/sample.

Differentially expressed genes were identified through bioinformatic analysis, performed according to the pipeline depicted in Annex, **Figure S6**. The quality of the raw reads was checked with FastQC version 0.10.1[175] and multiqc version 1.7 [176]. All the sequenced samples contained more than 33M reads, which were assumed by the sequencing run (Annex, **Figure S7**). The FastQC analysis proved overall high quality of the analysed sequences within each sample file. Performed analysis detected

presence of the adapter sequence among all of the sample files. Therefore, remaining adapter sequences were trimmed with cutadapt[177] version 1.9.1 and remaining dsAPL1A and dsAPL1C fragments were removed using samtools version 1.9[178]. Spliced Transcripts Alignment to a Reference (STAR) alignment tool [179] version 2.5.0a was used for alignment against the reference genome of *Anopheles gambiae* str. PEST version AgamP4 (from VectorBase). Reads summarization was performed using featureCounts version 1.6.1[180]. Counts data were analysed with SARTools package[181], using R version 3.6.1 (R Core Team (2018). R: A language and environment for statistical computing. R Foundation for Statistical Computing, Vienna, (Austria), and the Bioconductor package DESeq2 version 1.24.0[182] using default parameters. Due to the batch effect caused by time difference of RNA collection between replicate nr 1 and replicates nr 2, 3 and 4, the replicate nr 1 was excluded from the final RNAseq analysis. A generalized linear model was applied in order to test for inter-condition differences. For each pairwise comparison, raw p-values were adjusted for multiple testing using the Benjamini and Hochberg procedure[130]. Genes with adjusted p-values below 0.05 were considered differentially expressed.

Figures: 1, 2, 6, 20, 22, 29, S1, S5, S6 were created with BioRender.com

REFERENCES

1 Chandrasegaran, K., Lahondere, C., Escobar, L. E. & Vinauger, C. Linking Mosquito Ecology, Traits, Behavior, and Disease Transmission. *Trends Parasitol* **36**, 393-403, (2020).

2 Rosenberg, R. & Beard, C. B. Vector-borne infections. *Emerg Infect Dis* **17**, 769-770, (2011).

3 WHO_World_Malaria_Report_2019. WHO_World_Malaria_Report_2019.

4 Cox, F. E. G. History of the discovery of the malaria parasites and their vectors. *Parasites & Vectors* **3**, 5, (2010).

5 Chernin, E. Sir Patrick Manson: an annotated bibliography and a note on a collected set of his writings. *Rev Infect Dis* **5**, 353-386, (1983).

6 Hagan, P. & Chauhan, V. Ronald Ross and the problem of malaria. *Parasitology Today* **13**, 290-295, (1997).

7 Patterson, G. M. Looking Backward, Looking Forward: The Long, Torturous Struggle with Mosquitoes. *Insects* **7**, (2016).

8 Becker, N. *et al.* in *Mosquitoes and Their Control* 433-439 (Springer Berlin Heidelberg, 2010).

9 Rieckmann, K. H. The chequered history of malaria control: are new and better tools the ultimate answer? *Ann Trop Med Parasitol* **100**, 647-662, (2006).

10 Raghavendra, K., Barik, T. K., Reddy, B. P. N., Sharma, P. & Dash, A. P. Malaria vector control: from past to future. *Parasitology Research* **108**, 757-779, (2011).

11 Bhatt, S. *et al.* The effect of malaria control on Plasmodium falciparum in Africa between 2000 and 2015. *Nature* **526**, 207-211, (2015).

12 Keiser, J., Singer, B. H. & Utzinger, J. Reducing the burden of malaria in different eco-epidemiological settings with environmental management: a systematic review. *The Lancet Infectious Diseases* **5**, 695-708, (2005).

13 Benelli, G. & Beier, J. C. Current vector control challenges in the fight against malaria. *Acta Tropica* **174**, 91-96, (2017).

14 Liu, N. Insecticide Resistance in Mosquitoes: Impact, Mechanisms, and Research Directions. *Annual Review of Entomology* **60**, 537-559, (2015).

15 Wilson, A. L. *et al.* The importance of vector control for the control and elimination of vector-borne diseases. *PLOS Neglected Tropical Diseases* **14**, e0007831, (2020).

16 Jayaraj, R., Megha, P. & Sreedev, P. Organochlorine pesticides, their toxic effects on living organisms and their fate in the environment. *Interdiscip Toxicol* **9**, 90-100, (2016).

17 Ogunah, J. A., Lalah, J. O. & Schramm, K.-W. Malaria vector control strategies. What is appropriate towards sustainable global eradication? *Sustainable Chemistry and Pharmacy* **18**, 100339, (2020).

18 HELI.

19 Cohuet, A., Harris, C., Robert, V. & Fontenille, D. Evolutionary forces on Anopheles: what makes a malaria vector? *Trends Parasitol* **26**, 130-136, (2010).

20 Beerntsen, B. T., James, A. A. & Christensen, B. M. Genetics of mosquito vector competence. *Microbiol Mol Biol Rev* **64**, 115-137, (2000).

21 Powell, J. R. An evolutionary perspective on vector-borne diseases. *Frontiers in Genetics* **10**, (2019).

22 Carter, R. & Mendis, K. N. Evolutionary and historical aspects of the burden of malaria. *Clin Microbiol Rev* **15**, 564-594, (2002).

23 Tuteja, R. Malaria − an overview. *The FEBS Journal* **274**, 4670-4679, (2007).

24 White, N. J. Plasmodium knowlesi: the fifth human malaria parasite. *Clin Infect Dis* **46**, 172-173, (2008).

25 Davidson, G. Anopheles gambiae Complex. *Nature* **196**, 907-907, (1962).

26 Coluzzi, M., Sabatini, A., della Torre, A., Di Deco, M. A. & Petrarca, V. A Polytene Chromosome Analysis of the Anopheles gambiae Species Complex. *Science* **298**, 1415-1418, (2002).

27 Riehle, M. M. *et al.* A cryptic subgroup of Anopheles gambiae is highly susceptible to human malaria parasites. *Science* **331**, 596-598, (2011).

28 Aly, A. S. I., Vaughan, A. M. & Kappe, S. H. I. Malaria Parasite Development in the Mosquito and Infection of the Mammalian Host. *Annual Review of Microbiology* **63**, 195-221, (2009).

29 Siciliano, G. & Alano, P. Enlightening the malaria parasite life cycle: bioluminescent Plasmodium in fundamental and applied research. *Frontiers in microbiology* **6**, (2015).

30 Josling, G. A. & Llinás, M. Sexual development in Plasmodium parasites: knowing when it's time to commit. *Nature Reviews Microbiology* **13**, 573-587, (2015).

31 Vlachou, D., Schlegelmilch, T., Runn, E., Mendes, A. & Kafatos, F. C. The developmental migration of Plasmodium in mosquitoes. *Current opinion in genetics & development* **16**, 384-391, (2006).

32 Baton, L. A. & Ranford-Cartwright, L. C. Spreading the seeds of million-murdering death: metamorphoses of malaria in the mosquito. *Trends Parasitol* **21**, 573-580, (2005).

33 Shahabuddin, M. Plasmodium ookinete development in the mosquito midgut: a case of reciprocal manipulation. *Parasitology* **116 Suppl**, S83-93, (1998).

34 Guttery, D. S., Holder, A. A. & Tewari, R. Sexual Development in Plasmodium: Lessons from Functional Analyses. *PLOS Pathogens* **8**, e1002404, (2012).

35 Smith, R. C. & Barillas-Mury, C. Plasmodium oocysts: overlooked targets of mosquito immunity. *Trends in parasitology* **32**, 979-990, (2016).

36 Siciliano, G. *et al.* Critical Steps of Plasmodium falciparum Ookinete Maturation. *Frontiers in microbiology* **11**, 269, (2020).

37 White, B. J., Collins, F. H. & Besansky, N. J. Evolution of Anopheles gambiae in Relation to Humans and Malaria. *Annual Review of Ecology, Evolution, and Systematics* **42**, 111-132, (2011).

38 Smith, R. C., Vega-Rodriguez, J. & Jacobs-Lorena, M. The Plasmodium bottleneck: malaria parasite losses in the mosquito vector. *Mem Inst Oswaldo Cruz* **109**, 644-661, (2014).

39 Pumpuni, C. B., Demaio, J., Kent, M., Davis, J. R. & Beier, J. C. Bacterial population dynamics in three anopheline species: the impact on Plasmodium sporogonic development. *The American journal of tropical medicine and hygiene* **54**, 214-218, (1996).

40 Rodgers, F. H., Gendrin, M., Wyer, C. A. S. & Christophides, G. K. Microbiota-induced peritrophic matrix regulates midgut homeostasis and prevents systemic infection of malaria vector mosquitoes. *PLoS Pathog* **13**, e1006391, (2017).

41 Jupatanakul, N., Sim, S. & Dimopoulos, G. The insect microbiome modulates vector competence for arboviruses. *Viruses* **6**, 4294-4313, (2014).

42 Dong, Y., Manfredini, F. & Dimopoulos, G. Implication of the mosquito midgut microbiota in the defense against malaria parasites. *PLoS Pathog* **5**, e1000423, (2009).

43 Wang, S. & Jacobs-Lorena, M. Genetic approaches to interfere with malaria transmission by vector mosquitoes. *Trends in Biotechnology* **31**, 185-193, (2013).

44 Sinden, R. E. Plasmodium differentiation in the mosquito. *Parassitologia* **41**, 139-148, (1999).

45 Rosenberg, R. & Rungsiwongse, J. The Number of Sporozoites Produced by Individual Malaria Oocysts. *The American Journal of Tropical Medicine and Hygiene* **45**, 574-577, (1991).

46 Hillyer, J. F., Barreau, C. & Vernick, K. D. Efficiency of salivary gland invasion by malaria sporozoites is controlled by rapid sporozoite destruction in the mosquito haemocoel. *International journal for parasitology* **37**, 673-681, (2007).

47 Graumans, W., Jacobs, E., Bousema, T. & Sinnis, P. When Is a Plasmodium-Infected Mosquito an Infectious Mosquito? *Trends in Parasitology* **36**, 705-716, (2020).

48 Barrangou, R. & Marraffini, L. A. CRISPR-Cas systems: Prokaryotes upgrade to adaptive immunity. *Mol Cell* **54**, 234-244, (2014).

49 Charles A. Janeway, J. & Medzhitov, R. Innate Immune Recognition. *Annual Review of Immunology* **20**, 197-216, (2002).

50 Cooper, M. D. & Herrin, B. R. How did our complex immune system evolve? *Nature Reviews Immunology* **10**, 2-3, (2010).

51 Buchmann, K. Evolution of Innate Immunity: Clues from Invertebrates via Fish to Mammals. *Frontiers in Immunology* **5**, (2014).

52 Govind, S. Innate immunity in Drosophila: Pathogens and pathways. *Insect Sci* **15**, 29-43, (2008).

53 Buchon, N., Silverman, N. & Cherry, S. Immunity in Drosophila melanogaster--from microbial recognition to whole-organism physiology. *Nat Rev Immunol* **14**, 796-810, (2014).

54 Enkhbayar, P., Kamiya, M., Osaki, M., Matsumoto, T. & Matsushima, N. Structural principles of leucine-rich repeat (LRR) proteins. *Proteins* **54**, 394-403, (2004).

55 Govind, S. Control of development and immunity by rel transcription factors in Drosophila. *Oncogene* **18**, 6875-6887, (1999).

56 Anderson, K. V., Jurgens, G. & Nusslein-Volhard, C. Establishment of dorsal-ventral polarity in the Drosophila embryo: genetic studies on the role of the Toll gene product. *Cell* **42**, 779-789, (1985).

57 Valanne, S., Wang, J.-H. & Rämet, M. The Drosophila Toll Signaling Pathway. *The Journal of Immunology* **186**, 649-656, (2011).

58 Rutschmann, S., Kilinc, A. & Ferrandon, D. Cutting edge: the toll pathway is required for resistance to gram-positive bacterial infections in Drosophila. *J Immunol* **168**, 1542-1546, (2002).

59 Anderson, K. V. Toll signaling pathways in the innate immune response. *Curr Opin Immunol* **12**, 13-19, (2000).

60 Arnot, C. J., Gay, N. J. & Gangloff, M. Molecular mechanism that induces activation of Spatzle, the ligand for the Drosophila Toll receptor. *The Journal of biological chemistry* **285**, 19502-19509, (2010).

61 Hu, X., Yagi, Y., Tanji, T., Zhou, S. & Ip, Y. T. Multimerization and interaction of Toll and Spätzle in Drosophila. *Proceedings of the National Academy of Sciences of the United States of America* **101**, 9369-9374, (2004).

62 Ooi, J. Y., Yagi, Y., Hu, X. & Ip, Y. T. The Drosophila Toll-9 activates a constitutive antimicrobial defense. *EMBO Rep* **3**, 82-87, (2002).

63 Nakamoto, M. *et al.* Virus recognition by Toll-7 activates antiviral autophagy in Drosophila. *Immunity* **36**, 658-667, (2012).

64 Xu, Y. *et al.* Structural basis for signal transduction by the Toll/interleukin-1 receptor domains. *Nature* **408**, 111-115, (2000).

65 Brennan, C. A. & Anderson, K. V. Drosophila: The Genetics of Innate Immune Recognition and Response. *Annual Review of Immunology* **22**, 457-483, (2004).

66 Leulier, F. & Lemaitre, B. Toll-like receptors--taking an evolutionary approach. *Nat Rev Genet* **9**, 165-178, (2008).

67 Abreu, M. T. & Arditi, M. Innate immunity and toll-like receptors: clinical implications of basic science research. *The Journal of Pediatrics* **144**, 421-429, (2004).

68 Kawai, T. & Akira, S. TLR signaling. *Seminars in Immunology* **19**, 24-32, (2007).

69 Jin, M. S. *et al.* Crystal structure of the TLR1-TLR2 heterodimer induced by binding of a tri-acylated lipopeptide. *Cell* **130**, 1071-1082, (2007).

70 Medzhitov, R. Toll-like receptors and innate immunity. *Nature Reviews Immunology* **1**, 135-145, (2001).

71 Oliveira-Nascimento, L., Massari, P. & Wetzler, L. M. The Role of TLR2 in Infection and Immunity. *Front Immunol* **3**, 79, (2012).

72 Lee, B. L. & Barton, G. M. Trafficking of endosomal Toll-like receptors. *Trends Cell Biol* **24**, 360-369, (2014).

73 Langjahr, P. *et al.* Metalloproteinase-dependent TLR2 ectodomain shedding is involved in soluble toll-like receptor 2 (sTLR2) production. *PLoS One* **9**, e104624, (2014).

74 LeBouder, E. *et al.* Soluble Forms of Toll-Like Receptor (TLR)2 Capable of Modulating TLR2 Signaling Are Present in Human Plasma and Breast Milk. *The Journal of Immunology* **171**, 6680-6689, (2003).

75 Cattaneo, C. *et al.* Analysis of Toll-Like Receptors in Human Milk: Detection of Membrane-Bound and Soluble Forms. *J Immunol Res* **2019**, 4078671, (2019).

76 Akira, S., Takeda, K. & Kaisho, T. Toll-like receptors: critical proteins linking innate and acquired immunity. *Nature Immunology* **2**, 675-680, (2001).

77 Medzhitov, R. & Janeway, C., Jr. The Toll receptor family and microbial recognition. *Trends Microbiol* **8**, 452-456, (2000).

78 Takeda, K. & Akira, S. TLR signaling pathways. *Seminars in Immunology* **16**, 3-9, (2004).

79 El-Zayat, S. R., Sibaii, H. & Mannaa, F. A. Toll-like receptors activation, signaling, and targeting: an overview. *Bulletin of the National Research Centre* **43**, 187, (2019).

80 Viala, J., Sansonetti, P. & Philpott, D. J. Nods and 'intracellular' innate immunity. *Comptes Rendus Biologies* **327**, 551-555, (2004).

81 Schroder, K. & Tschopp, J. The inflammasomes. *Cell* **140**, 821-832, (2010).

82 Wilmanski, J. M., Petnicki-Ocwieja, T. & Kobayashi, K. S. NLR proteins: integral members of innate immunity and mediators of inflammatory diseases. *Journal of Leukocyte Biology* **83**, 13-30, (2008).

83 Franchi, L., Warner, N., Viani, K. & Nunez, G. Function of Nod-like receptors in microbial recognition and host defense. *Immunol Rev* **227**, 106-128, (2009).

84 Athman, R. & Philpott, D. Innate immunity via Toll-like receptors and Nod proteins. *Current opinion in microbiology* **7**, 25-32, (2004).

85 Bonardi, V., Cherkis, K., Nishimura, M. T. & Dangl, J. L. A new eye on NLR proteins: focused on clarity or diffused by complexity? *Current Opinion in Immunology* **24**, 41-50, (2012).

86 Padmanabhan, M., Cournoyer, P. & Dinesh-Kumar, S. The leucine-rich repeat domain in plant innate immunity: a wealth of possibilities. *Cellular microbiology* **11**, 191-198, (2009).

87 Chisholm, S. T., Coaker, G., Day, B. & Staskawicz, B. J. Host-microbe interactions: shaping the evolution of the plant immune response. *Cell* **124**, 803-814, (2006).

88 DeYoung, B. J. & Innes, R. W. Plant NBS-LRR proteins in pathogen sensing and host defense. *Nature immunology* **7**, 1243-1249, (2006).

89 Takken, F. L. & Goverse, A. How to build a pathogen detector: structural basis of NB-LRR function. *Current opinion in plant biology* **15**, 375-384, (2012).

90 Belkhadir, Y., Subramaniam, R. & Dangl, J. L. Plant disease resistance protein signaling: NBS–LRR proteins and their partners. *Current opinion in plant biology* **7**, 391-399, (2004).

91 Pancer, Z. *et al.* Somatic diversification of variable lymphocyte receptors in the agnathan sea lamprey. *Nature* **430**, 174-180, (2004).

92 Sutoh, Y. & Kasahara, M. The immune system of jawless vertebrates: insights into the prototype of the adaptive immune system. *Immunogenetics*, (2020).

93 Herrin, B. R. *et al.* Structure and specificity of lamprey monoclonal antibodies. *Proceedings of the National Academy of Sciences* **105**, 2040-2045, (2008).

94 Alder, M. N. *et al.* Diversity and function of adaptive immune receptors in a jawless vertebrate. *Science* **310**, 1970-1973, (2005).

95 Herrin, B. R. & Cooper, M. D. Alternative adaptive immunity in jawless vertebrates. *The Journal of Immunology* **185**, 1367-1374, (2010).

96 Christophides, G. K. *et al.* Immunity-Related Genes and Gene Families in Anopheles gambiae. *Science* **298**, 159-165, (2002).

97 Nene, V. *et al.* Genome sequence of Aedes aegypti, a major arbovirus vector. *Science* **316**, 1718-1723, (2007).

98 Mitri, C. & Vernick, K. D. Anopheles gambiae pathogen susceptibility: the intersection of genetics, immunity and ecology. *Current opinion in microbiology* **15**, 285-291, (2012).

99 Riehle, M. M. *et al.* Natural malaria infection in Anopheles gambiae is regulated by a single genomic control region. *Science* **312**, 577-579, (2006).

100 Menge, D. M. *et al.* Quantitative trait loci controlling refractoriness to Plasmodium falciparum in natural Anopheles gambiae mosquitoes from a malaria-endemic region in western Kenya. *Genetics* **173**, 235-241, (2006).

101 Riehle, M. M. *et al.* A major genetic locus controlling natural Plasmodium falciparum infection is shared by East and West African Anopheles gambiae. *Malar J* **6**, 87, (2007).

102 Riehle, M. M. *et al.* Anopheles gambiae APL1 is a family of variable LRR proteins required for Rel1-mediated protection from the malaria parasite, Plasmodium berghei. *PLoS One* **3**, e3672, (2008).

103 Mitri, C. *et al.* Fine pathogen discrimination within the APL1 gene family protects Anopheles gambiae against human and rodent malaria species. *PLoS Pathog* **5**, e1000576, (2009).

104 Mitri, C. *et al.* An evolution-based screen for genetic differentiation between Anopheles sister taxa enriches for detection of functional immune factors. *PLoS pathogens* **11**, (2015).

105 Rottschaefer, S. M. *et al.* Exceptional diversity, maintenance of polymorphism, and recent directional selection on the APL1 malaria resistance genes of Anopheles gambiae. *PLoS biology* **9**, (2011).

106 Holm, I. *et al.* Diverged alleles of the Anopheles gambiae leucine-rich repeat gene APL1A display distinct protective profiles against Plasmodium falciparum. *PloS one* **7**, (2012).

107 Waterhouse, R. M., Povelones, M. & Christophides, G. K. Sequence-structure-function relations of the mosquito leucine-rich repeat immune proteins. *BMC Genomics* **11**, 531, (2010).

108 Baxter, R. H. *et al.* A heterodimeric complex of the LRR proteins LRIM1 and APL1C regulates complement-like immunity in Anopheles gambiae. *Proceedings of the National Academy of Sciences of the United States of America* **107**, 16817-16822, (2010).

109 Povelones, M., Waterhouse, R. M., Kafatos, F. C. & Christophides, G. K. Leucine-rich repeat protein complex activates mosquito complement in defense against Plasmodium parasites. *Science* **324**, 258-261, (2009).

110 Fraiture, M. *et al.* Two Mosquito LRR Proteins Function as Complement Control Factors in the TEP1-Mediated Killing of Plasmodium. *Cell host & microbe* **5**, 273-284, (2009).

111 Povelones, M., Upton, L. M., Sala, K. A. & Christophides, G. K. Structure-function analysis of the Anopheles gambiae LRIM1/APL1C complex and its interaction with complement C3-like protein TEP1. *PLoS Pathog* **7**, e1002023, (2011).

112 Christophides, G. K. *et al.* Immunity-related genes and gene families in Anopheles gambiae. *Science* **298**, 159-165, (2002).

113 Osta, M. A., Christophides, G. K. & Kafatos, F. C. Effects of mosquito genes on Plasmodium development. *Science* **303**, 2030-2032, (2004).

114 Moita, L. F. *et al.* In vivo identification of novel regulators and conserved pathways of phagocytosis in A. gambiae. *Immunity* **23**, 65-73, (2005).

115 Blandin, S. *et al.* Complement-like protein TEP1 is a determinant of vectorial capacity in the malaria vector Anopheles gambiae. *Cell* **116**, 661-670, (2004).

116 Baxter, R. H. *et al.* Structural basis for conserved complement factor-like function in the antimalarial protein TEP1. *Proceedings of the National Academy of Sciences* **104**, 11615-11620, (2007).

117 Blandin, S. A., Marois, E. & Levashina, E. A. Antimalarial responses in Anopheles gambiae: from a complement-like protein to a complement-like pathway. *Cell host & microbe* **3**, 364-374, (2008).

118 Ricklin, D., Hajishengallis, G., Yang, K. & Lambris, J. D. Complement: a key system for immune surveillance and homeostasis. *Nat Immunol* **11**, 785-797, (2010).

119 Le, B. V., Williams, M., Logarajah, S. & Baxter, R. H. Molecular basis for genetic resistance of Anopheles gambiae to Plasmodium: structural analysis of TEP1 susceptible and resistant alleles. *PLoS Pathog* **8**, e1002958, (2012).

120 Levashina, E. A. *et al.* Conserved role of a complement-like protein in phagocytosis revealed by dsRNA knockout in cultured cells of the mosquito, Anopheles gambiae. *Cell* **104**, 709-718, (2001).

121 Blandin, S. A. *et al.* Dissecting the genetic basis of resistance to malaria parasites in Anopheles gambiae. *Science* **326**, 147-150, (2009).

122 Reyes Ruiz, V. M. *et al.* Stimulation of a protease targeting the LRIM1/APL1C complex reveals specificity in complement-like pathway activation in Anopheles gambiae. *PloS one* **14**, (2019).

123 Reddy, J. T. & Locke, M. The size limited penetration of gold particles through insect basal laminae. *Journal of Insect Physiology* **36**, 397-407, (1990).

124 Vernick, K. D., Fujioka, H. & Aikawa, M. Plasmodium gallinaceum: a novel morphology of malaria ookinetes in the midgut of the mosquito vector. *Exp Parasitol* **91**, 362-366, (1999).

125 Ukegbu, C. V. *et al.* Plasmodium berghei P47 is essential for ookinete protection from the Anopheles gambiae complement-like response. *Scientific reports* **7**, 6026, (2017).

126 Volohonsky, G. *et al.* Kinetics of Plasmodium midgut invasion in Anopheles mosquitoes. *bioRxiv*, 2020.2002.2006.937276, (2020).

127 Kwon, H. & Smith, R. C. Chemical depletion of phagocytic immune cells in Anopheles gambiae reveals dual roles of mosquito hemocytes in anti-Plasmodium immunity. *Proceedings of the National Academy of Sciences* **116**, 14119-14128, (2019).

128 Castillo, J. C., Ferreira, A. B. B., Trisnadi, N. & Barillas-Mury, C. Activation of mosquito complement antiplasmodial response requires cellular immunity. *Science immunology* **2**, (2017).

129 Blandin, S. *et al.* Complement-like protein TEP1 is a determinant of vectorial capacity in the malaria vector Anopheles gambiae. *Cell* **116**, 661-670, (2004).

130 Benjamini, Y. & Hochberg, Y. Controlling the false discovery rate: A practical and powerful approach to multiple testing. JR Statist. Soc. B, 57, 289–300. *Find this article online*, (1995).

131 Blandin, S. & Levashina, E. A. Thioester-containing proteins and insect immunity. *Molecular Immunology* **40**, 903-908, (2004).

132 Povelones, M. *et al.* The CLIP-domain serine protease homolog SPCLIP1 regulates complement recruitment to microbial surfaces in the malaria mosquito Anopheles gambiae. *PLoS pathogens* **9**, (2013).

133 Veillard, F., Troxler, L. & Reichhart, J.-M. Drosophila melanogaster clip-domain serine proteases: Structure, function and regulation. *Biochimie* **122**, 255-269, (2016).

134 Kanost, M. R. & Jiang, H. Clip-domain serine proteases as immune factors in insect hemolymph. *Current opinion in insect science* **11**, 47-55, (2015).

135 Yassine, H., Kamareddine, L., Chamat, S., Christophides, G. K. & Osta, M. A. A serine protease homolog negatively regulates TEP1 consumption in systemic infections of the malaria vector Anopheles gambiae. *J Innate Immun* **6**, 806-818, (2014).

136 Abraham, E. G. *et al.* An immune-responsive serpin, SRPN6, mediates mosquito defense against malaria parasites. *Proceedings of the National Academy of Sciences of the United States of America* **102**, 16327-16332, (2005).

137 Pinto, S. B., Kafatos, F. C. & Michel, K. The parasite invasion marker SRPN6 reduces sporozoite numbers in salivary glands of Anopheles gambiae. *Cell Microbiol* **10**, 891-898, (2008).

138 Meister, S. *et al.* Immune signaling pathways regulating bacterial and malaria parasite infection of the mosquito Anopheles gambiae. *Proceedings of the National Academy of Sciences of the United States of America* **102**, 11420-11425, (2005).

139 Dong, Y., Taylor, H. E. & Dimopoulos, G. AgDscam, a hypervariable immunoglobulin domain-containing receptor of the Anopheles gambiae innate immune system. *PLoS Biol* **4**, e229, (2006).

140 Oliveira Gde, A., Lieberman, J. & Barillas-Mury, C. Epithelial nitration by a peroxidase/NOX5 system mediates mosquito antiplasmodial immunity. *Science* **335**, 856-859, (2012).

141 Kajla, M. *et al.* Silencing of Anopheles stephensi Heme Peroxidase HPX15 Activates Diverse Immune Pathways to Regulate the Growth of Midgut Bacteria. *Frontiers in microbiology* **7**, 1351, (2016).

142 Salzet, M., Deloffre, L., Breton, C., Vieau, D. & Schoofs, L. The angiotensin system elements in invertebrates. *Brain Res Brain Res Rev* **36**, 35-45, (2001).

143 Abu Hasan, Z. *et al.* The toxicity of angiotensin converting enzyme inhibitors to larvae of the disease vectors Aedes aegypti and Anopheles gambiae. *Scientific reports* **7**, 45409, (2017).

144 Burnham, S., Smith, J. A., Lee, A. J., Isaac, R. E. & Shirras, A. D. The angiotensin-converting enzyme (ACE) gene family of Anopheles gambiae. *BMC Genomics* **6**, 172, (2005).

145 Ekbote, U., Looker, M. & Isaac, R. E. ACE inhibitors reduce fecundity in the mosquito, Anopheles stephensi. *Comp Biochem Physiol B Biochem Mol Biol* **134**, 593-598, (2003).

146 Midega, J. *et al.* Discovery and characterization of two Nimrod superfamily members in Anopheles gambiae. *Pathog Glob Health* **107**, 463-474, (2013).

147 Bi, W. J. *et al.* Scavenger receptor B protects shrimp from bacteria by enhancing phagocytosis and regulating expression of antimicrobial peptides. *Developmental and comparative immunology* **51**, 10-21, (2015).

148 Zaidman-Remy, A. *et al.* The Drosophila amidase PGRP-LB modulates the immune response to bacterial infection. *Immunity* **24**, 463-473, (2006).

149 Kurata, S. Peptidoglycan recognition proteins in Drosophila immunity. *Dev Comp Immunol* **42**, 36-41, (2014).

150 Neyen, C., Poidevin, M., Roussel, A. & Lemaitre, B. Tissue- and ligand-specific sensing of gram-negative infection in drosophila by PGRP-LC isoforms and PGRP-LE. *J Immunol* **189**, 1886-1897, (2012).

151 Schnitger, A. K., Yassine, H., Kafatos, F. C. & Osta, M. A. Two C-type lectins cooperate to defend Anopheles gambiae against Gram-negative bacteria. *J Biol Chem* **284**, 17616-17624, (2009).

152 Bishnoi, R. *et al.* Solution structure, glycan specificity and of phenol oxidase inhibitory activity of Anopheles C-type lectins CTL4 and CTLMA2. *Scientific reports* **9**, 15191, (2019).

153 Matsushita, M. The Complement System of Agnathans. *Front Immunol* **9**, 1405, (2018).

154 Castillo, J. C., Robertson, A. E. & Strand, M. R. Characterization of hemocytes from the mosquitoes Anopheles gambiae and Aedes aegypti. *Insect Biochem Mol Biol* **36**, 891-903, (2006).

155 Hillyer, J. F. & Strand, M. R. Mosquito hemocyte-mediated immune responses. *Current opinion in insect science* **3**, 14-21, (2014).

156 Luckhart, S., Vodovotz, Y., Cui, L. & Rosenberg, R. The mosquito Anopheles stephensi limits malaria parasite development with inducible synthesis of nitric oxide. *Proceedings of the National Academy of Sciences of the United States of America* **95**, 5700-5705, (1998).

157 Kumar, S. & Barillas-Mury, C. Ookinete-induced midgut peroxidases detonate the time bomb in anopheline mosquitoes. *Insect biochemistry and molecular biology* **35**, 721-727, (2005).

158 Pompon, J. & Levashina, E. A. A New Role of the Mosquito Complement-like Cascade in Male Fertility in Anopheles gambiae. *PLoS Biol* **13**, e1002255, (2015).

159 Okuda, K. *et al.* Cell death and regeneration in the midgut of the mosquito, Culex quinquefasciatus. *J Insect Physiol* **53**, 1307-1315, (2007).

160 Viljakainen, L. Evolutionary genetics of insect innate immunity. *Brief Funct Genomics* **14**, 407-412, (2015).

161 Wang, X., Zhang, Y., Zhang, R. & Zhang, J. The diversity of pattern recognition receptors (PRRs) involved with insect defense against pathogens. *Current opinion in insect science* **33**, 105-110, (2019).

162 Ghosh, J. *et al.* Invertebrate immune diversity. *Developmental and comparative immunology* **35**, 959-974, (2011).

163 Mitri, C. *et al.* Gene copy number and function of the APL1 immune factor changed during Anopheles evolution. *Parasites & vectors* **13**, 18, (2020).

164 Redmond, S. N. *et al.* Association mapping by pooled sequencing identifies TOLL 11 as a protective factor against Plasmodium falciparum in Anopheles gambiae. *BMC genomics* **16**, 779, (2015).

165 Ishino, T., Orito, Y., Chinzei, Y. & Yuda, M. A calcium-dependent protein kinase regulates Plasmodium ookinete access to the midgut epithelial cell. *Mol Microbiol* **59**, 1175-1184, (2006).

166 Bhattacharyya, M. K. & Kumar, N. Effect of xanthurenic acid on infectivity of Plasmodium falciparum to Anopheles stephensi. *Int J Parasitol* **31**, 1129-1133, (2001).

167 Schindelin, J. *et al.* Fiji: an open-source platform for biological-image analysis. *Nat Methods* **9**, 676-682, (2012).

168 Blandin, S. *et al.* Reverse genetics in the mosquito Anopheles gambiae: targeted disruption of the Defensin gene. *EMBO Rep* **3**, 852-856, (2002).

169 Simonetti, A. B., Billingsley, P. F., Winger, L. A. & Sinden, R. E. Kinetics of expression of two major Plasmodium berghei antigens in the mosquito vector, Anopheles stephensi. *J Eukaryot Microbiol* **40**, 569-576, (1993).

170 Livak, K. J. & Schmittgen, T. D. Analysis of relative gene expression data using real-time quantitative PCR and the 2− ΔΔCT method. *methods* **25**, 402-408, (2001).

171 Gendrin, M. *et al.* Antibiotics in ingested human blood affect the mosquito microbiota and capacity to transmit malaria. *Nat Commun* **6**, 5921, (2015).

172 Kwon, H. & Smith, R. C. Chemical depletion of phagocytic immune cells in Anopheles gambiae reveals dual roles of mosquito hemocytes in anti-Plasmodium immunity. *Proc Natl Acad Sci U S A* **116**, 14119-14128, (2019).

173 Tavares, J., Formaglio, P., Medvinsky, A., Ménard, R. & Amino, R. in *Malaria* 401-410 (Springer, 2012).

174 Fisher, R. A. in *Mathematical Proceedings of the Cambridge Philosophical Society.* 700-725 (Cambridge University Press).

175 Andrews, S. (Babraham Bioinformatics, Babraham Institute, Cambridge, United Kingdom, 2010).

176 Ewels, P., Magnusson, M., Lundin, S. & Kaller, M. MultiQC: summarize analysis results for multiple tools and samples in a single report. *Bioinformatics* **32**, 3047-3048, (2016).

177 Martin, M. Cutadapt removes adapter sequences from high-throughput sequencing reads. *2011* **17**, 3, (2011).

178 Li, H. *et al.* The Sequence Alignment/Map format and SAMtools. *Bioinformatics* **25**, 2078-2079, (2009).

179 Dobin, A. *et al.* STAR: ultrafast universal RNA-seq aligner. *Bioinformatics* **29**, 15-21, (2013).

180 Liao, Y., Smyth, G. K. & Shi, W. featureCounts: an efficient general purpose program for assigning sequence reads to genomic features. *Bioinformatics* **30**, 923-930, (2014).

181 Varet, H., Brillet-Gueguen, L., Coppee, J. Y. & Dillies, M. A. SARTools: A DESeq2- and EdgeR-Based R Pipeline for Comprehensive Differential Analysis of RNA-Seq Data. *PLoS One* **11**, e0157022, (2016).

182 Love, M. I., Huber, W. & Anders, S. Moderated estimation of fold change and dispersion for RNA-seq data with DESeq2. *Genome Biol* **15**, 550, (2014).

ANNEX

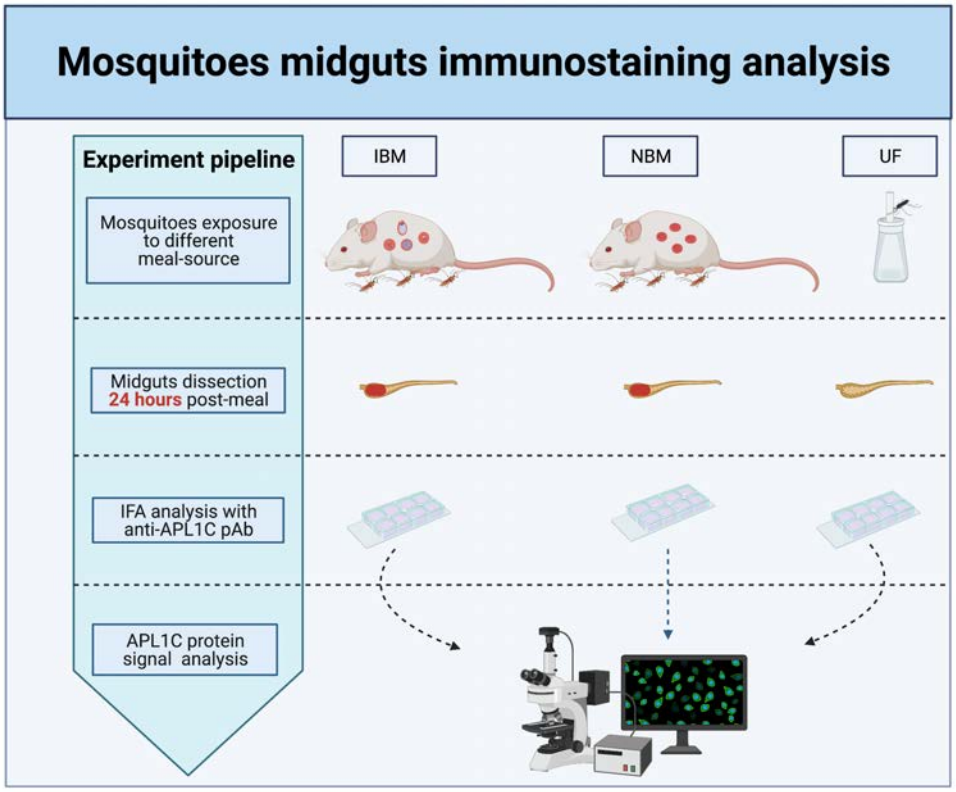

Figure S1. Workflow of IFA experiment. Mosquito midguts were dissected 24 h after *Plasmodium* infected bloodmeal (IBM), non-infected bloodmeal (NBM) or unfed (UF) and immunoassayed using anti-APL1C pAb. The signal corresponding to APL1C protein presence on the midguts was captured by laser scanning microscope (LSM), quantified by ImageJ v1.52p and the signal intensity from each midgut was compared between the tested conditions by Mann-Whitney test.

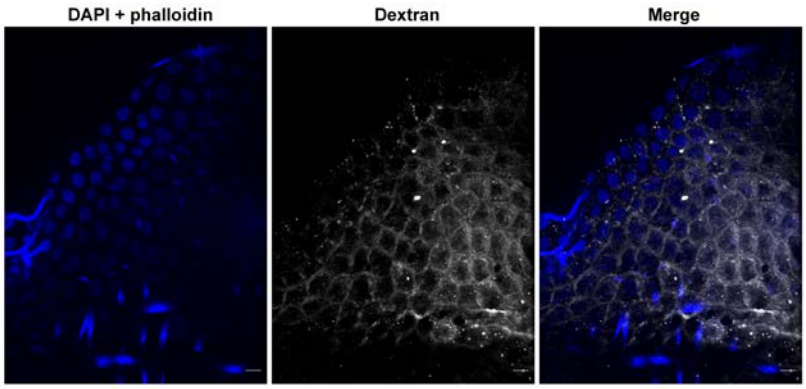

Figure S2. Mosquito hemolymph-injected dextran diffuses on mosquito midguts in a way resembling APL1C protein deposition. Immunostaining analysis of the midguts from dextran-injected mosquitoes shows that dextran diffuses through basal lamina and is deposed on the tissue. The scale bar is 10µm.

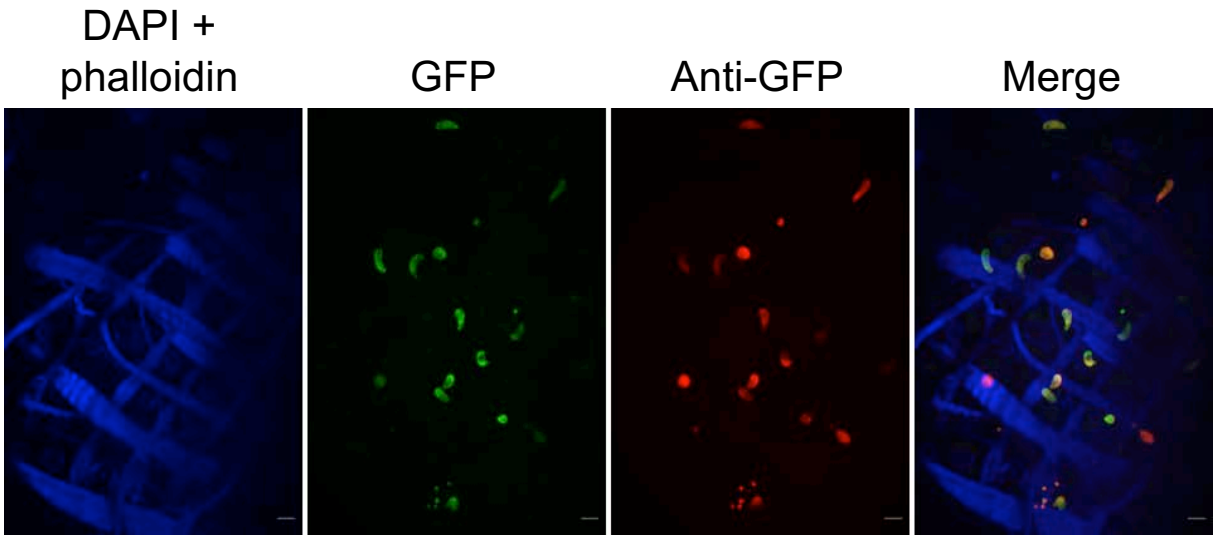

Figure S3. Tissue permeabilization enables antibody access to all the parasites present in mosquito midguts. IFA of *P. berghei*-infected mosquito midguts collected 24 h post-IBM and immunostained with anti-GFP conjugated antibody. GFP-expressing ookinetes (green) are also associated with anti-GFP protein (red). Nuclei and actin were stained with DAPI and Phalloidin (blue). The scale bar is 10 µm.

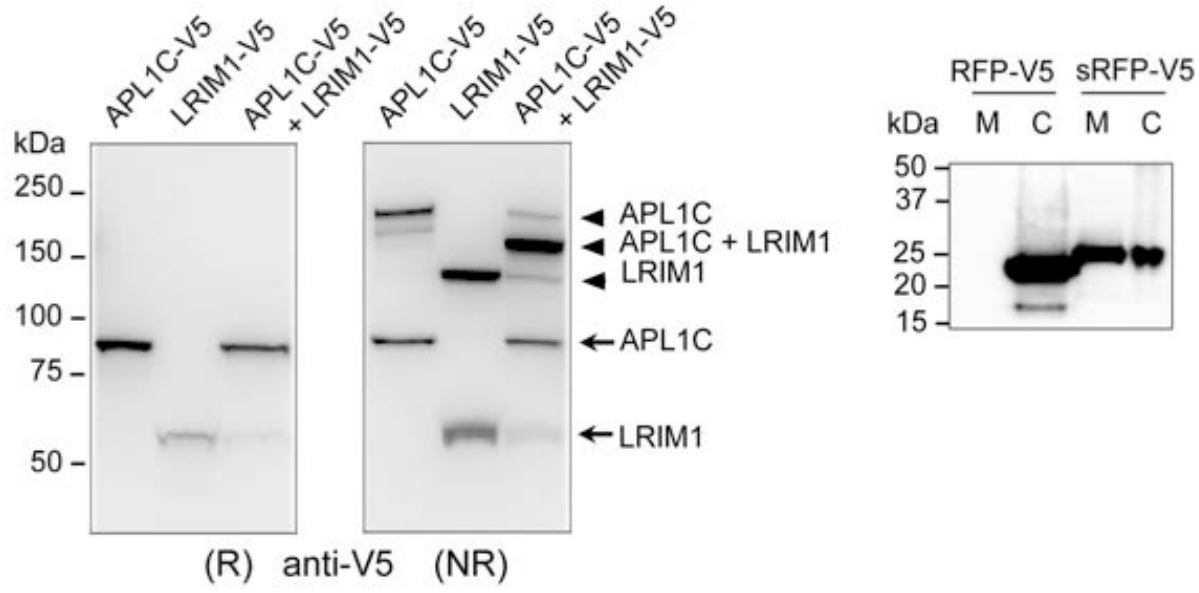

Figure S4. V5-tagged protein constructs are secreted from hemocyte-like cells. A. Immunoblot analysis using a mouse anti-V5 mAb and culture medium of the 4a3A hemocyte-like cell line transfected with plasmids encoding V5-tagged APL1C and LRIM1 under reducing (R) and non-reducing (NR) conditions. Estimated sizes of monomeric APL1C and LRIM1 forms including V5-tag are: 88 kDa (APL1C) and 60 kDa (LRIM1), respectively. The results show

that both V5-APL1C and V5-LRIM1 are secreted in the medium. **B.** Immunoblot analysis of cells (C) and culture medium (M) of the 4a3A hemocyte-like cell line transfected with plasmids encoding V5-tagged RFP (V5-RFP) and V5-tagged RFP fused with the signal sequence from APL1C (sRFP). Immunoblot was probed with a mouse anti-V5 mAb.

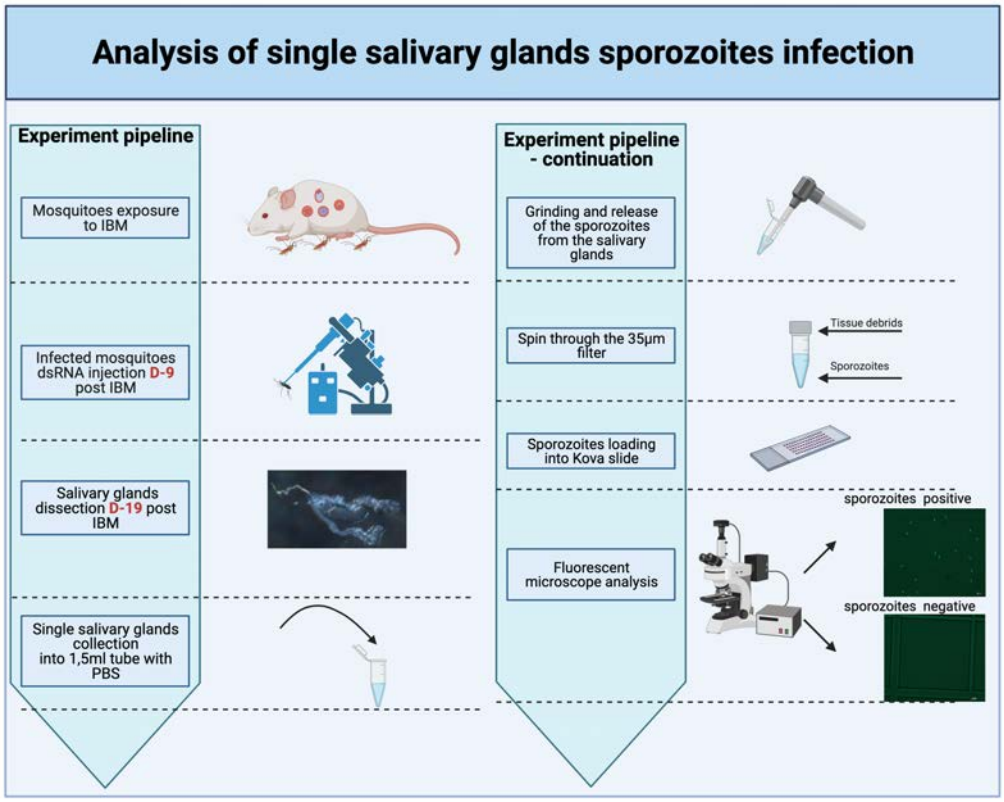

Figure S5. Workflow of salivary glands infection prevalence and intensity analysis after dsRNA treatment. Mosquitoes were injected 9 d post IBM with dsRNAs (dsAPL1C, dsTEP1, dsTEP3 or co-injected with dsTEP1/dsTEP3). DsGFP-injected mosquitoes served as a control. In the case of double treatment (dsTEP1/dsTEP3), a double dose of dsGFP was also injected in the control group. Salivary glands were dissected 19 d post IBM (10 d post dsRNA treatment) and collected separately in 1,5 ml tube with 20 µl of PBS. Sporozoites were released from the salivary gland tissues by grinding and filtering in order to get rid of tissue debrides. The collected sporozoites containing flow-through were subsequently loaded into a Kova slide and screened for measuring sporozoites infection prevalence and intensity.

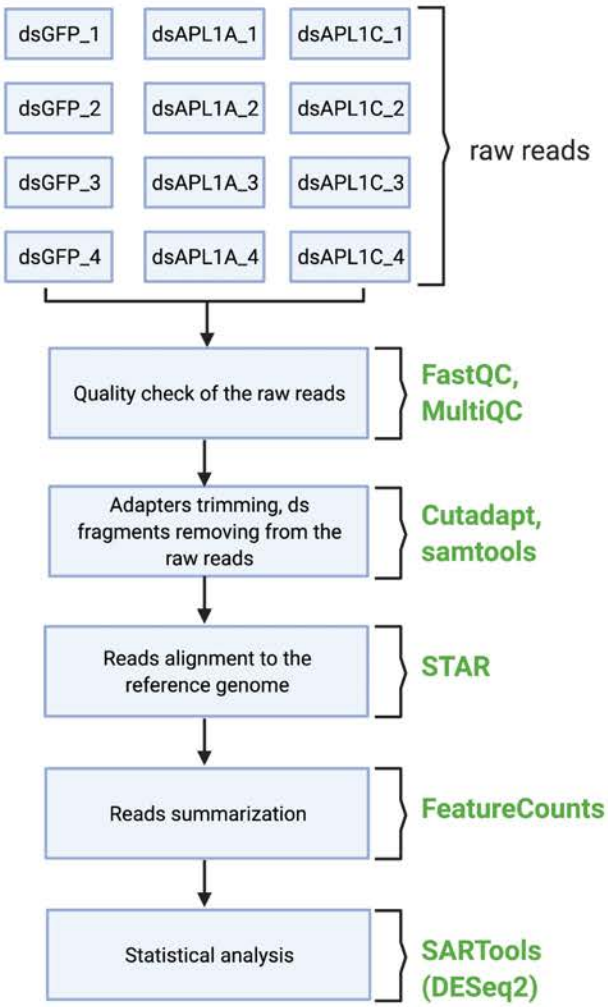

Figure S6. RNAseq bioinformatic analysis pipeline that identified differentially expressed genes in APL1A and APL1C depleted mosquitoes. Each step of the analysis is presented in blue bracket, and the bioinformatic tools used for each step are indicated in green font.

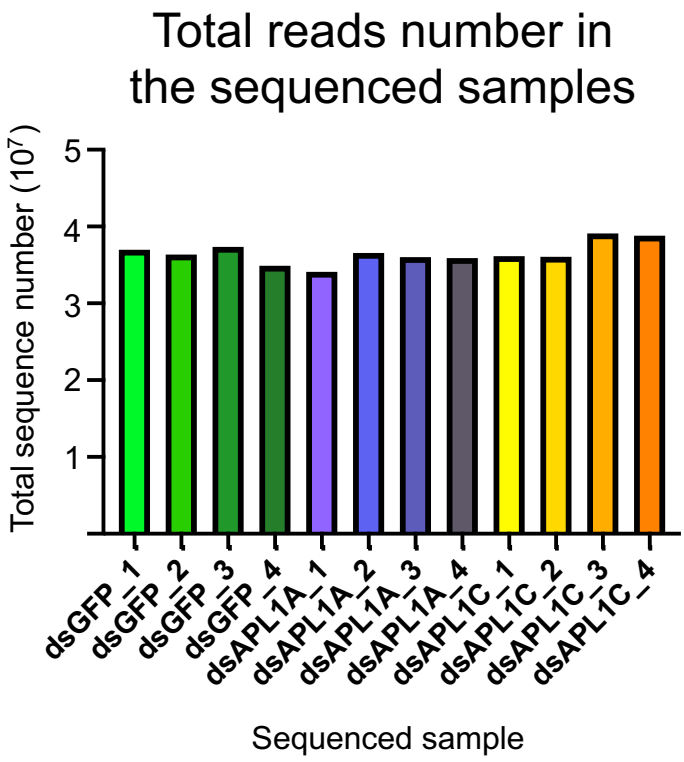

2592

2593 **Figure S7. Total sequence number reported in the RNAseq analysis for all the studied**
2594 **samples. The results show that all samples displayed a close total number of reads (30-**
2595 **40 M reads).**

Experiment #	Figure #[a]	Condition	Number of mosquitoes	Tested conditions	Median values [b]			individual p-value [c]	Fisher combined prob.[d]
1	7B	UF	4	-	-	-	-	-	-
2		UF	5	-	-	-	-	-	-
3		UF	4	-	-	-	-	-	-
4		UF	10	-	-	-	-	-	-
1		NBM	6	NBM vs UF	1,11E+08	vs	1,64E+07	0,0095	< 0.0001
2		NBM	4	NBM vs UF	1,20E+08	vs	3,28E+05	0,0159	
3		NBM	6	NBM vs UF	3,48E+08	vs	6,56E+06	0,0095	
4		NBM	10	NBM vs UF	1,78E+08	vs	3,03E+06	<0,0001	
3		IBM	5	IBM vs UF	6,06E+07	vs	6,56E+06	0,0317	< 0.0001
4		IBM	11	IBM vs UF	3,88E+08	vs	3,03E+06	<0,0001	
-	-	-	-	NBM vs IBM	3,48E+08	vs	6,06E+07	0,1775	NA
-	-	-	-	NBM vs IBM	1,78E+08	vs	3,88E+08	0,5573	
5	14C	LP	8	-	-	-	-	-	-
6		LP	8	-	-	-	-	-	-
7		LP	8	-	-	-	-	-	-
5		CLD	6	CLD vs LP	9,37E+06	vs	3,52E+07	0,0813	0,0087
6		CLD	10	CLD vs LP	1,42E+07	vs	1,19E+08	0,0676	
7		CLD	10	CLD vs LP	1,80E+07	vs	1,04E+08	0,0343	
8	15C	dsGFP	6	-	-	-	-	-	-
9		dsGFP	6	-	-	-	-	-	-
10		dsGFP	8	-	-	-	-	-	-
8		dsNOX5/HPX2	6	dsNOX5/HPX2 vs dsGFP	2,82E+07	vs	1,98E+08	0,0152	< 0.0001
9		dsNOX5/HPX2	7	dsNOX5/HPX2 vs dsGFP	3,25E+06	vs	7,05E+07	0,0012	
10		dsNOX5/HPX2	8	dsNOX5/HPX2 vs dsGFP	3,70E+07	vs	1,46E+08	0,0379	

[a] The corresponding figure numbers associated with the data.

[b] Median values of tested conditions in each replicate.

[c] Statistical differences for APL1C signal intensity on the midguts were tested in each replicate using the Wilcoxon–Mann–Whitney test.

[d] This p-value was calculated using the method of R.A. Fisher to combine independent tests of significance[174]. Notation NA (Not Applicable) indicates that the direction of phenotypic effect among experimental replicates was not consistent and therefore replicates were not statistically combined.

Table S1. Statistical analysis of APL1C signal on mosquito midguts. Summary data for all experimental replicates testing the APL1C protein signal as compared to control treatment. Statistically significant differences are indicated by green shading. Rows indicate the treatment for a given replicate, the experiment number, the number of mosquitoes used for the statistical analysis. Individual p-values were calculated for each replicate by statistical comparison between the corresponding control experiment shown in the column “Experiment #” and indicated in "Tested conditions" column. If the different replicates of a tested condition were consistent (display the same phenotypic direction), then the individual p-values were combined by Fisher's method “Fisher combined prob”. If the replicate phenotypes were not consistent, the individual p-values are shown but combining of p-values is not justified.

Experiment #	Figure # [a]	Injected dsRNA	Number of mosquitoes	Salivary glands infection prevalence (%)	Infection prevalence - individual p-value [b]	Infection prevalence - Fisher combined prob. [c]	Salivary glands infection intensity (median)	Infection intensity - individual p-value [d]	Infection intensity - Fisher combined prob. [c]
1	17C	dsGFP	30	70	-	-	-	-	-
2		dsGFP	20	25	-	-	6,40E+03	-	-
3		dsGFP	20	65	-	-	2,40E+03	-	-
4		dsGFP	36	47,22	-	-	2,90E+03	-	-
1		dsAPL1C	30	96,67	0,0056	< 0.0001	-	-	-
2		dsAPL1C	9	100	0,0002		4,44E+02	0,1898	NA
3		dsAPL1C	34	84,85	0,0942		4,25E+03	0,5657	
4		dsAPL1C	32	75	0,0195		1,90E+03	0,642	
5	19B	dsGFP	18	61,11	-	-	6,00E+03	-	
6		dsGFP	36	50	-	-	6,39E+02	-	-
7		dsGFP	27	48,15	-	-	4,20E+03	-	-
8		dsGFP	40	72,5	-	-	5,10E+03	-	-
5		dsTEP1	23	73,91	0,382	0,21	2,90E+03	0,4233	0,3517485
6		dsTEP1	43	67,44	0,1158		6,00E+02	0,598	
7		dsTEP1	26	61,54	0,3276		6,50E+02	0,1402	
5		dsTEP3	21	76,19	0,3091	0,26	2,55E+03	0,1303	NA
6		dsTEP3	36	63,89	0,234		5,80E+03	0,0035	
7		dsTEP1/TEP3	20	60	0,4208	0,57	1900	0,6591	NA
8		dsTEP1/TEP3	24	79,17	0,551		8,40E+03	0,4738	

[a] The corresponding figure numbers associated with data.

[b] Statistical differences for salivary glands infection prevalence were tested for each replicate (target gene vs dsGFP control) using the $\chi 2$ test.

[c] This p value was calculated using the method of R.A. Fisher to combine independent tests of significance[174]. Notation NA (Not Applicable) indicates that the direction of phenotypic effect among experimental replicates was not consistent and therefore replicates were not statistically combined.

[d] Statistical differences for salivary glands infection intensity were tested for each replicate (dstarget gene vs dsGFP control) using the Wilcoxon–Mann–Whitney test.

Table S2. Statistical analysis of *P. berghei* salivary glands infection prevalence following gene silencing. Summary data for all experimental replicates testing the effect of a targeted gene silencing as compared to control treatment dsGFP. Statistically significant differences are indicated by green shading. Rows indicate target gene tested (injected dsRNA) for a given replicate, with the corresponding replicates indicated in the following row(s) . Individual p-values were calculated for each replicate by statistical comparison between the dsRNA-targeted gene and the corresponding dsGFP control showed in column “Experiment #”. If the different replicates of a tested gene were consistent (display the same phenotypic direction), then the individual p-values were combined by Fisher's method “Fisher combined

prob". If the replicate phenotypes were not consistent, the individual p-values are shown but combining of p-values is not justified.

dsGFP	dsAPL1C
2 745	6 652

Table S3. APL1C controls sporozoite intensity in mosquito hemolymph. APL1C depletion results in higher number of sporozoites present in mosquito hemolymph. Infected mosquitoes were perfused 17 d post-*P. berghei* infection (8 d post dsAPL1C or dsGFP treatment). The number of perfused sporozoites was counted in both studied conditions and reported in the table.

ANNEX

Gene ID	Gene name	FoldChange	log2FoldChange	p-adj	Gene description	Gene description source
AGAP005503	SDR11	0,06	-4,055	3,95E-07	dehydrogenase/reductase SDR family member 11 precursor	VB
AGAP007033	APL1C	0,151	-2,726	2,90E-17	Anopheles Plasmodium-responsive Leucine-Rich Repeat 1C	VB
AGAP010058	PAS1	0,227	-2,139	0,0115104	neuronal PAS domain protein 1	VB
AGAP009217	CLIPB12	0,243	-2,043	0,01173398	CLIP-domain serine protease	VB
AGAP001669	CPR6	0,324	-1,625	0,04941549	cuticular protein RR-2 family 6	VB
AGAP008512	8512	0,332	-1,59	1,48E-05	NodB homology domain, Glycoside hydrolase/deacetylase, beta/alpha-barrel	IP
AGAP000113	113	0,341	-1,552	2,79E-07	Peptidase M14, carboxypeptidase A Cytosolic carboxypeptidase, N-terminal	IP
AGAP011509	COEunkn	0,359	-1,478	0,0087826	carboxylesterase	VB
AGAP013201	3201	0,363	-1,462	0,04950774	Ecdysteroid kinase-like, Protein kinase-like domain superfamily, CHK kinase-like	IP
AGAP006400	APH2	0,403	-1,31	0,00950344	alkaline phosphatase 2	VB
AGAP007319	7319	0,432	-1,212	0,00889759	N/A	N/A
AGAP010057		0,44	-1,186	0,02827811	nicotinic acetylcholine receptor, beta-2 subunit	VB
AGAP008444	CPLCG1	0,446	-1,164	0,00160066	cuticular protein CPLCG family (CPLCG1)	VB
AGAP010854	SCF45	0,453	-1,141	0,00952942	solute carrier family 45, member 1/2/4	VB
AGAP011564	GGT	0,455	-1,137	0,04950774	glucosyl/glucuronosyl transferases	VB
AGAP012648		0,46	-1,121	0,03487263	Sulfotransferase domain, P-loop containing nucleoside triphosphate hydrolase	IP
AGAP029110	9110	0,469	-1,093	0,02867749	C-type lectin-like/link domain superfamily	IP
AGAP003334	CPLCX2	0,474	-1,077	0,02778496	cuticular protein unclassified	VB
AGAP001748	ChS	0,476	-1,072	0,01545946	chitin synthase	VB
AGAP029383		0,477	-1,069	0,04961506	Pyruvate kinase, C-terminal domain superfamily	IP
AGAP001470	1470	0,486	-1,041	0,00667323	Leucine-rich repeat, typical subtype	IP
AGAP005496	LRIM12	0,487	-1,039	0,01760889	leucine-rich immune protein (Short)	VB
AGAP028512		0,504	-0,99	0,02877573	N/A	N/A
AGAP005459	CPR16	0,505	-0,985	0,028741	cuticular protein RR-1 family 16	VB
AGAP003600		0,508	-0,978	0,02279322	Elongation of very long chain fatty acids protein	UP
AGAP006480		0,509	-0,974	0,03487263	N/A	N/A
AGAP013507		0,509	-0,974	0,01960246	N/A	N/A
AGAP001969		0,51	-0,972	0,04950774	polyubiquitin	VB
AGAP009623	GAPDH	0,513	-0,964	0,0115104	glyceraldehyde 3-phosphate dehydrogenase	VB
AGAP007045	LRIM15	0,514	-0,961	0,01484981	leucine-rich immune protein (TM)	VB
AGAP013192		0,514	-0,96	0,04875578	venom allergen	VB
AGAP028028	LRIM16A	0,514	-0,959	0,01173009	Leucine-rich immune protein (TM)	UP
AGAP010814	TEP6	0,517	-0,952	0,0238129	thioester-containing protein 6	VB
AGAP003692		0,518	-0,948	0,03379828	Aminopeptidase	UP
AGAP007416		0,519	-0,945	0,02784284	SMAD domain, Dwarfin-type, SMAD/FHA domain superfamily	IP
AGAP005952		0,52	-0,943	0,01964634	N/A	N/A
AGAP001594		0,526	-0,926	7,71E-05	GNAT domain, Acyl-CoA N-acyltransferase	IP
AGAP008368	TEP14	0,527	-0,924	0,03909671	thioester-containing protein 14	VB
AGAP029054	NimB2	0,527	-0,923	0,01800364	nimrod B2	VB
AGAP000424		0,528	-0,921	0,03250892	N/A	N/A
AGAP004809	APN1	0,528	-0,92	0,00889759	alanyl aminopeptidase N 1	VB
AGAP009871	CPR75	0,531	-0,913	0,01317147	cuticular protein RR-1 family 75	VB
AGAP012718		0,535	-0,903	0,00057426	proline oxidase	VB
AGAP028064	LRIM16B	0,535	-0,901	0,04181769	Leucine-rich immune protein (TM)	UP
AGAP006898	Cht6	0,537	-0,897	0,03680706	chitinase	VB
AGAP013245		0,538	-0,894	0,03922705	N/A	N/A
AGAP010385		0,545	-0,875	0,03182168	N/A	N/A
AGAP010562		0,546	-0,872	0,03494485	Amino acid/polyamine transporter I, Cationic amino acid transporter, C-terminal	IP
AGAP003060		0,55	-0,861	4,37E-05	N/A	N/A
AGAP008209	CYP6M1	0,552	-0,858	0,00645541	cytochrome P450	VB
AGAP004799		0,553	-0,856	0,0005304	N/A	N/A
AGAP002204	CYP325D1	0,554	-0,853	0,03487263	cytochrome P450	VB
AGAP001603		0,557	-0,845	0,0114621	mitochondrial 18 kDa protein	VB
AGAP003354	A5R3	0,557	-0,845	0,01317147	antigen 5 related protein 3	VB
AGAP028680		0,558	-0,842	0,02503675	Leucine-rich repeat, cysteine-containing subtype, F-box domain	IP
AGAP028612		0,563	-0,828	0,0330731	N/A	N/A
AGAP003695		0,571	-0,807	0,02075811	aminopeptidase N	VB
AGAP008091	CLIPE1	0,573	-0,804	0,00051006	CLIP-domain serine protease	VB
AGAP003775		0,575	-0,798	0,04464053	N/A	N/A
AGAP029055		0,577	-0,793	0,02215262	EGF-like domain	IP
AGAP005837	COEJHE5E	0,58	-0,786	0,01173009	carboxylesterase	VB
AGAP007717		0,581	-0,783	0,03161692	SH3 domain	IP
AGAP028167		0,581	-0,783	0,03383209	Proteinase, regulatory CLIP domain, Serine proteases, trypsin domain, Peptidase S1A, chymotrypsin family, Peptidase S1, PA clan	IP
AGAP013061		0,582	-0,781	0,02160989	Haemolymph juvenile hormone binding, Takeout superfamily	IP
AGAP001375	SRPN12	0,587	-0,768	0,01173398	serine protease inhibitor (serpin) 12	VB
AGAP029185		0,587	-0,768	0,03890513	CBM21 (carbohydrate binding type-21) domain	IP
AGAP001181		0,588	-0,767	0,01484981	N/A	N/A
AGAP001344		0,593	-0,754	0,04919363	Transcription factor, T-box p53-like transcription factor, DNA-binding	IP
AGAP013202		0,596	-0,746	0,03049047	N/A	N/A
AGAP011666		0,598	-0,742	0,01271696	N/A	N/A
AGAP005094		0,599	-0,74	0,0114621	Protein of unknown function DUF1397	IP
AGAP011911		0,606	-0,722	0,04405244	F-box protein 39	UP
AGAP000198	Cht5-5	0,607	-0,719	0,03823344	Chitinase	UP

2644

AGAP029297		0,611	-0,711	0,03524546	Major facilitator superfamily	IP
AGAP001486		0,612	-0,707	0,04822763	N/A	N/A
AGAP005450		0,621	-0,687	0,03414776	Kazal domain	IP
AGAP011749		0,621	-0,687	0,0179084	Major facilitator superfamily domain	IP
AGAP029820		0,621	-0,686	0,01484981	ATP:guanido phosphotransferase, Glutamine synthetase/guanido kinase, catalytic domain	IP
AGAP006835		0,627	-0,674	0,02237205	N/A	N/A
AGAP008059	CSP1	0,628	-0,671	0,0179084	chemosensory protein 1	VB
AGAP009415		0,629	-0,668	0,01811537	lysophosphatidate acyltransferase	VB
AGAP009982		0,63	-0,666	0,00551591	N/A	N/A
AGAP013459		0,632	-0,662	0,02129007	N/A	N/A
AGAP004936		0,638	-0,649	0,02341124	EGF-like domain	IP
AGAP007974	drm	0,638	-0,649	0,02362829	Protein drumstick	UP
AGAP011341		0,641	-0,641	0,02984576	Ets domain, Pointed domain, Sterile alpha motif/pointed domain superfamily, Winged helix DNA-binding domain superfamily	IP
AGAP007349		0,642	-0,64	0,02867749	N/A	IP
AGAP013106		0,644	-0,635	0,0478941	Niemann-Pick Type C-2	VB
AGAP003038		0,648	-0,625	0,02373187	Major facilitator, sugar transporter-like, Sugar transporter, conserved site	IP
AGAP005470		0,648	-0,625	0,01426511	N/A	IP
AGAP007786		0,648	-0,625	0,03909671	isocitrate dehydrogenase (NAD+)	VB
AGAP007939		0,649	-0,624	0,04375476	starch phosphorylase	VB
AGAP000986	CPAP3-D	0,652	-0,618	0,04997375	cuticular protein	VB
AGAP001417		0,658	-0,603	0,03653976	Brain protein 44-like protein	VB
AGAP001052		0,66	-0,598	0,04989706	ubiquitin carboxyl-terminal hydrolase 2/21	VB
AGAP001799		0,661	-0,598	0,03494485	tropomyosin 1	VB
AGAP006260		0,661	-0,597	0,0478941	Z band alternatively spliced PDZ-motif protein 66	VB
AGAP003860		0,665	-0,588	0,01650848	proline dehydrogenase	VB
AGAP008640		0,666	-0,586	0,02488032	N/A	N/A
AGAP010229		0,666	-0,586	0,03282155	beta-ureidopropionase	VB
AGAP004846	SCRB9	0,667	-0,583	0,01746087	Class B Scavenger Receptor (CD36 domain).	VB
AGAP012515	ATPsynF	0,667	-0,584	0,01746087	F-type H+-transporting ATPase subunit f	VB
AGAP012643		0,668	-0,581	0,00979108	solute carrier family 7 (cationic amino acid transporter, y+ system)	VB
AGAP007611		0,669	-0,579	0,0179084	SEA domain, EGF-like domain, Cellulose/chitin-binding protein, N-terminal, DOMON domain, Galactose-binding-like domain superfamily	IP
AGAP009200		0,669	-0,579	0,03564164	collagen type IV alpha	VB
AGAP011355		0,671	-0,576	0,04483169	Domain of unknown function DB, Immunoglobulin subtype 2, Fibronectin type III	IP
AGAP029127	CSP5	0,672	-0,574	0,03681021	chemosensory protein 5	VB
AGAP001313		0,673	-0,571	0,02279322	Muscular protein 20	VB
AGAP005010		0,673	-0,572	0,0055572	Homeobox KN domain, Iroquois-class homeodomain protein	IP
AGAP004643	SCRB6	0,674	-0,569	0,0114621	Class B Scavenger Receptor (CD36 domain).	VB
AGAP010145		0,674	-0,569	0,03681021	Yellow	UP
AGAP010230		0,675	-0,566	0,0112639	MAGUK p55 subfamily member 3	VB
AGAP001303	SAP1	0,676	-0,564	0,02450875	chemosensory protein 6	VB
AGAP003620		0,678	-0,56	0,01890109	N/A	N/A
AGAP006900		0,678	-0,56	0,04961506	Zinc finger, RING-type, Lon, substrate-binding domain, Tetratricopeptide-like helical domain superfamily, PUA-like superfamily	IP
AGAP005878		0,682	-0,552	0,04464053	POU domain transcription factor, class 3	VB
AGAP028061		0,682	-0,551	0,01261935	Protein SOGA	IP
AGAP004834		0,683	-0,549	0,02318625	PMP-22/EMP/MP20/Claudin superfamily	IP
AGAP008400		0,683	-0,551	0,00979108	Laminin G domain, Concanavalin A-like lectin/glucanase domain superfamily, CSPG repeat	IP
AGAP002859		0,684	-0,548	0,02847867	solute carrier family 8 (sodium/calcium exchanger)	VB
AGAP007876		0,684	-0,549	0,01327857	N/A	N/A
AGAP001582		0,688	-0,54	0,03681021	Ankyrin repeat-containing domain superfamily	IP
AGAP005043		0,688	-0,541	0,03187828	Inactive dipeptidyl peptidase 10	VB
AGAP004263	TO1	0,689	-0,538	0,00889759	takeout 1	VB
AGAP007061		0,69	-0,535	0,03487263	Leucine-rich repeat, typical subtype	IP
AGAP012447	GLURIIe	0,691	-0,534	0,03823344	ionotropic receptor GLURIIe	VB
AGAP010193	CTLGA3	0,693	-0,529	0,03441075	C-type lectin (CTL) - galactose binding	VB
AGAP010891		0,694	-0,528	0,03225499	ariadne-1	VB
AGAP029564		0,694	-0,527	0,03718961	Immunoglobulin-like domain, CD80-like, immunoglobulin C2-set	IP
AGAP007849		0,695	-0,526	0,03049047	laminin, alpha 1/2	VB
AGAP007963		0,695	-0,525	0,0282315	Sarcoplasmic calcium-binding protein	VB
AGAP009224		0,695	-0,525	0,02705207	GroES-like superfamily, Polyketide synthase, enoylreductase domain, NAD(P)-binding domain superfamily	IP
AGAP012256		0,695	-0,525	0,04528598	Polypeptide N-acetylgalactosaminyltransferase	UP
AGAP012399		0,696	-0,523	0,01850004	maltase	VB
AGAP028496		0,7	-0,514	0,02222595	Zinc finger C2HC domain-containing protein	IP
AGAP001369		0,701	-0,512	0,03282155	SH3 domain, IMD/I-BAR domain, AH/BAR domain superfamily, I-BAR domain containing protein IRSp53/IRTKS/Pinkbar	IP
AGAP006452		0,701	-0,513	0,03681021	Thioredoxin domain	IP
AGAP007373		0,701	-0,512	0,03379828	Tetraspanin	UP
AGAP010233		0,701	-0,512	0,025216	integrin beta 1	VB

2645

AGAP004457		0,702	-0,51	0,03718961	Sugar transporter ERD6-like 4	VB
AGAP004237		0,704	-0,505	0,03182418	nuclear lamin L1 alpha	VB
AGAP001413		0,705	-0,505	0,02373187	N/A	N/A
AGAP006179		0,706	-0,502	0,01271696	troponin C	VB
AGAP002456		0,707	-0,5	0,03049047	P-loop containing nucleoside triphosphate hydrolase, Dynamin-type guanine nucleotide-binding (G) domain, EH domain-containing protein, N-terminal	IP
AGAP029561		0,708	-0,497	0,00889759	N/A	N/A
AGAP010502		0,709	-0,497	0,04372467	N/A	N/A
AGAP004642	NPF	0,71	-0,495	0,03374923	Neuropeptide F	UP
AGAP008516		0,71	-0,494	0,02561527	nicotinate phosphoribosyltransferase	VB
AGAP010750		0,71	-0,493	0,0375236	ryanodine receptor 2	VB
AGAP000305		0,711	-0,492	0,04961506	SPARC	VB
AGAP007629	LANB2	0,711	-0,492	0,00944157	laminin gamma 1	VB
AGAP001366		0,712	-0,49	0,02279322	Serine proteases, trypsin domain, Peptidase S1A, chymotrypsin family, Serine protease gd, N-terminal domain	IP
AGAP007791		0,713	-0,489	0,03201638	sodium/potassium-transporting ATPase subunit beta	VB
AGAP008702	GPRNPR2	0,713	-0,487	0,03161692	Putative neuropeptide receptor 2	UP
AGAP005247		0,714	-0,486	0,03282155	Protein of unknown function DUF4728	IP
AGAP003785		0,716	-0,482	0,03653976	glucose dehydrogenase (acceptor)	VB
AGAP003843		0,716	-0,482	0,04950774	cytochrome c heme-lyase	VB
AGAP010394		0,717	-0,481	0,0431993	Patched-related	UP
AGAP010938		0,718	-0,477	0,03909671	Trp repressor/replication initiator, Brinker DNA-binding domain	IP
AGAP000847		0,72	-0,473	0,03462588	CDC-like kinase	VB
AGAP008366	TEP2	0,72	-0,475	0,01847926	thioester-containing protein 2	VB
AGAP009693		0,721	-0,473	0,03618715	RNA pseudouridylate synthase domain-containing protein 2	VB
AGAP006063		0,722	-0,47	0,0179084	N/A	N/A
AGAP007556		0,724	-0,465	0,03487263	Immunoglobulin subtype 2, Fibronectin type III	IP
AGAP009569		0,724	-0,466	0,01271696	syntenin-1 isoform 1	VB
AGAP010436		0,729	-0,456	0,03049047	adenylate cyclase 2	VB
AGAP002492		0,733	-0,448	0,04748468	nuclear respiratory factor 1	VB
AGAP004596	PyK	0,735	-0,444	0,01800364	pyruvate kinase	VB
AGAP029620		0,735	-0,445	0,03078378	Thrombospondin type-1 (TSP1) repeat, Somatomedin B domain	IP
AGAP004335		0,736	-0,442	0,02117272	filamin	VB
AGAP009579		0,736	-0,442	0,04961506	dihydropyridine-sensitive l-type calcium channel	VB
AGAP007005		0,738	-0,438	0,02650679	N/A	N/A
AGAP007788		0,739	-0,437	0,02925868	E3 ubiquitin-protein ligase RNF31	VB
AGAP002513		0,743	-0,428	0,0005304	Defective in cullin neddylation protein	UP
AGAP007833		0,744	-0,426	0,02143453	FAM21/CAPZIP domain	IP
AGAP029606		0,747	-0,421	0,01261935	IQ motif, EF-hand binding site, Myosin head, motor domain, P-loop containing nucleoside triphosphate hydrolase,	IP
AGAP002010		0,751	-0,413	0,04981479	N/A	N/A
AGAP000331		0,752	-0,412	0,02741115	low density lipoprotein-related protein 2]	VB
AGAP000815	INTB	0,753	-0,409	0,02318625	integrin beta subunit	VB
AGAP001590		0,754	-0,408	0,03618715	DBB domain, Ankyrin repeat-containing domain superfamily	IP
AGAP005057		0,754	-0,408	0,01569346	Resistance to inhibitors of cholinesterase protein 3, N-terminal	IP
AGAP008914		0,757	-0,401	0,02561527	Basic-leucine zipper domain	IP
AGAP007198		0,759	-0,398	0,02535361	N/A	N/A
AGAP002898	GSTZ1	0,761	-0,393	0,03489037	glutathione S-transferase zeta class 1	VB
AGAP009638		0,761	-0,394	0,03494485	Stabilizer of axonemal microtubules 1/2	IP
AGAP000304		0,765	-0,386	0,04989706	Protein twisted gastrulation	VB
AGAP008254		0,766	-0,384	0,03379828	VWFC domain	IP
AGAP005032		0,767	-0,384	0,04950774	calnexin	VB
AGAP012305		0,773	-0,372	0,04950774	Muscle LIM protein at 84B	VB
AGAP007049		0,774	-0,369	0,01441075	N/A	N/A
AGAP006389		0,776	-0,366	0,01944884	ribonuclease kappa	VB
AGAP005400		0,78	-0,358	0,03057533	four and a half LIM domains	VB
AGAP008763		0,78	-0,359	0,01932857	MIF4G-like, type 3, Armadillo-type fold	IP
AGAP001023		0,793	-0,334	0,03681021	myofilin variant B	VB
AGAP008046		0,793	-0,335	0,03414776	Protein kinase C and casein kinase substrate in neurons 2 protein	UP
AGAP004689		0,797	-0,327	0,0282315	Plexin domain-containing protein	IP
AGAP011459		0,804	-0,315	0,03909671	Cyclic nucleotide-binding domain, Ion transport domain, RmlC-like jelly roll fold	IP
AGAP006645		0,809	-0,307	0,03374923	Leucine-rich repeat, typical subtype	IP
AGAP007474		0,823	-0,281	0,02721754	Talin-1	VB
AGAP009668		0,85	-0,234	0,03161692	lysosomal-associated membrane protein 1/2	VB

Table S4. Full list of genes, which expression was downregulated upon APL1C depletion in RNAseq experiment. Genes are enlisted according to the descending expression fold change between “dsAPL1C” and “dsGFP” (control) treatments. The columns include gene ID referred as the AGAP numbers; gene names, N/A means not annotated gene; expression foldchange and log2foldchange; adjusted p-value (p-adj); gene description including encoded protein function or predicted protein domain based on the databases: VB-VectorBase Community Annotation, IP-Interpro, UP-UniPro. Red dotted line indicates the cutoff tested by qPCR. Genes in purple treatments were tested by qPCR. For the rest of the genes within the cutoff, the specific primers were not available. APL1C was excluded from qPCR analysis. The “Gene name” column includes the abbreviation used in qPCR analysis. Gene name in black correspond to the annotated gene name. Gene name in red correspond to abbreviation of gene function, whereas the genes without annotated function are called by the four last digits of their AGAP number and are depicted in green.

Gene ID	Gene name	FoldChange	log2FoldChange	p-adj	Gene description	Gene description source
AGAP006728	COEAE7G	10,483	3,39	4,20E-10	carboxylesterase	VB
AGAP029790	9790	10,297	3,364	0,0324689	Domain of unknown function DUF4806	IP
AGAP008246	GBD	2,577	1,366	0,016879105	gamma-butyrobetaine dioxygenase	VB
AGAP029411	9411	2,419	1,274	0,024111017	N/A	N/A
AGAP009381	CRBP	2,36	1,239	0,0375236	Cellular retinaldehyde-binding protein	UP
AGAP012477	GBD_2	2,32	1,214	0,013171475	gamma-butyrobetaine dioxygenase	VB
AGAP011676	UP2M	2,264	1,179	7,71E-05	uncoupling protein 2, mitochondrial	VB
AGAP003350	GTP	2,246	1,167	0,019596342	phosphoenolpyruvate carboxykinase (GTP)	VB
AGAP029623	9623	2,147	1,103	0,010492105	Sulfotransferase domain P-loop containing nucleoside triphosphate hydrolase	IP
AGAP007300	AP	2,122	1,085	0,019602457	alkaline phosphatase	VB
AGAP007959	7959	2,113	1,079	0,006046664	N/A	N/A
AGAP013642	U1	2,041	1,029	0,030548251	U1 spliceosomal RNA [Source:RFAM;Acc:RF00003]	
AGAP001423	BPBP	2,026	1,018	0,013739866	Bifunctional purine biosynthesis protein	VB
AGAP007122	TU1	2,018	1,013	0,000530401	tubulin, alpha 1	VB
AGAP012894		1,997	0,998	0,015519838	Histone H2B	UP
AGAP001352	1352	1,973	0,98	0,023186247	Haemolymph juvenile hormone binding Takeout superfamily	IP
AGAP005296	U11_1	1,971	0,979	0,01964634	U11/U12 small nuclear ribonucleoprotein 65 kDa protein	VB
AGAP007364	7364	1,956	0,968	0,009791078	Maternal protein exuperantia	IP
AGAP006241	INX2	1,954	0,967	9,44E-05	Innexin inx2	VB
AGAP000162	CBS	1,931	0,949	0,015459457	Cystathionine beta-synthase	UP
AGAP029317		1,912	0,935	0,039588096	Exoribonuclease, phosphorolytic domain 1 Ribosomal protein S5 domain 2-type fold PNPase/RNase PH domain superfamily	IP
AGAP000772	772	1,881	0,912	0,019328566	N/A	N/A
AGAP009751	ANCE2	1,868	0,901	0,006046664	angiotensin-converting enzyme 2	VB
AGAP003086		1,861	0,896	0,001831642	TMEM192 family	IP
AGAP004038	HPX8	1,858	0,893	0,003199427	heme peroxidase 8	VB
AGAP010540	540	1,852	0,889	0,010020081	N/A	N/A
AGAP005829	MAS_1	1,844	0,883	0,008897593	microtubule-associated protein, RP/EB family	VB
AGAP000180	PC	1,84	0,88	0,0112639	phosphoribosylaminoimidazole carboxylase	VB
AGAP004036	HPX7	1,838	0,878	0,02739326	heme peroxidase 7	VB
AGAP028655	8655	1,829	0,871	0,006887628	N/A	N/A
AGAP003591	LRR1	1,826	0,869	0,009441568	LRR-repeat protein 1	VB
AGAP007991		1,822	0,866	0,034317264	Triacylglycerol lipase family Lipase/vitellogenin Alpha/Beta hydrolase fold Lipase, N-terminal	IP
AGAP002387		1,82	0,864	0,004983856	acid phosphatase	VB
AGAP003087		1,816	0,861	0,009953441	TMEM192 family	IP
AGAP011145		1,811	0,856	0,033798283	ATP-dependent RNA helicase DDX56/DBP9	VB
AGAP000427		1,802	0,85	0,005953354	vitellogenin receptor	VB
AGAP008015		1,795	0,844	0,005266262	lamin	VB
AGAP009606		1,791	0,841	0,01042075	Domain of unknown function DUF3421 DM9 repeat	IP
AGAP011858		1,791	0,841	0,011510398	zinc finger HIT domain-containing protein 3	VB
AGAP001333	st	1,783	0,834	0,011462104	protein scarlet	VB
AGAP002581		1,782	0,833	0,019328566	MCM domain Nucleic acid-binding, OB-fold Mini-chromosome maintenance protein MCM, AAA-lid domain	IP
AGAP007549		1,774	0,827	0,030783776	Six-bladed beta-propeller, TolB-like Major royal jelly protein/protein yellow	IP
AGAP002532		1,765	0,82	0,004238876	Cyclin, C-terminal domain Cyclin, N-terminal	IP
AGAP005844		1,76	0,816	0,006233202	Bifunctional purine biosynthesis protein	VB
AGAP007505		1,76	0,816	0,014849805	vitellogenic carboxypeptidase-like protein	VB
AGAP011845		1,751	0,808	0,022152616	Histone H2A	UP
AGAP011713		1,734	0,794	0,016059772	ribonuclease P protein subunit POP4	VB
AGAP006404		1,733	0,793	0,018003641	N/A	N/A
AGAP012040		1,724	0,786	0,032254989	N/A	N/A

2660

AGAP012040		1,724	0,786	0,032254989	N/A	N/A
AGAP009792		1,719	0,781	0,000530401	importin subunit alpha-2	VB
AGAP001699		1,713	0,777	0,048918391	fatty-acid amide hydrolase 2	VB
AGAP012192		1,712	0,776	0,008897593	DNA mismatch repair protein MLH1	VB
AGAP002846		1,711	0,775	0,041598991	Trunk	VB
AGAP002378		1,71	0,774	0,023876565	Adenylosuccinate lyase	UP
AGAP006727	COEAE6G	1,707	0,772	0,015519838	carboxylesterase	VB
AGAP012375		1,698	0,764	0,017608886	protein aurora borealis	VB
AGAP003974		1,695	0,761	0,008897593	tRNA (cytidine32/guanosine34-2'-O)-methyltransferase	VB
AGAP003552		1,69	0,757	0,023186247	SET and MYND domain-containing protein 5	VB
AGAP000479		1,687	0,755	0,017422566	pre-rRNA-processing protein IPI3	VB
AGAP005581		1,685	0,753	0,00105879	3-hydroxyisobutyrate dehydrogenase	UP
AGAP002478		1,684	0,752	0,008897593	cyclin B	VB
AGAP005800		1,682	0,75	0,01612065	DNA replication licensing factor MCM7	VB
AGAP013023		1,664	0,735	0,03161692	Histone RNA stem-loop-binding protein SLBP1/SLBP2 Histone RNA hairpin-binding protein, RNA-binding domain	IP
AGAP011887		1,663	0,734	0,017908403	nuclear pore complex protein Nup37	VB
AGAP005260		1,661	0,732	0,011510398	dTMP kinase	VB
AGAP008290	TRYP6	1,66	0,731	0,020786941	trypsin 6	VB
AGAP006438		1,655	0,727	0,006046664	ribosomal biogenesis protein LAS1	VB
AGAP005052		1,654	0,726	0,03653976	deoxyribodipyrimidine photo-lyase	VB
AGAP011897		1,65	0,722	0,018003641	N/A	N/A
AGAP010918		1,645	0,718	0,038914815	cleavage stimulation factor subunit 2	VB
AGAP029627		1,645	0,718	0,049973746	Copper type II, ascorbate-dependent monooxygenase, N-terminal DOMON domain PHM/PNGase F domain superfamily Tyramine beta-hydroxylase/Dopamine beta-hydroxylase	IP
AGAP012686		1,644	0,717	0,049507741	Zinc finger C2H2-type	IP
AGAP001522		1,641	0,714	0,009529416	Thyroid receptor-interacting protein 13	VB
AGAP011652		1,641	0,714	0,024988431	AAA family ATPase, CDC48 subfamily protein	VB
AGAP008738		1,638	0,712	0,048387263	Eukaryotic translation initiation factor 4E binding protein	IP
AGAP029470		1,633	0,707	0,019448835	Sterile alpha motif domain K Homology domain	IP
AGAP010789		1,624	0,7	0,023352255	EB domain	IP
AGAP029584		1,623	0,698	0,023196353	N/A	N/A
AGAP029679		1,623	0,699	0,034944849	Zinc finger, AD-type Zinc finger C2H2-type	IP
AGAP006092		1,618	0,694	0,027272801	U3 small nucleolar RNA-associated protein 4	VB
AGAP011393		1,617	0,693	0,018115369	integrator complex subunit 7	VB
AGAP000650		1,613	0,689	0,015519838	ribonucleases P/MRP protein subunit RPP40	VB
AGAP003740		1,606	0,684	0,046466887	N/A	N/A
AGAP010941		1,601	0,679	0,027784962	Zinc finger C2H2-type Zinc finger protein 511	IP
AGAP003545	Osk	1,6	0,678	0,020044331	protein oskar	VB
AGAP004825		1,598	0,676	0,022564284	PapD-like superfamily Immunoglobulin-like fold ADP-ribose pyrophosphatase, mitochondrial	IP
AGAP004008		1,597	0,676	0,029845759	Protein kinase domain Serine-threonine/tyrosine-protein kinase, catalytic domain	IP
AGAP007817		1,597	0,675	0,017908403	Protein NEDD1	UP
AGAP029259		1,591	0,67	0,0112639	N/A	N/A
AGAP007145		1,584	0,663	0,017908403	N/A	N/A
AGAP007823		1,582	0,662	0,049415485	Nucleotide-binding alpha-beta plait domain superfamily Meiosis regulator and mRNA stability factor 1 OST-HTH/LOTUS domain	IP
AGAP009048		1,582	0,662	0,049897056	protein arginine N-methyltransferase 5	VB
AGAP010609		1,582	0,662	0,049507741	DnaJ (Hsp40) homolog subfamily C	VB
AGAP012154		1,581	0,661	0,017624312	solute carrier family 15 member 1	VB
AGAP008578		1,58	0,66	0,023186247	ATP-dependent RNA helicase DDX4	VB
AGAP006938	Art7	1,578	0,658	0,033798283	Protein arginine N-methyltransferase 7	UP
AGAP007775		1,578	0,658	0,03823344	ATP-dependent DNA helicase PIF1	UP
AGAP012964		1,578	0,658	0,017608886	Sarcospan	IP
AGAP004108		1,574	0,654	0,023812903	Amalgam	VB
AGAP010791		1,569	0,65	0,008897593	polyribonucleotide nucleotidyltransferase	VB
AGAP001656		1,568	0,649	0,029622655	ribosomal RNA-processing protein 7	VB
AGAP011457		1,565	0,646	0,013171475	ribose 5-phosphate isomerase A	VB
AGAP010453		1,56	0,642	0,021290069	ribosome biogenesis protein NSA1	VB
AGAP012107		1,557	0,638	0,036201432	SUMO-conjugating enzyme UBC9	VB
AGAP012216		1,557	0,639	0,006887628	sterol O-acyltransferase	VB
AGAP010406		1,554	0,636	0,035660224	origin recognition complex subunit 3	VB
AGAP007502		1,551	0,633	0,008897593	kinesin family member 11	VB
AGAP008063		1,547	0,629	0,036201432	exosome complex component CSL4	VB
AGAP001453		1,546	0,629	0,049973746	N/A	N/A
AGAP011454		1,544	0,626	0,001831642	rotatin	VB
AGAP008879		1,539	0,622	0,011462104	Protein of unknown function DUF389	IP
AGAP003883		1,537	0,62	0,000709794	peptidyl-tRNA hydrolase, PTH2 family	VB
AGAP003578		1,535	0,618	0,033798283	aldehyde dehydrogenase (NAD+)	VB
AGAP001166		1,532	0,616	0,021172723	GINS complex subunit 4	VB

2661

AGAP010722		1,529	0,612	0,028086615	RNA recognition motif domain Tudor domain Nucleotide-binding alpha-beta plait domain superfamily SNase-like, OB-fold superfamily RNA-binding domain superfamily	IP
AGAP003090		1,528	0,612	0,013462018	ubiquitin-conjugating enzyme E2 O	VB
AGAP013324		1,528	0,612	0,036267067	putative G-protein coupled receptor GPCR	VB
AGAP028639		1,526	0,609	0,014757327	N/A	N/A
AGAP004239		1,518	0,602	0,034317264	polo-like kinase 1	VB
AGAP001529		1,515	0,6	0,001102944	H/ACA ribonucleoprotein complex subunit	UP
AGAP007417		1,515	0,599	0,029157396	E3 ubiquitin-protein ligase SHPRH	VB
AGAP007635		1,511	0,595	0,014849805	60S ribosomal protein L7	VB
AGAP000719	Ahcy13	1,51	0,595	0,028478668	Adenosylhomocysteinase	UP
AGAP011534		1,51	0,594	0,023015671	Ankyrin repeat Ankyrin repeat and LEM domain-containing protein 2	IP
AGAP005149		1,498	0,583	0,006127055	H/ACA ribonucleoprotein complex subunit 3	VB
AGAP002967		1,497	0,582	0,016802001	bloom syndrome protein	VB
AGAP003890		1,492	0,577	0,024880322	U3 small nucleolar ribonucleoprotein protein IMP4	VB
AGAP010538		1,492	0,578	0,0381339	M-phase phosphoprotein	VB
AGAP003594		1,491	0,576	0,036857325	Zinc finger, AD-type Zinc finger C2H2-type Transcription factor Grauzone	IP
AGAP009825		1,491	0,576	0,018500044	TRM13/UPF0224 family, U11-48K-like CHHC zinc finger domain Zinc finger C2H2 superfamily	IP
AGAP013441		1,487	0,572	0,023186247	SS18 family	IP
AGAP004018		1,486	0,571	0,023186247	PDZ domain Harmonin	IP
AGAP008487		1,486	0,571	0,026506785	Sphingomyelin phosphodiesterase	UP
AGAP000168	GPRFZ3	1,482	0,568	0,030490471	Putative frizzled receptor 3	UP
AGAP006233		1,481	0,566	0,023015671	Phospholipase D-like domain	IP
AGAP002088		1,48	0,566	0,018596807	U3 small nucleolar RNA-associated protein 15	VB
AGAP005174		1,473	0,559	0,02827811	nucleoporin SEH1	VB
AGAP008771		1,472	0,558	0,036187152	DNA-directed RNA polymerases I and III subunit RPAC1	VB
AGAP002394		1,471	0,557	0,036810206	DNA-directed RNA polymerase III subunit RPC3	VB
AGAP002706		1,471	0,556	0,023812903	small nuclear ribonucleoprotein G	VB
AGAP028653		1,47	0,555	0,028478668	Pleckstrin homology domain	IP
AGAP002117		1,469	0,555	0,034944849	Cell death regulator Aven	IP
AGAP005629		1,469	0,555	0,03823344	N/A	N/A
AGAP009024		1,469	0,554	0,035419211	RNA polymerase I-specific transcription initiation factor RRN3	VB
AGAP027988		1,467	0,553	0,034910795	Zinc finger, AD-type Zinc finger C2H2-type	IP
AGAP008163		1,464	0,55	0,029845759	U4/U6 small nuclear ribonucleoprotein SNU13	VB
AGAP009488		1,464	0,55	0,034910795	histone transcription regulator	VB
AGAP001595	RpS29	1,46	0,546	0,010729313	40S ribosomal protein S29	VB
AGAP029794		1,459	0,545	0,031358359	Serine proteases, trypsin domain Peptidase S1A, chymotrypsin family	IP
AGAP002409		1,457	0,543	0,006127055	tRNA pseudouridine38-40 synthase	VB
AGAP002121		1,453	0,539	0,016879105	DNA-directed RNA polymerase II subunit RPB7	VB
AGAP005320		1,45	0,536	0,039878744	U3 small nucleolar RNA-interacting protein 2	VB
AGAP009336		1,45	0,536	0,022152616	RNA recognition motif domain Nucleotide-binding alpha-beta plait domain superfamily RNA-binding domain superfamily	IP
AGAP002535		1,449	0,535	0,023186247	serine/threonine-protein phosphatase PGAM5	VB
AGAP007413		1,445	0,531	0,033798283	BRCT domain Microcephalin-like	IP
AGAP000785		1,444	0,53	0,034872633	Synaptic vesicle protein	VB
AGAP002594		1,443	0,529	0,032821552	apolipoprotein D	VB
AGAP000666		1,442	0,528	0,03823344	ubiquitin carboxyl-terminal hydrolase 16/45	VB
AGAP029449		1,441	0,527	0,014751272	Helicase, C-terminal DEAD/DEAH box helicase domain Helicase superfamily 1/2, ATP-binding domain P-loop containing nucleoside triphosphate hydrolase	IP
AGAP009512		1,44	0,526	0,019885369	E3 ubiquitin-protein ligase UBR7	VB
AGAP000535		1,438	0,524	0,030035206	Acyltransferase 3 Nose resistant-to-fluoxetine protein, N-terminal	IP
AGAP001380		1,434	0,52	0,023933025	translation initiation factor 6	VB
AGAP000681		1,429	0,515	0,0436892	tRNA:m4X modification enzyme	VB
AGAP000496		1,422	0,508	0,019328566	geminin	VB
AGAP006941		1,42	0,506	0,037189609	ATP-dependent RNA helicase DDX51/DBP6	VB
AGAP009442		1,419	0,505	0,049415485	cyclin-dependent kinase regulatory subunit CKS1	VB
AGAP009431	RpS21	1,415	0,501	0,00055617	40S ribosomal protein S21	UP
AGAP003205		1,411	0,497	0,036174833	Major facilitator superfamily MFS transporter superfamily	IP

AGAP011383		1,41	0,495	0,037458371	rRNA-processing protein EBP2	VB
AGAP000549		1,409	0,494	0,049507741	2-oxoisovalerate dehydrogenase E2 component (dihydrolipoyl transacylase)	VB
AGAP002961		1,409	0,495	0,036810206	ribosomal RNA-processing protein 12	VB
AGAP009830		1,406	0,491	0,01612065	Chitin binding domain	IP
AGAP008292	TRYP4	1,403	0,489	0,036201432	trypsin 4	VB
AGAP001224		1,402	0,488	0,025215999	cleavage and polyadenylation specificity factor subunit 3	VB
AGAP005917		1,399	0,484	0,036201432	ATP-dependent DNA helicase Q4	VB
AGAP013400		1,399	0,485	0,014432066	Cytosolic fatty-acid binding Lipocalin/cytosolic fatty-acid binding domain Calycin Intracellular lipid binding protein	IP
AGAP029374		1,398	0,484	0,039588096	Zinc finger, AD-type Domain of unknown function DUF4806	IP
AGAP006234		1,397	0,483	0,049507741	protein SHQ1	VB
AGAP011966		1,397	0,482	0,036187152	transcription termination factor 2	VB
AGAP005922		1,392	0,477	0,044831691	DNA-directed RNA polymerase III subunit RPC5	VB
AGAP028053		1,389	0,474	0,047484681	N/A	N/A
AGAP007668	eIF3g	1,387	0,472	0,006887628	Eukaryotic translation initiation factor 3 subunit G	UP
AGAP002151		1,386	0,471	0,033160605	Regulator of chromosome condensation, RCC1 Regulator of chromosome condensation 1/beta-lactamase-inhibitor protein II	IP
AGAP008118		1,385	0,47	0,023352255	serine/threonine-protein kinase Chk1	VB
AGAP007020	TPX5	1,378	0,462	0,049615058	thioredoxin peroxidase 5	VB
AGAP000374		1,377	0,461	0,034944849	anaphase-promoting complex subunit 1	VB
AGAP003029		1,375	0,459	0,036201432	Forkhead-associated (FHA) domain Zinc finger, PHD-type SMAD/FHA domain superfamily PHD finger protein 12, MRG binding domain superfamily	IP
AGAP002337	eIF3d	1,366	0,45	0,027842842	Eukaryotic translation initiation factor 3 subunit D	UP
AGAP000416		1,364	0,448	0,030053919	hydroxyacylglutathione hydrolase	VB
AGAP002106		1,363	0,447	0,0324689	xeroderma pigmentosum group C-complementing protein	VB
AGAP002113		1,363	0,446	0,023409625	cytochrome b5	VB
AGAP002985		1,363	0,447	0,017608886	Structural maintenance of chromosomes protein 6	UP
AGAP002653		1,357	0,44	0,045285977	phenylalanyl-tRNA synthetase alpha chain	VB
AGAP003264		1,355	0,438	0,036810206	histone acetyltransferase 1	VB
AGAP007026	Ccs	1,355	0,439	0,043199303	copper chaperone for superoxide dismutase	VB
AGAP011309		1,355	0,438	0,044633666	nuclear GTP-binding protein	VB
AGAP010978		1,346	0,429	0,037106786	nuclear pore complex protein Nup62	VB
AGAP006997	Aats-ala-m	1,345	0,428	0,036201432	alanyl-tRNA synthetase, mitochondrial	VB
AGAP002404		1,343	0,425	0,049615058	cullin 5	VB
AGAP001141		1,339	0,421	0,044831691	Zinc finger C2H2-type	IP
AGAP009862		1,335	0,417	0,048227633	WD40 repeat WD40/YVTN repeat-like-containing domain superfamily	IP
AGAP010586	AIMP1	1,335	0,417	0,029255508	aminoacyl tRNA synthase complex-interacting multifunctional protein 1	VB
AGAP011677		1,335	0,417	0,020085987	Elongation factor EFG, domain V-like Transcription factor, GTP-binding domain Translation elongation factor EFTu-like, domain 2	IP
AGAP008000		1,334	0,416	0,044640528	sepiapterin reductase	VB
AGAP002968		1,324	0,405	0,048634299	thiamine pyrophosphokinase	VB
AGAP005115		1,323	0,404	0,044831691	N/A	N/A
AGAP003063		1,319	0,399	0,044831691	Rwd domain-containing protein	VB
AGAP009091		1,317	0,397	0,034625882	aromatic-L-amino-acid decarboxylase	VB
AGAP004563	ANCE9	1,313	0,393	0,049507741	angiotensin-converting enzyme 9	VB
AGAP006947		1,311	0,391	0,044831691	Cytochrome B561-related	IP
AGAP003486		1,302	0,38	0,034625882	N/A	N/A
AGAP008090		1,302	0,38	0,036201432	nuclear pore complex protein Nup205	VB
AGAP008635		1,295	0,373	0,032228725	protein SDA1	VB
AGAP005990		1,285	0,362	0,046758013	glycolipid transfer protein domain-containing protein 1	VB
AGAP008795		1,285	0,362	0,029622655	Zinc finger, AD-type Zinc finger C2H2-type	IP
AGAP009920	RpL37a	1,283	0,359	0,035903402	60S ribosomal protein L37a	VB
AGAP000826		1,282	0,358	0,044052437	cap-specific mRNA (nucleoside-2'-O-)-methyltransferase 1	VB
AGAP011173	RpL11	1,278	0,354	0,039015507	60S ribosomal protein L11	VB
AGAP009572	RpS15a-2	1,276	0,351	0,033798283	40S ribosomal protein S15a	VB
AGAP002539		1,269	0,343	0,035419211	integrator complex subunit 3	VB
AGAP007740	RpLP1	1,264	0,338	0,027842842	60S ribosomal protein LP1	VB
AGAP012219	Med1	1,253	0,326	0,03589132	mediator of RNA polymerase II transcription subunit 1	VB
AGAP002525		1,223	0,29	0,049507741	eukaryotic translation initiation factor 2A	VB

2663

Table S5. Full list of genes, which expression is upregulated upon APL1C depletion in RNAseq experiment. Genes are enlisted according to the ascending expression fold change between “dsAPL1C” and “dsGFP” (control) treatments. The columns include gene ID referred as the AGAP numbers; gene names, where N/A means not annotated gene; expression foldchange and log2foldchange; adjusted p-value (p-adj); gene description including encoded protein function or predicted protein domain based on the databases: VB- VectorBase Community Annotation, IP-Interpro, UP-UniPro. Genes in purple treatments were tested by qPCR. For the rest of the genes within the cutoff, the specific primers were not available. The “Gene name” column include the abbreviation used in qPCR analysis. Gene name in black correspond to the annotated gene name. Gene name in red correspond to abbreviation of gene function, whereas the genes without annotated function are called by the four last digits of their AGAP number and are depicted in green.

Gene_orientation_restriction	Primer sequence
APL1C_5'_EcoRI	TTGAATTCGAGCATTGAGTACCACAATGTGCTGGTTACACGCCG
APL1C_3'_V5Xba	CCTCTAGACTTTGTAACGCGACGCGTATC
LRIM1_5'_EcoRI	TTGAATTCAACGCGAAACGAAAGATGATGTCG
LRIM1_3'_V5Xba	CCTCTAGATCCCAGCTGGCTCGCTAAATTCTGC
RFPAPL1C_5’_EcoRI	TTGAATTCGAGCATTGAGTACCACAATGTGCTGGTTACACGCCG
RFPAPL1C_3’_SacII	AACCGCGGTGCAACACTACCACATGTG

Table S6. Primers sequences used for the plasmids construction.

Annotation_ID[a]	Gene_name	Primer_f 5'-3'[b]	Primer_r 5'-3'[b]	Source[c]	Purpose
N/A	GFP	GAATTGTAATACGACTCACTATAGGGCATGGTGAGCAAGGGCGAG	GAATTGTAATACGACTCACTATAGGGCTTACTTGTACAGCTCGTC	https://doi.org/10.1371/journal.ppat.1005306	dsRNA synthesis
AGAP007036	APL1A	TAATACGACTCACTATAGGACTACCACCAGCCGAAAGATG	TAATACGACTCACTATAGGATCTGGTCTTGTATAGTACAATGG	https://doi.org/10.1371/journal.ppat.1005306	dsRNA synthesis
AGAP007033	APL1C	TAATACGACTCACTATAGGAGGCCAAGAAGAACCGCAATCC	TAATACGACTCACTATAGGATCACAGTGATTTCAGGGTGTGC	https://doi.org/10.1371/journal.ppat.1005306	dsRNA synthesis
AGAP008072	NOX5	TAATACGACTCACTATAGGGTCGTACGAATGGTCGAGTGA	TAATACGACTCACTATAGGGCCAAACTGGTCGCACTTGTA	DOI: 10.1126/sciimmunol.aal1505	dsRNA synthesis
AGAP009033	HPX2	TAATACGACTCACTATAGGGACGACGACGGTGTGTACAAG	TAATACGACTCACTATAGGGATACTCGGCCGAATCGAAC	DOI: 10.1126/sciimmunol.aal1505	dsRNA synthesis
AGAP010815	TEP1	TAATACGACTCACTATAGGTTTGTGGGCCTTAAAGCGCTG	TAATACGACTCACTATAGGACCACGTAACCGCTCGGTAAG	https://doi.org/10.1371/journal.ppat.0020052	dsRNA synthesis
AGAP010816	TEP3	TAATACGACTCACTATAGGGCACCTCGACTGAGAAAGGTTTG	TAATACGACTCACTATAGGGCTGATTATTTATATAGTTTTAC	https://doi.org/10.1371/journal.ppat.1005306	dsRNA synthesis
AGAP010592	S7	CACCGCCGTGTACGATGCCA	ATGGTGGTCTGCTGGTTCTT	https://doi.org/10.1371/journal.ppat.1005306	qPCR
N/A	16S_V4q	GTGCCAGCMGCCGCGGTAA	GGACTACHVGGGTWTCTAAT	https://doi.org/10.1371/journal.pntd.0008059	qPCR
AGAP007036	APL1A	GACTGCAAGCCGAGATCGATACC	CATCCATCTGGTCCTTGAGCTTA	https://doi.org/10.1371/journal.ppat.1005306	qPCR
AGAP007033	APL1C	AAGCAGGCTGAGTTGAGACAGG	GCCCAAGTAACATCATACACAC	https://doi.org/10.1371/journal.ppat.1005306	qPCR
AGAP012386	eater	TTCACCCGTCTGCGAGGGATGCAAGC	GTCAACGTGCATAGTAGCGTCTCCGTAGC	DOI: 10.1073/pnas.1900147116	qPCR
AGAP009762	nimrodB2	CAATCTGCTCAAATGGCTGCTTCCACG	GCTGCAAACATTCGGTCCAGTGCATTC	DOI: 10.1073/pnas.1900147116	qPCR
AGAP009033	HPX2	CCGCTTCTACAACACGATGA	CGACCAGATGGGCAAGTAT	DOI: 10.1126/sciimmunol.aal1505	qPCR
AGAP008072	NOX5	TCATGCATCGCTACTGGAAG	CCAGAAAAGTCCACCTTGG	DOI: 10.1126/sciimmunol.aal1505	qPCR
AGAP010815	TEP1	AAAGCTGTTGCGTCAGGG	TTCTCCCACACACCAAACGAA	10.1371/journal.ppat.1002023	qPCR
AGAP010816	TEP3	ACCGCCAGGCGTACGTGATGG	CAAACCTTTCTCAGTCGAGGT	https://doi.org/10.1371/journal.ppat.1005306	qPCR
AGAP005503	SDR11	CAGTGTGGTAGGCCATACGG	TTCAGCTCACTAGGGACCG	TM	qPCR
AGAP010058	PAS1	CTCGGACACAACGTAGTTGG	AGCTGGAAGATCGCACTGGC	TM	qPCR
AGAP009217	CLIPB12	ATAATTCTCAGATGTGTGCG	CCATCCCAAAAGCATGTGCC	TM	qPCR
AGAP001669	CPR6	AAGACTGTTTGATGTTGACC	AGATCCATCTCGTTTTTGCC	TM	qPCR
AGAP008512	8512	TTGGAACGCCTTTTGGACCG	CTTGTGGTGAAACATTTGCG	TM	qPCR
AGAP000113	113	CAACTTCGCGAAACCTCGCC	CTGTTCGACAGAAAGCTGCC	TM	qPCR
AGAP011509	COE	GTGCCATACACGGGGATGAT	ATCAACTCCACTGTCCAGCG	TM	qPCR
AGAP013201	3201	ATGATGTTTCAATTCGAGCC	AGATCTATCCCTGGAGAACCG	TM	qPCR
AGAP006400	APH2	CATGTCCCAGACAACCGTGA	TGCCGAGGTTCGATTTCACA	TM	qPCR
AGAP007319	7319	TTATGAAGTGAAAGCTGACGC	CCTCCGCAACCTGGTTATGCC	TM	qPCR
AGAP010854	SCF45	ACCTGTAGGACCTTAGCACGCC	AAGGTGCTAAAGTAGCTCGC	TM	qPCR
AGAP011564	GGT	ATTACCGGGATCATGACGG	CGTTCACGACCGCCATCGCTG	TM	qPCR
AGAP012648	2648	GGTCCATGCCTCAAGAAGTC	AAGATTGCAAACGGTGCGAG	TM	qPCR
AGAP029110	9110	CGAGCTACTAACGCTTGGGC	GGGAATTCAGGATTACGCGG	TM	qPCR
AGAP003334	CPLCX2	GTCCACCACGCCCCGGTCGTG	CCACCGGGACCGGGTGCACGGA	TM	qPCR
AGAP001748	ChS	GCGTACTTCGAACGCTGGCG	TCGTCATCCTCAATTACCGG	TM	qPCR
AGAP001470	1470	GAAGGTAAGCTCCGACACCT	CTGGCCGGCCTGCTCGAGCT	DOI: 10.1073/pnas.1900147116	qPCR
AGAP006728	COEAE7G	CGGTGTAACGCATGGCACGC	TGCGACCGGTGCTGGTACCG	TM	qPCR
AGAP029790	9790	GCAAGTAGGCTGAAGTAG	TCATGCGCTGATCGAAAACG	TM	qPCR
AGAP008246	GBD_46	GGTCGGGACTGTGAACAAGAA	ACGAGGGTTTCGACGAACAAT	TM	qPCR
AGAP029411	9411	GCGATTTCTAGCCTTCGTGC	CGTGTCGTAGTGAGCGTAGG	TM	qPCR
AGAP009381	CRBP	GTGTGCGAATCCAAGTCAGC	CCACTCTACCCTGCAACCTG	TM	qPCR
AGAP012477	GBD_77	CCATGTCACTGGTTCGCTG	ATAGAGGCCGATTGTGTGGC	TM	qPCR
AGAP011676	UP2M	TTGCTTGAAGCTCTCACCGT	AAGACGAAAAATCCCCGCGA	TM	qPCR
AGAP003350	GTP	TCAGTTCAGCAGAACCAATCCA	GCACTTAGGCACGAGAGTGT	TM	qPCR
AGAP029623	9623	CGATGAAGCGATCGAACCTC	GCAAGTTGCTGCTCGATGAA	TM	qPCR
AGAP007300	AP	AGTTTCCCGACGTTGGTCTC	CACCGAGCGTTGCATAGTTG	TM	qPCR
AGAP007959	7959	TTGCCGTGAATATCGTGCCT	ACCGCCGCTGTTGCTATTAT	TM	qPCR
AGAP001423	BPBP	ATTATTGCGCGCGAAGTGTC	TCTTCTTCTTGCGCAGCACT	TM	qPCR
AGAP007122	TU1	GCTTTCTGCTGTTCCACTCG	GGGTAGACGGCGAACTGTAG	TM	qPCR
AGAP001352	1352	GTTTCTTCTGCCTCAACCGC	AGAGCCGGATTGGGACAAAC	TM	qPCR
AGAP005296	U11 5296	GAAGGGACAGGCGTTCGTTA	CGCTTGGTCGATGCAGTTTT	TM	qPCR
AGAP007364	7364	CGAGTCGGTTAAGTCCTTCG	TCGTCCAAAACTAACTTCGCT	TM	qPCR
AGAP006241	INX2	GGTCCAGAGTGTGTCGAAGG	CACACGCCTTCCTCATCGTA	TM	qPCR
AGAP000162	CBS	GCAACGACGTTCGGTATTCG	TCCAAAACTGCCAACAGGGT	TM	qPCR
AGAP000772	772	TGCTAGGGGTACACGTGAGA	GCCCCAGCACAATGCAAAAT	TM	qPCR
AGAP009751	ANCE2	ACTCCGGTGTGGAGCCGCCGG	CACGTACTCGCCCGCCAGCG	TM	qPCR
AGAP004038	HPX8	ACGGGCCCCGGACCAATCCG	CCGCTAGTGACCCCTCCAGG	TM	qPCR
AGAP010540	540	GATTGGCCGGAAGGAAGTGA	CACGTGTTTGCAGACGATCC	TM	qPCR
AGAP005829	MAS 5829	GGAAGGAGTACGATCCGCAG	GTTCGTATCACCCATCCGCT	TM	qPCR
AGAP000180	PC	AGCGAGGAGCAGATTGTGTG	CTTCATGTCGATCAGCGCAC	TM	qPCR
AGAP004036	HPX7	GTACGCTGTACCAGGAGGCG	TACCGATGGGTTGGTGTGCG	TM	qPCR
AGAP028655	8655	TACAAGTACAGCTCCGTGCG	GGGGGCACTTCCTACCTAGA	TM	qPCR
AGAP003591	LRR1	GTTCGTCACACCCGAGCACG	TTCCCCACGGTAAGACACGG	TM	qPCR
AGAP007036	APL1A_GSP	CATTTGCTGCACGTGGAACGTAACCAGC	N/A	TM	RACE
AGAP007033	APL1C_GSP	GGCAAGCGTTTAAGTTGGGCGAAACGCA	N/A	DOI: 10.1371/journal.pone.0003672	RACE
AGAP007036	APL1A_GSP_ne	TAGGCTGGAAAACCTTTACCTCGACCAC	N/A	TM	RACE
AGAP007033	APL1C_GSP_	GTTGGATAATAAGAGGGCAAAGCAGGC	N/A	TM	RACE

[a] Applicable to mosquito genes; ID based on the Reference Strain Anopheles gambiae PEST.

[b] T7 sequence is underlined.

[c] In case of published primers sequence, link to the publication source is indicated. TM refers to the primers designed in this manuscript.

Table S7. List of the primers used for dsRNA synthesis, qPCR and RACE.

ABSTRACT

Abstract: *Anopheles* mosquito is a vector of *Plasmodium* parasite, the causative agent of malaria. The Anopheles leucine-rich immune molecule (LRIM) family members are leucine-rich repeat (LRR) proteins, which certain were described as key antagonists of *Plasmodium* parasites in *Anopheles* mosquito midgut. APL1C (*Anopheles Plasmodium-responsive factor*) is a representative of LRIM members which specifically protects against rodent malaria parasites by stabilizing the complement-like protein TEP1. By combining cell biology with functional genomic approaches, this study shows that mosquito bloodmeal induce the presence of an extracellular layer of APL1C protein surrounding the midgut beneath of the basal lamina. Consistently with the formation of this layer, APL1C binds to the ookinetes that emerged on the basal side of the midgut. This presence occurs independently from TEP1 function, requires the contribution of the phagocytic cells and nitration pathway. In addition, APL1C defence function is not restricted to the ookinete in the midgut but it also acts against the latest Plasmodium stage, the sporozoites. APL1C inhibits salivary glands infection prevalence, and consistently, it also binds to the surface of the sporozoites in the hemocoel. However, unlike to the midgut stages, anti-sporozoites APL1C-dependent mechanism involves different partners. Moreover, RNAseq study revealed APL1C gene targets, including genes with immune-like function. These results generate novel biological insight for the function of APL1C, and probably other LRIM and LRR family members, as a pathogen recognition receptor inducing immune response against pathogens that come in contact with mosquito hemolymph compartment.

Key words: *Anopheles,* leucine-rich repeat, pathogen recognition, immune signalling, complement-like pathway, *Plasmodium.*

Résumé : L'anophèle est le moustique vecteur du parasite *Plasmodium*, responsable du paludisme. Chez ce moustique, des protéines de la famille LRIM (*Anopheles leucine-rich immune molecule*) ont été décrites comme antagonistes du développement de *Plasmodium*. L'une d'entre elles, APL1C (*Anopheles Plasmodium-responsive factor*) protège spécifiquement le moustique contre les parasites *Plasmodium* de rongeurs en collaboration avec la protéine TEP1 du complément. En combinant des approches de biologie cellulaire et de génomique fonctionnelle, mon travail de thèse montre que le repas sanguin des moustiques induit le recrutement d'APL1C au niveau du pôle basal de l'épithélium digestif. Ce positionnement d'APL1C lui permet de se lier aux stades ookinètes du parasite émergeant du côté basal de l'épithélium, et ce, indépendamment de la fonction de TEP1. Néanmoins, cette action d'APL1C requiert la contribution des phagocytes et de la Nitration. Par ailleurs, mon travail montre que l'action d'APL1C ne se restreint pas à l'ookinète car elle agit aussi contre le dernier stade de développement de *Plasmodium*, les sporozoïtes. Avec la

capacité de se lier aux sporozoites, APL1C contrôle la prévalence d'infection des glandes salivaires du moustique, mais avec des partenaires différents de ceux agissant sur les ookinètes. Finalement, une étude transcriptomique m'a permis d'identifier des facteurs agissant en aval d'APL1C. L'ensemble de ces résultats génère de nouvelles connaissances relatives à la fonction des membres de la famille LRIM en tant que récepteurs de reconnaissance d'agents pathogènes capable de déclencher une réponse immunitaire dans différents compartiments tissulaires du moustique.

Mots clés : *Anopheles,* motifs riches en leucines, reconnaissance microbienne, signalisation immunitaire, système assimilé au complément, *Plasmodium.*